HU ISSN 2063-6997

GEOSCIENCES AND ENGINEERING

A Publication of the University of Miskolc

Volume 9, Number 14 (2021)

Miskolc, University Press

GEOSCIENCES AND ENGINEERING
A Publication of the University of Miskolc
Volume 9, Number 14 (2021)
Miskolc, University Press
UNIVERSITY OF MISKOLC
FACULTY OF EARTH SCIENCE & ENGINEERING
HU ISSN 2063-6997

TABLE OF CONTENTS

Geosciences and Engineering, Vol. 9, No. 14 (2021), pp. 5–16.
https://doi.org/10.33030/geosciences.2021.14.005

GEOLOGY AND PETROGRAPHY OF MUBARAK AREA, CENTRAL EASTERN DESERT, EGYPT

MOHAMED ABDELHADI BADAWI,[1, 2,*], FARID M. ALI MAKROUM[2], AHMED SHALABY[2], NORBERT NÉMETH[1]

[1]*Institute of Mineralogy and Geology, University of Miskolc, 3515 Miskolc, Hungary*
[2]*Geology Department, Faculty of Science, Mansoura University, Mansoura 35516, Egypt*
**mohamedabdelhadi@mans.edu.eg*

Abstract: The Mubarak region is covered by two major rock units: the Island Arc Association and granitoids. This Island Arc Association is represented by metaandesite, hornblende-actinolite schist, and amphibolite, which were metamorphosed up to amphibolite facies. Granitoids are classified based on the petrographic mineral composition into two phases: the syn- to late-orogenic phase and the post-orogenic phase. According to field observations and petrographic analyses, these granitoids are magmatic rocks with isotropic texture, as opposed to the Island Arc Association, which is strongly foliated, indicating that a NW shortening occurred prior to the emplacement of the weakly metamorphosed granodiorite and the non-metamorphic post-orogenic intrusives.

Keywords: *granite, Pan-African Orogeny, intrusive, Island Arc Association*

1. INTRODUCTION

The Neoproterozoic crystalline basement rocks of Egypt's Eastern Desert and Sinai comprise the northern edges of the Arabian-Nubian Shield (ANS) juvenile arc terrain, which was cratonized during the late Neoproterozoic Pan-African Orogeny (900–550 Ma) *(Figure 1a)* [1]. This section of the ANS is also covered by a diverse range of rock types, including gneisses and ophiolitic mélange, which have been intruded by syn- to late-orogenic tectonic granitoids with adjacent volcanic formations and are covered by molasse-type sediments of late Proterozoic age *(Figure 1b)* [2–4]. Gneisses and migmatites comprise the Egyptian basement complex's rocks, as well as the ANS [5, 6]. The ophiolites are variably dismembered and are divided into three units that display a sequence from mantle section upward through mafic crust to the overlying mafic volcanic rocks [7]. These units include (1) serpentinites, (2) meta-pyroxenites, and (3) metagabbro and metavolcanic rocks.

The rock assemblage of the Island Arc Association (IAA) is composed of (1) an intrusive gabbro-diorite-tonalite suite, (2) calc-alkaline metavolcanics and meta-tuffs and (3) rare sedimentary iron deposits and shallow-marine carbonate facies [8–11].

Granite rocks are divided into three categories: (1) older grey calc-alkaline granites, (2) younger pink granites, and (3) A-type (alkaline/peralkaline) granites [12–17]. Additionally, the ANS calc-alkaline magmatism is divided into two distinct

series: syn- to late-orogenic island arc intrusive (625–650 Ma) and post-orogenic (590–625 Ma) with less deformation [18, 19]. Gabbroic rocks are found across the Eastern Desert basement complex and are classified into two age groups, the ophiolitic meta-gabbros and fresh post-orogenic gabbros.

The distribution of these lithologies structurally divides the Eastern Desert into three distinct regions, the northern, central, and southern Eastern Desert, along two structural axes: the ENE dextral Qena-Safaga shear zone and the WNW sinistral Kom Ombo-Houdin shear zone, respectively *(Figure 1b)* [20]. In comparison to the northern and southern Eastern Deserts, which are dominated by granitic rocks and low-grade cover nappe, respectively, the central Eastern Desert is dominated by massive gneissic rocks. Additionally, the exhumation of these gneissic rocks is controlled and limited laterally by the NW-trending sinistral Najd Fault System (NFS) [21–23].

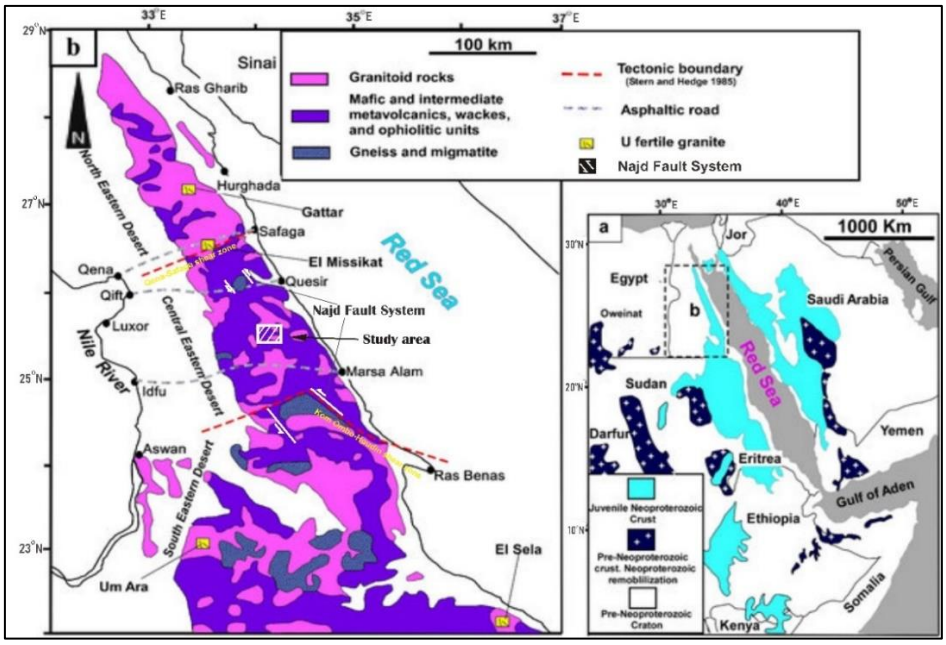

Figure 1

(a) Map of the Arabian-Nubian Shield (ANS) modified after [27], *showing the location of Eastern Desert of Egypt (frame b) and regions of pre-Neoproterozoic crust outcrops; (b) Generalized map of Eastern Desert, showing the distribution of lithologies, and major tectonic boundaries, modified after* [28]

In sharp contrast to the NFS and associated structures, the Mubarak belt usually runs east–west to northeast–southwest *(Figure 1b)*. Based on this, Shalaby and his co-authors concluded that considering the Mubarak belt as a conjugate fault to the NFS provides the most convincing explanation for its deformation model and is consistent

with the central Eastern Desert tectonic framework [24]. This belt is shaped like a wedge by post-accretionary lower greenschist facies surrounded by less deformed metavolcanics [25, 26]. It is composed mainly of a dense sequence of low-grade volcano-sedimentary rocks with arc and back-arc affinities. Furthermore, it contains significant granitoids of unclear tectonic origin. This belt is bisected by the Mubarak–Dabr Metagabbro–Diorite Complex from the south [26].

The aim of this study is to classify the rock types found in the Mubarak area of the central Eastern Desert of Egypt based on the lithological groupings that have emerged in the ANS and their petrographic descriptions. This study is based on field observations and sample collection from all lithologies exposed in the area for petrographic classification. The sampling sites are chosen along the Mubarak belt to represent the change in the grade of metamorphism and mineral composition, on the rim and core of the granitoid intrusions as well. This paper presents the rock types based on optical microscopy, which is a contribution to the comprehensive study of the larger Um Nar area. This area is currently investigated completely through the integration of structural, geochemistry, and remote sensing data to analyze its tectonic framework in greater depth [24].

2. LOCATION OF THE STUDY AREA

Wadi Mubarak is located in the central Eastern Desert and covers approximately 300 kilometers between longitudes 34º11'E and 34º28'E and latitudes 25º10'N and 25º22'N. It is located near the city of Mersa Alam and is accessible by the Mersa Alam-Idfu asphaltic road *(Figure 2a)*. Along with the arid climate and sparse vegetation, this area is characterized by rigid topography due to the presence of multiple steep peaks, especially Gebel El Mayit (830 m).

3. GEOLOGIC SETTING

The rocks of Wadi Mubarak can be classified into three major lithological units: (1) Pan-African nappe assemblages, (2) Syn- to late-orogenic calc-alkaline intrusives, and (3) Post-orogenic granitic and gabbroic intrusions.

3.1. Pan-African nappe assemblage

The Pan-African nappe assemblage is represented by the IAA of the Mubarak belt. Unlike the Najd Fault System and its accompanying structures, this belt extends east–west to northeast–southwest (see *Figure 4*). The Mubarak belt is typically shaped like a sliver border and possesses nearly vertical layers of a metamorphic association of volcanic and volcano-sedimentary origin including amphibolites, schists, and low-grade metaandesites *(Figure 2b)*.

On the eastern side of the Mubarak belt, the medium-grade schists and amphibolites are abundant, which are strongly foliated in contrast with the metaandesites, which are widely exposed on the western side and distinguished by being massive, weakly metamorphosed volcanic slabs (*Figures 3a* and *b*).

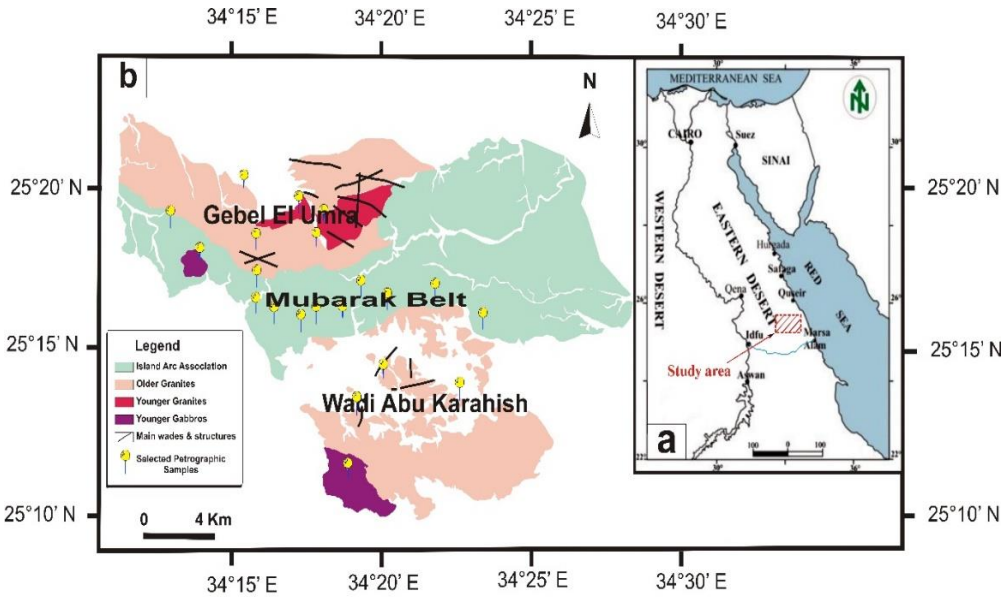

Figure 2
(a) Location map of the Eastern Desert of Egypt showing the study area, (b) Geological map of the Mubarak area showing different lithologic units

3.2. Syn- to late-orogenic calc-alkaline granites

The older "grey" granites may be found in the areas of El Umra and Abu Karahish, which are located to the north and south of the Mubarak belt, respectively, and are considered to be younger than the Mubarak belt *(Figure 2b)*. Granitic bodies in El Umra have an E-W elongated ellipsoidal form, whereas Abu Karahish granite is exposed as irregular bodies which are covered mostly by sand deposits.

These rocks are coarse-grained equigranular magmatic rocks of granodioritic composition *(Figure 3d)*. These granodiorites are exposed as sporadic low hills showing extensive weathering features (e.g., exfoliation and fractures) and devoid of any features of metamorphism *(Figure 3c)*.

3.3. Post-orogenic intrusives

The Mubarak region exhibits numerous plutons of post-orogenic granitic and gabbroic composition. The post-orogenic granites are referred to as "pink younger granites" and are found in El Umra area as non-deformed irregular intrusive bodies forming sharp contacts with the previously formed older granites (*Figures 2b* and *3e*). The post-orogenic gabbros bodies have circular outlines. They are mostly exposed in the western and southern parts of the mapped area (*Figures 2b* and *3f*).

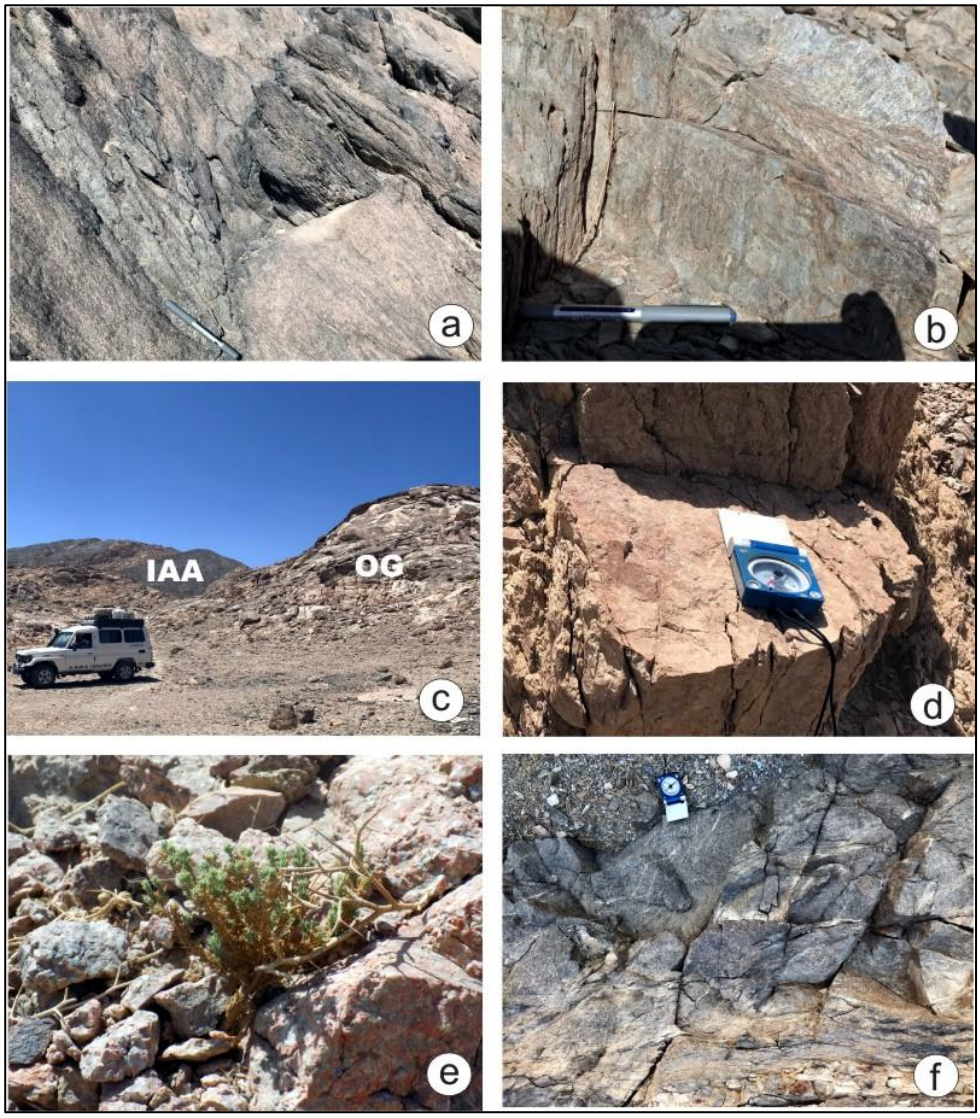

Figure 3
Field observations showing (a) the amphibolites and schists of the Mubarak belt, (b) the Island Arc metavolcanics, (c) older granites of Abu Karahish area, (d) older granites of Gebel El Umrah, (e) post-orogenic granites, and (f) post-orogenic gabbros

4. PETROGRAPHY

This description is based on twenty-three representative petrographic thin sections for the different lithologies dominating the Mubarak area *(Table 1)*.

Table 1

Selected petrographic samples with their rock types and geographic coordinates

Rock Sample	Rock Name	Longitude	Latitude
D11	Amphibolite	34°23'16.44"E	25°16'0.91"N
D12	Amphibolite	34°23'25.07"E	25°16'8.22"N
D13	Amphibolite	34°23'22.55"E	25°15'54.81"N
D13 b	syn-to-late orogenic granodiorite	25°15'44.14"N	34°23'4.76"E
N15	post-orogenic gabbro	34°19'6.28"E	25°11'51.85"N
N17	syn-to-late orogenic granodiorite	34°19'24.15"E	25°13'49.69"N
N18	syn-to-late orogenic granodiorite	34°20'6.39"E	25°13'42.20"N
N20	Amphibolite	34°19'7.20"E	25°16'8.06"N
N22	post-orogenic gabbro	34°13'50.91"E	25°16'57.89"N
N25	Hornblende-actinolite schist	34°16'6.62"E	25°16'32.17"N
N29	syn-to-late orogenic granodiorite	34°17'7.60"E	25°18'7.29"N
N 30 b	post-orogenic granite	34°17'53.82"E	25°18'21.90"N
N31	syn-to-late orogenic granodiorite	34°13'4.58"E	25°21'54.69"N
N32	syn-to-late orogenic granodiorite	34°13'10.78"E	25°19'3.94"N
N34	Meta-andesite	34°14'13.97"E	25°17'26.72"N
N35	Meta-andesite	34°13'38.51"E	25°17'49.77"N
N36	post-orogenic gabbro	34°13'19.99"E	25°17'32.78"N
N37	Meta-andesite	34°11'26.43"E	25°18'47.08"N
N38	Meta-andesite	34°11'4.73"E	25°18'33.62"N
N39	Meta-andesite	34°10'56.33"E	25°19'0.37"N
5	Hornblende-actinolite schist	34°18'26.53"E	25°15'58.45"N
6	Hornblende-actinolite schist	34°17'47.52"E	25°16'10.03"N
7	Hornblende-actinolite schist	34°16'54.16"E	25°16'22.21"N

4.1. Pan-African nappe assemblage

4.1.a. Amphibolite

Amphibolite is foliated, hard, massive, and fine-grained rocks of dark green in color *(Figure 4a)*. This rock is essentially composed of amphibole phenocrysts embedded in a fine-grained groundmass of quartz, plagioclase, and minor biotite. Chlorite, epidote, sericite, and iron oxides are abundant as subsequent mineral phases overgrown on amphiboles. **Amphiboles** form subhedral, oriented prismatic crystals reaching up to (265 μm × 80 μm) in size and are mostly represented by actinolite and scarce hornblende. Felsic minerals fill the space between amphibole crystals aligned according to the foliation. **Quartz** occurs as equant crystals with undulate extinction (45 μm × 40 μm). **Chlorite** occurs frequently (700 μm × 274 μm) as large flakes surrounding amphibole crystals but are not oriented. **Sericite** is common within plagioclase relics. **Iron oxides** form anhedral crystals, partly concentrated on the cleavage planes of amphibole crystals.

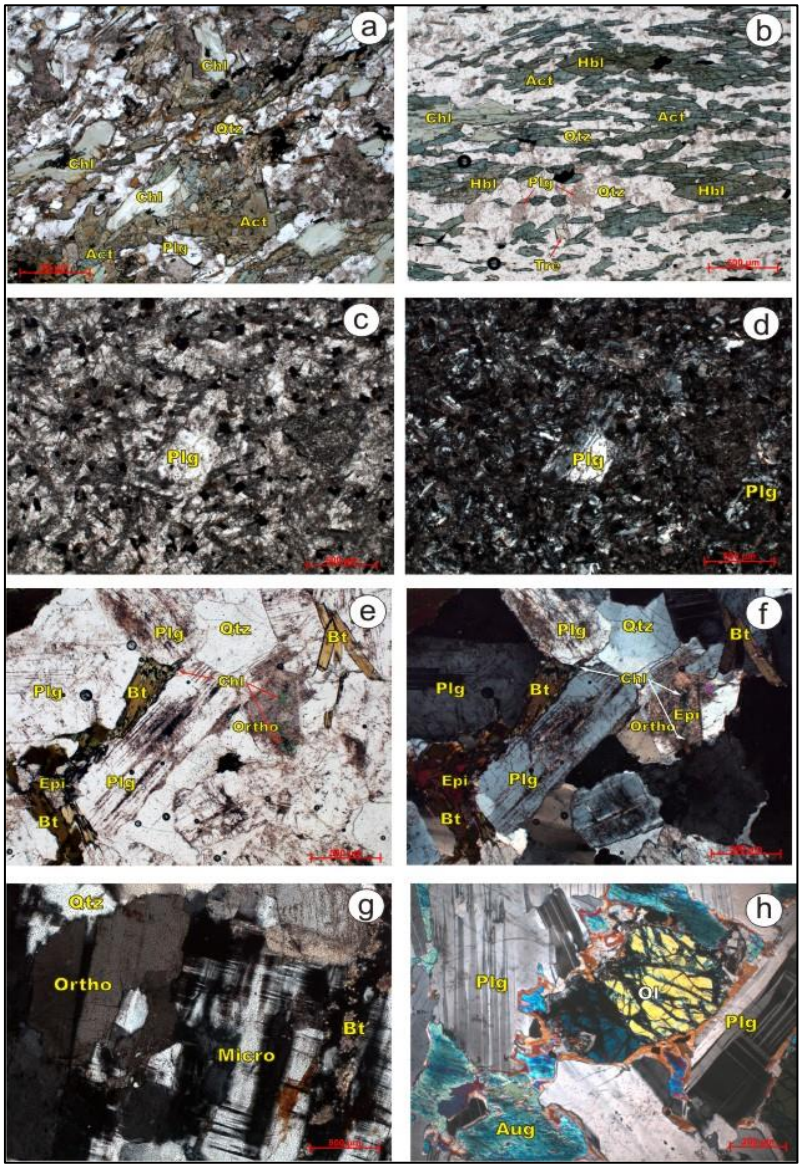

Figure 4

Thin-section photomicrographs of the lithologies of Mubarak area showing (a) foliated and heavily altered amphibolite (ppl), (b) foliation of Hbl schist (ppl), (c&d) plagioclase phenocryst embedded in the fine-grained groundmass of meta-andesite (ppl&xN), (e&f) partial alteration of primary minerals of granodiorite (ppl&xN), (g) cross-hatching and simple twinning of K-feldspars of younger granites (xN) and (h) younger gabbro (xN). Abbreviations, Qtz: quartz, Plg: plagioclase, Hbl: hornblende, Act: actinolite, Trem: tremolite, Bt: biotite, Chl: chlorite, Epi: epidote, Ortho: orthoclase, Micro: microcline, Aug: augite, Ol: olivine.

4.1.b. Hornblende-actinolite Schist

Hornblende-actinolite schist is strongly foliated rocks of greyish green color *(Figure 4b)*. It is composed of 50% of mafic minerals: hornblende and actinolite with minor tremolite, and 50% felsic minerals dominated by quartz with minor plagioclase. Chlorite and iron oxides represent subsequent mineral phases overgrown on amphiboles. The distinctive feature from amphibolite is the higher proportion of felsic minerals and the amphibole composition. Amphiboles occur as aggregates elongated in one direction. **Hornblende** occurs as relics of heavily fractured subhedral to anhedral prismatic crystals (400 μm-250 μm), where these fractures extend along its long axe and parallel to the foliation. **Actinolite** occurs as tabular subhedral crystals (600 μm × 75 μm). Minor tremolite occurs as subhedral short prismatic crystals. **Quartz** is frequent as anhedral subrounded crystals of serrated edges (30 μm-20 μm) filling the space between amphiboles. **Plagioclase** is rare and occurs as anhedral short prismatic crystals and are heavily sericitized. **Chlorite** is frequently present (700 μm × 275 μm) overgrown on amphiboles.

4.1.c. Metaandesite

This rock is hard, massive, fine-grained of a dark green color (*Figures 4c* and *d*). It is composed essentially of plagioclase, biotite, quartz, hornblende, and chlorite. Accessory minerals include iron oxides and epidote. Plagioclase phenocrysts are embedded in fine grained groundmass of plagioclase, biotite, chlorite, epidote, and iron oxides. **Plagioclase** phenocrysts (700 μm × 400 μm) occur as subhedral prismatic crystals of andesine composition (according to the Michel-Lévy diagram) that are partly fractured and altered to sericite.

4.2. Syn-to-late orogenic granodiorite

This rock is coarse-grained and grey in color, composed mainly of plagioclase, quartz, biotite, and K-feldspars (*Figures 4e* and *f*). Sericite, epidote, kaolinite, chlorite, and iron oxides represent the metamorphic phases. **Plagioclase** (up to 1450 μm × 450 μm in size) occurs as prismatic subhedral crystals of andesine composition. It shows faint lamellar zonation while alteration to sericite partly destroys its crystal lattice. **Quartz** (620 μm × 600 μm) occurs as strained anhedral crystals, exhibiting uneven, wavy and undulose extinctions. **Biotite** (250 μm × 50 μm) occurs as flaky and elongated crystals. It is commonly altered into chlorite and iron oxides, particularly on the peripheries and along its cleavage planes. **Kaolinite** is very common due to the heavy weathering indicating complete alteration of K-feldspars. **Chlorite** occurs as pale green, small flake-like crystals, or irregular patches.

4.3. Post-orogenic intrusives

4.3.a. Post-orogenic granite

This rock is coarse-grained and red in color *(Figure 4g)*. It is composed mainly of quartz, orthoclase, microcline, biotite, and minor plagioclase. Kaolinite, epidote,

sericite, and iron oxides represent the metamorphic phases. **Quartz** occurs as an essential mineral, generally anhedral, medium-grained crystals up to (300 μm × 200 μm) deformed into wavy extinction. **K-feldspars,** represented by orthoclase and microcline (1000 μm × 700 μm – 1400 μm × 1050 μm), exhibit simple twinning and cross hatching twinning and are slightly altered to dusty kaolinite. **Biotite** occurs as subhedral flakes associated with epidote and iron oxides. **Plagioclase** is rare and occurs as prismatic subhedral crystals that are mostly zoned and exhibit albite twin lamellae. Granophyric and perthitic textures are common due to intergrowth of quartz and K-feldspars and between albite and K-feldspars, respectively.

4.3.b. Post-orogenic gabbro

This rock is hard, massive, and very coarse-grained of dark green to greenish black in color *(Figure 4h)*. It is composed of plagioclase, augite, and olivine. Iron oxide, calcite and epidote are accessory minerals. **Plagioclase** (2260 μm × 890 μm) occurs as euhedral to subhedral lath-shaped crystals that are partly altered to fine sericite scales and shows strong lamellar twinning of labradorite composition. **Augite** (915 μm × 670 μm) in size exists as subhedral crystals that are occasionally replaced by secondary amphibole, iron oxides, and chlorite. Augite crystals enclose plagioclase laths, forming ophitic and sub-ophitic textures. **Olivine** is commonly found as rounded crystals (up to 1250 μm × 900 μm in size), with a distinctive mesh texture where serpentine is an alteration product. Iron oxides occur as anhedral crystals replacing augite or along its peripheries and cleavage planes.

5. CONCLUSIONS

Field observations of the Mubarak area reveal that the Pan African nappe assemblage and syn- to late-orogenic granodiorites are the dominant rock units. The rocks representing the Pan African assemblage in the area belong to the IAA, outcropping as nearly vertical, E-W striking sheets. Ophiolites of the ANS were not found here.

The IAA rocks encompass a range of medium-grade metamorphic rock units of amphibolite facies, indicated by the presence of amphiboles defining the foliation in amphibolites and schists. Amphiboles appear as relic minerals supplanted by low-grade minerals (e.g., chlorite and epidote), implying a retrograde phase. Additionally, the extensively fragmented hornblende and serrated quartz in the schist reflect the late stage of compression at a shallow crustal level as a result of the NW tectonic escape [21] related to the Pan-African Orogeny.

Granitoids are commonly found in the area, and they are aligned with the Mubarak belt from north and south. These granitoids are classified into two distinct phases: (1) syn- tolate- orogenic and (2) post-orogenic granitoids. Although granodiorite seems to be petrographically the plutonic equivalent of the IAA rocks, particularly the metaandesite, it belongs to the late orogenic group, emplaced after the NW shortening tectonic phase. This is clearly shown by the isotropic texture devoid of any elongation and foliation features. Additionally, the quartz grains reveal undulate extinction and interior fractures, indicating that they were subjected to brittle

deformation at a shallow crustal level. According to that, the IAA rocks were deformed ductilely at a deeper crustal level prior to the emplacement of granodiorite. Post-orogenic intrusive rocks do not bear the low-grade metamorphic assemblage of the previous groups. These granitoids show a higher grade of differentiation than the granodiorite, according to their mineral composition. The non-metamorphic gabbros of the area belong to the fresh post-orogenic gabbros of the Eastern Desert.

REFERENCES

[1] Stern, R. J. (1994). Arc assembly and continental collision in the neoproterozoic East African orogen: implications for the consolidation of Gondwanaland. *Annual Review of Earth and Planetary Sciences*, 22, pp. 319–351.

[2] Ries, A. C., Shackelton, R. M., Graham, R. H., Fitches, W. R. (1983). Pan-African structures, ophiolites and melange in the Eastern Desert of Egypt: a traverse at 26° N. *Journal of the Geological Society London*, 140, pp. 75–95.

[3] El-Gaby, S., List, F. K., Tehrani, R. (1988): Geology, evolution and metallogenesis of the pan-African Belt in Egypt. In: El-Gaby S., Greiling R. O. (eds.). *The pan-African belt of Northeast Africa and adjacent areas*. Vieweg & Sohn, Wiesbaden, pp. 17–68.

[4] Stern, R. J., Johanson, P. R., Kroner, A., Yibas, B. (2004). Neoproterozoic ophiolites of the Arabian-Nubian shield. In: Kusky, T. M. (ed.). *Precambrian Ophiolites and Related Rocks*. Elsevier, Amsterdam, pp. 95–128.

[5] Bennett, J. D., Mosley, P. N. (1987). Tiered tectonics and evolution, Eastern Desert and Sinai. In: Matheis, G., Schandelmeier, H. (eds.). *Current research in African Earth Sciences*. Balkema, Rotterdam, pp 79–82.

[6] Greiling, R. O., Abdeen, M. M., Dardir, A. A., El Akhal, H., El Ramly, M. F., Kamal El Din, G. M., Osman A. F., Rashwan, A. A., Rice, A. H., Sadek, M. F. (1994). A structural synthesis of the Proteorozoic Arabian-Nubian Shield in Egypt. *Geologische Rundschau*, 83, pp. 484–501.

[7] Gahlan, H. A. (2006). *Petrological characteristics of the mantle section in the Proterozoic ophiolites from the Pan-African Belt*. Ph.D. thesis, Kanazawa University, Kanazawa, Japan, p 227.

[8] El-Gaby, S., El Nady, O., Khudeir, A. (1984). Tectonic evolution of the basement complex in the central Eastern Desert of Egypt. *Geologische Rundschau*, 73, pp. 1019–1036.

[9] Mohamed, F. H., Hassanen, M. A. (1996). Geochemical evolution of arc-related mafic plutonism district, Eastern Desert of Egypt. *Journal of African Earth Science*, 22, pp. 269–283.

[10] Abu El-Ela, F. F. (1997). Geochemistry of an island-arc volcanic suit: Wadi Dabr intrusive complex, Eastern Desert, Egypt. *Journal of African Earth Science*, 24, pp. 473–496.

[11] Kharbish, S. (2010). Geochemistry and magmatic setting of Wadi El-Markh island-arc gabbro–diorite suite, central Eastern Desert, Egypt. *Chemie der Erde*, 70, pp. 257–266.

[12] El-Ramly, M. F., Akaad, M. K. (1960). The basement complex in the CED of Egypt between lat. 24°30′ and 25°40′. *Geological Survey Egypt*, 8, p. 33.

[13] El-Gaby, S. (1975). Petrochemistry and geochemistry of some granites from Egypt. *Neues Jahrbuch für Mineralogie Abhandlungen*, 124, pp. 147–189.

[14] Hussein, A. A., Aly, M. M., El Ramly, M. F. (1982). A proposed new classification of the granites of Egypt. *Journal of Volcanology and Geothermal Research*,14, pp. 187–198.

[15] Farahat, E. S., Abdel Ghani, M. S., Ahmed, A. F. (2004a). Mineral chemistry as a guide to magmatic evolution of I- and A-type granitoids, Eastern Desert, Egypt. *Proceedings of the 6th international conference on geochemistry*, Alexandria University, Egypt, pp. 1–23.

[16] Farahat, E. S., Mohamed, H. A., Ahmed, A. F., El Mahallawi, M. M. (2007). Origin of I- and A-type granitoids from the Eastern Desert of Egypt: implications for crustal growth in the northern Arabian-Nubian shield. *Journal of African Earth Science*, 49, pp. 43–58.

[17] Ali, K., Wilde, S., Stern, R. J., Moghazi, A., Mahbubul Ameen, S. (2013). Hf isotopic composition of single zircons from Neoproterozoic arc volcanics and post-collision granites, Eastern Desert of Egypt: implications for crustal growth and recycling in the Arabian-Nubian Shield. *Precambrian Research*, 239, pp. 42–55.

[18] Be'eri-Shlevin, Y., Katzir, Y., Whitehouse, M. (2009b). Post collisional tectono-magmatic evolution in the northern Arabian-Nubian Shield (ANS): time constraints from ion probe U-Pb dating of zircon. *Journal of the Geological Society London*, 166 (1), pp. 71–8.

[19] Be'eri-Shlevin, Y., Samuel, M. D., Azer, M. K., Rämö, O. T., Whitehouse, M. J., Moussa, H. E. (2011). The Ediacaran Ferani and Rutig volcano-sedimentary successions of the northernmost Arabian– Nubian Shield (ANS): new insights from zircon U-Pb geochronology, geochemistry, and O-Nd isotope ratios. *Precambrian Research*, 188, pp. 21–44.

[20] El-Gaby, S., El Aref, M., Khudeir, A., El Habbak, G. (1994). Geology and genesis of banded iron formation at Wadi Kareim, Eastern Desert, Egypt. *7th Ann. Meeting, Min Soc*, Egypt. Abstract.

[21] Fritz, H., Wallbrecher, E., Khudier, A. A., Abu El Ela, F., Dallmeyer, R. D. (1996). Formation of Neoproterozoic metamorphic core complexes during oblique convergence, Eastern Desert, Egypt. *Journal of African Earth Science*, 23, pp. 311–329.

[22] Loizenbauer, J., Wallbrecher, E., Fntz, H., Neumayr, P., Khudeir, A. A., Kloetzil, U. (2001). Structural geology, single zircon ages and fluid inclusion studies of the Meatiq metamorphic core complex. Implications for Neoproterozoic tectonics in the Eastern Desert of Egypt. *Precambrian Research*, 110, pp. 357–383.

[23] Bregar, M., Bauernhofer, A., Pelz, K., Kloetzli, U., Fritz, H., Neumayr, P. (2002). A late Neoproterozoic magmatic core complex in the Eastern Desert of Egypt; emplacement of granitoids in a wrench-tectonic setting. *Precambrian Research*, 118, pp. 59–82.

[24] Shalaby, A., Stüwe, K., Makroum, F., Fritz, H., Kebede, T., Klotzli, U. (2005). The Wadi Mubarak belt, Eastern Desert of Egypt: a neoproterozoic conjugate shear system in the Arabian-Nubian Shield. *Precambrian Research*, 136, pp. 27–50.

[25] Abd El-Wahed, M. A. (2014). Oppositely dipping thrusts and transpressional imbricate zone in the central Eastern Desert of Egypt. *Journal of African Earth Science*, 100, pp. 42–59.

[26] Akaad, M. K. (1996). Rock succession of the basement: an autobiography and assessment. *Proc. The Egyptian geological survey centennial conference*, paper no. 71, p. 87.

[27] Stern, R. J., Avigad, D., Miller, N. R., Beyth, M. (2006). Evidence for the Snowball Earth Hypothesis in the Arabian–Nubian Shield and the East African Orogen. *Journal of African Earth Science*, 44, pp. 1–20.

[28] Stern, R. J., Hedge, C. E. (1985). Geochronologic and isotopic constraints on late precambrian crustal evolution in the Eastern Desert of Egypt. *American Journal of Science*, 258, pp. 97–127.

Geosciences and Engineering, Vol. 9, No. 14 (2021), pp. 17–28.
https://doi.org/10.33030/geosciences.2021.14.017

STATE OF THE ART OF GEOTHERMAL ENERGY SYSTEM ENHANCEMENT: A LITERATURE REVIEW

FRANKLIN GÓMEZ* – ANIKÓ N. TÓTH

University of Miskolc, Faculty of Earth Science and Engineering
oljfrank@uni-miskolc.hu

Abstract: The application of hydraulic fracturing in geothermal reservoirs requires the consideration of aspects related to temperature, geology, and in-situ stresses. This research compares the application of hydraulic fracturing for geothermal purposes in Rotliegend sandstones of sedimentary origin in the North German Basin with that of a Granodiorite reservoir in the Pohang site in South Korea. Furthermore, some recommendations are proposed for the application of hydraulic fracturing in Ecuadorian plays for thegeneration of geothermal energy. The basement reservoirs have a hard structure and are prone to pre-existing natural fractures, especially in reservoirs for geothermal purposes, because they normally have active tectonism due to their location. In contrast, sedimentary reservoirs are not necessarily in areas with active tectonism and their more ductile structure does not make them prone to natural fractures, but their temperature gradient should be analyzed to verify their feasibility. The stress analysis, the coefficient of fracture conductivity (FCD), the Folds of Increase (FOI) and the temperature gradient are complementary factors for determining the economic viability of geothermal reservoirs. Consequently, the application of hydraulic fracturing in geothermal reservoirs requires the analysis of S_v (overburden) stress, S_{h1} (horizontal 1) stress, S_{h2} (horizontal 2) stress, temperature, FCD, and FOI. This is particularly true for the Chachimbiro Ecuadorian geothermal reservoir, where there is high temperature and active tectonism.

Keywords: *Coefficient of fracture, Conductivity FCD, Folds of Increase FOI, geothermal reservoir, Hydraulic Fracturing, overburden stress*

1. INTRODUCTION

This research compares the application of hydraulic fracturing for geothermal energy purposes in sedimentary-hosted geothermal reservoirs to that of a granodiorite reservoir. In particular, the comparison will focus on the hydraulic fracturing applied in Rotliegend sandstones in the North German Basin reservoirs and in a granodiorite reservoir in basement in the Pohang site in South Korea. In addition, some recommendations are made for the application of hydraulic fracturing for geothermal energy generation in Ecuadorian plays.

Hydraulic fracturing is the process of injecting fluid into a well to create tensile stresses in a formation, so that these stresses exceed the tensile strength of the rock and fracture it [1]. The main reason for creating these fractures is to create conductivity in the reservoir, for different purposes. One of these purposes is to produce

geothermal energy from the earth's crust, which is defined as extending from the surface to a depth of ten kilometers or more, with a volume of several hundred cubic kilometers. The heat stored in this zone can be used for the generation of energy, also known as geothermal energy [2, 3].

The process of designing a fracture requires analyzing the stresses and pressure of the reservoirs (upper and lower layers), measuring the temperature of the reservoir, determining fracture conductivity (FCD) and folds of increase (FOI), estimating the fracture geometry, and calculating Fluid Loss C, spurt loss, and fluid selection-apparent viscosity (cp) for fracturing. The process also requires calibrating the model (Stresses-DFIT and Fluid loss, and efficiency-minifrac), matching the pressure history, and carrying out an economic analysis [4, 5]. Each of these steps will be analyzed in order to determine the advantages and disadvantages of applied hydraulic fracturing in sedimentary and basement reservoirs for geothermal purposes.

2. METHODOLOGY

The methodology for comparing the basement and sedimentary reservoirs follows the process of *Figure 1*. The methodology is taken from Smith et al. [5], adapted to geothermal reservoirs. The main difference between conventional-oil and geothermal reservoirs is that the active tectonic areas where geothermal reservoirs – and even some sedimentary reservoirs – are normally located can be a source of geothermal energy. Also, the temperature of geothermal reservoirs is normally higher than that of petroleum reservoirs. In this context, the fracturing will be affected by stresses and temperature when it is applied in geothermal reservoirs.

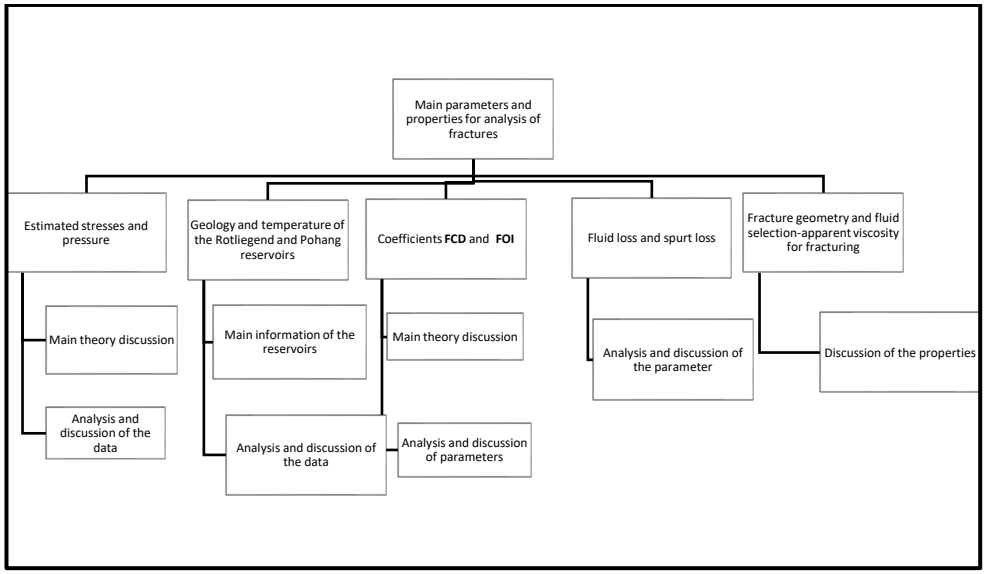

Figure 1. *Methodology flow chart for analysis of the fracturing applied to the geothermal reservoirs* [5]

2.1 Estimating Stresses and Pressures

The fractures propagate in a perpendicular direction to the minimum in situ stress; thus, the injection pressure must be greater than the minimum in situ stress. Hence, the stresses determine the orientation of the fractures. There are three main principle stresses: S_v (overburden), Sh_1 (maximum horizontal), and Sh_2 (minimum horizontal). The orientation of the fracture may be either horizontal or vertical in the majority of the cases. Moreover, Sh_2 is normally the minimum horizontal stress (the pressure where a fracture is mechanically closed) and thus the fractures in the majority of the cases are vertical. Sometimes it is possible to have inclined fractures in active tectonic areas [5, 6].

The vertical stress S_v (also called overburden stress) varies between 1 to 1.05 psi/ft, based on Smith et al. [5] and is the pressure generated for the layers over the reservoir. Then, if the reservoir is shallow the overburden is small. The horizontal stress is a reaction to the overburden stress and a reaction to geologic forces of the local structure. Consequently, if the rock is isotropic H = h1 = h2 then the horizontal stress is X * S_v. And X is defined for Poisson's ratio, lithology, pore pressure, porosity and cofining stress. However, it is important to note that because of the geological structure, the type of fault and the type of rock define the success or failure of fracturing. Of the three kind of faults, the most convenient for fracturing are the normal faults, because in this case the fractures will be vertical and there is less loss of natural fracture fluid [6]. With reverse faults, the horizontal stress is larger than vertical stress and thus the fractures are horizontal. In this case a lot of fluids can be lost. On the other hand, if there are strike-slip faults, one of the horizontal stresses is greater than the vertical stress, and the fractures should be vertical, following the fault orientation [6].

In the earth's crust, the situation of natural fractures is more complex because in the relevant geological age the directions of the main stress could change orientation according to tectonic plate movement. There are some cases, for instance, where a transpressional stress regime which began with reverse faults later changed to a strike-slip fault orientation. A specific explanation can be found in Zoback [6].

Analysis and Discussion

The estimation and analysis of the stresses and natural fracture direction are descrobed in *Table 1*.

The analysis of the stress regime is important because the natural fractures can define the conductivity of the fracture and of course the loss of fluid. In the case of the basement in the Pohang site in South Korea, there is a transpressional stress regime. That means that natural fractures in the reservoir start at the inclination of the fault slip for the compressional stresses, but then the natural faults change direction, becoming vertical in accordance with strike-slip faults. Thus, there is a disordered fracture system in the reservoir.

Table 1

Analysis and comparison of stress and pressures between Rotliegend sandstones in the North German Basin reservoirs and in a granodiorite reservoir in basement of the Pohang site in South Korea [7, 8, 9, 10, 11]

Reservoir		**magnitude of stress**	**stress regime**	**observations**
Basement in Pohang site in South of Korea [7, 8, 9]	S_v[MPa]	107	strike-slip/reverse (Transpressional)	Reverse natural fractures are expected to dip and strike normal to the direction of S_{h1} which is N100°E
	S_{h1}[MPa]	133-153		
	S_{h2}[MPa]	98-119		
Rotliegend sandstones in the North German Basin reservoirs [10, 11]	S_v[MPa]	100	Normal faulting/strike-slip	strike-slip natural fractures are expected to be vertical and strike 40.36° from the S_{h1}
	S_{h1}[MPa]	78–100		
	S_{h2}[MPa]	53		
	S_v[MPa]	100	Normal faulting/strike-slip	
	S_{h1}[MPa]	78–100		
	S_{h2}[MPa]	58.6		

If a well reaches the reservoir basement, the development of artificial fractures can produce a disordered flow of fluids, as depicted in *Figure 2*.

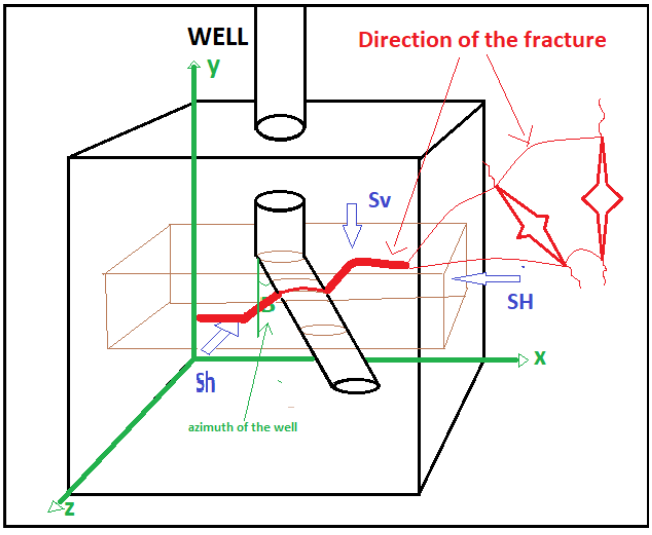

Figure 2

Change in the orientation of the fractures for transpressional regime [7]

Whereas the basement in Pohang site in South Korea has a transpressional regime with strike-slip/reverse regime, the Rotliegend sandstones in the North German Basin reservoirs have a Normal faulting/strike-slip. There, the natural fractures are expected to be vertical. However, like the sandstones it is not common to find natural fractures. Furthermore, if fractures are developed, these are vertical in the offset angle of the direction of the fault. In this case the angle is 40.36° from the direction of S_{h1}, the value calculated by Moeck and Schandelmeier [11] and Legarth, Huenges and Zimmermann [10].

2.2 Geology and Temperature of the Reservoirs

In addition to the stress analysis, the geology and the temperature also are important because they define the hardness and ductility of the reservoir. The main reservoir's characteristics are described here.

Sedimentary Geothermal Reservoir in Rotliegend: Temperature of at least 120 °C. Upper Rotliegend: reservoir compound of silt, sandstones and conglomerate. Lower Rotliegend: reservoir compound comprised of volcanic rocks (Mg-andesites, pyroclastites with interlayered sediments). In the middle, there is a layer of clay with low permeability with higher anisotropy. Permeability over 200 md, Pay zone: 4130–4190 m, 4078–4118 m. Clastic sediments without carbonate cements [10, 11].

Closure stress: lower interval 8.4 MPa of effective closure stress. Identified stress gradients are dpc/dz = 12.7 and 14.3 MPa/km respectively [11].

A granodiorite reservoir in basement in Pohang site in South Korea: The temperature here is at least 160 °C [8]. Granodiorite is an intrusive igneous rock with a phaneritic texture and crystals of medium size (2 mm–5 mm). It is normally made out of quartz, sodium plagioclase and amphibole. The basement rock in Pohang is covered by Cretaceous sedimentary rock (sandstones and mudstones) mixed with sequences of tuff andesite layers. Permeability 0.00018 D, 0.5% porosity [7, 9].

Analysis and Discussion

The temperature for the basement reservoir is higher than for the sedimentary reservoir. Normally, the temperature depends on the reservoir's location. Many geothermal reservoirs are close to places with volcanic activity, at hot spots, rifts, or the union of tectonic plates [12]. The deeper the reservoir, the higher the temperature, so the basement has higher temperatures than those of sedimentary reservoirs [12]. When applying hydraulic fracturing, it is important to have the right temperature when choosing the fluid, especially when using proppant. The proppant must be able to withstand high temperatures in the reservoir conditions, i.e., the proppant's properties should not change at high temperatures. The equipment used for hydraulic fracturing must also support higher temperatures (160 °C to +300 °C) than is common for equipment used in petroleum reservoirs [13].

2.3 Coefficient of Fracture conductivity (FCD) and Folds of increase (FOI)

The coefficient of fracture conductivity (FCD) is defined as the product of high fracture permeability and width in the reservoir over the reservoir permeability and penetration.

$$FCD = \frac{Kf*w}{K*Xf}, \tag{1}$$

where Kf is fracture permeability (a term used for permeability in mD); W is width in m; K is reservoir permeability in mD ; Xf is fracture half-length in m. The FCD indicates the transport capacity of the fluid fed into the fracture. According to Smith and Montgomery [5] the FCD value must be 2 or greater for higher permeabilities, and 10 for lower permeabilities.

The folds of increase (FOI) is the ratio between initial reservoir productivity and reservoir productivity after stimulation (evaluated with various proppants and frac lengths) [5].

$$FOI = \frac{IP_{BEFORE}}{IP_{AFTER}}, \tag{2}$$

where IP_{Before} is the index of productivity before the fracturing in BFPD/psia, and IP_{After} is the index of productivity after fracturing in BFPD/psia. The stimulation ratios or indices of productivity are individual values and have to be determined for each reservoir or fracture setting [10].

Stimulation ratios increase with increasing FCD, reaching a half-length dependent maximum. High values of FCD can be caused by low matrix permeabilities and increases in stimulation ratio can only be achieved by increasing fracture length. A good FOI with a bad FCD means that even with a bad fracture design, the results are good with an effective wellbore radius, which is the apparent wellbore radius:

$$r_{wa} = r_w * e^s, \tag{3}$$

where r_{wa} is effective wellbore radius in feet, r_w is wellbore radius in feet, and s is skin factor.

Analysis and Discussion

The values of FCD and FOI for the Rotliegend sedimentary reservoir and Pohang basement reservoir are given in *Tables 2–4*.

Table 2

Coefficient of fracture conductivity of Pohang reservoir

	Pohang	units	**source**
K_f (fracture permeability)	7599.38 to 50662.51	mD	[7]
K (matrix permeability)	1.82385E-6	mD	[7]
w (width)	0.00006–0.00012	m	[7]
x_f (half fracture length)	15	m	[9]
FCD	16666.67–222222.22		**calculated**

Table 3

Coefficient of fracture conductivity of Rotliegend reservoir

	Rotliegend	**units**	**source**
conductivity (K_f*w)	0.003 to 0.005	mD.m	[10]
k matrix permeability	1.99995E-5	mD	
X_f (half fracture length)	3236	m	
FCD	1.6–1.8 (4.41–7.35 designed)		**calculated**

Table 4

Folds of increase of Pohang and Rotliegend reservoirs

RESERVOIR	FOI	Source
Pohang	7.5	calculated with process of Smith and Montgomery [5]
Rotliegend	1.6–1.8	[10]

According to the theory, the FCD must be a value close to 2. The Pohang reservoir has extremely high FCD values *(Table 2)*, meaning that the reservoir has good conductivity, which might be a product of the natural fractures in the transpressional stress regime and that fracturing is unnecessary. For the case of the Rotliegend reservoir, the FCD was designed to get a value between 4 and 7, but the results give a value between 1.6 and 1.8 *(Table 3)*. This means that the fracture has an acceptable value for the petroleum industry, although it was designed for better results. For the purposes of petroleum engineering the fracture was successful, but for geothermal purposes it was not, as the flow rate was not high enough for optimum geothermal energy production.

The FOI for Pohang reservoir is high *(Table 4)*, and without any other parameter it means that the fracture was successful. However, combined with the results of the FCD, that no longer applies. Additionally, in the Rotliegend reservoir the FOI value means that the conductivity of the reservoir improves, but production results would not necessary be economically profitable *(Table 4)*.

2.4 Fluid Loss and Spurt Loss

Fluid loss is calculated by two parameters, the C fluid loss coefficient and the V spurt. The C fluid loss coefficient is a function of formation permeability, reservoir pressure, reservoir temperature, formation fluid properties, fracturing fluid viscosity, and the wall building characteristics of the fracturing fluid. Typical values of C are from 0.0005 to 0.01 ft/min$^{1/2}$. The fluid loss coefficient is affected by the permeability of the formation. If the formation permeability is bigger there will be more loss of fluids, because a filter cake will not form. The fluid loss coefficient is formed by three more coefficients Cv also known as CI, CII and Cw: Cv is the filtrate viscosity

effect, CII the reservoir fluid compressibility effect and Cw the wall building effect coefficient, which is related to the V spurt. Specific explanations can be found in Smith and Montgomery [5].

Analysis and Discussion:

There is no practical way to calculate the C fluid loss coefficient for the Rotliegend sedimentary and the Pohang basement reservoirs. However, the low permeability improves the possibility of a filter cake forming in the fracture, so in this case that parameter is better for basement reservoirs. For the other side, the kind of fluid used is important because it directly affects the calculus of Cv and CII partial coefficients of the fluid loss coefficient. The Cw is calculated only if there is no filter cake [5]. The fluid loss coefficient is normally calculated for petroleum reservoirs but it could be important for the design of fractures in geothermal reservoirs. Besides, the Cv will be affected by relative permeability of the kind of fluid used (for geothermal, usually water) and by the temperature of the reservoirs, especially as geothermal reservoirs require higher temperatures.

The spurt loss is big when there is no wall cake . The geothermal reservoirs in this case have small permeabilities, so filter cake is formed. The Cw wall building coefficient typically is 0 for permeabilities between 0.1–0.5 mD [5].

2.5 Fracture Geometry and Fluid selection-apparent viscosity for fracturing

When selecting the fluid, the viscosity is extremely important, not only for volume considerations but also for the geometry of the fracture. Furthermore, a bad viscosity design can cause the fracture fluid to extend fractures too far, mis-apply the proppant, increase costs, and raise reservoir pressures too high.

The geometry of a fracture relates the permeability with the length and width of a fracture. The petroleum industry uses the FCD coefficient of fracture conductivity for economically profitable designs of fractures. *Table 5* shows the ranges of permeability, length of fractures and width for petroleum designs of fractures.

Table 5

Range of X_f with K and FCD, designed for a petroleum well's fracture geometry [5]

K reservoir permeability[mD]	**Xf Desirable[m]**	**FCD**	**K_fW [m^2-m]**
0.0001	1,066.8	250	2.63E-14
0.0005	1,005.84	125	6.20E-14
0.001	853.44	50	4.21E-14
0.005	609.6	25	7.52E-14
0.01	548.64	10	5.41E-14
0.1	274.32	5	1.35E-13
0.5	213.36	2	2.11E-13

K reservoir permeability[mD]	Xf Desirable[m]	FCD	K_fW [m^2-m]
1	121.92	2	2.41E-13
5	91.44	2	9.02E-13
10	57.912	2	1.14E-12
20	45.72	2	1.80E-12
50	30.48	2	3.01E-12
100	15.24	2	3.01E-12

Analysis and discussion:

According to the dominant theory of the petroleum industry, the Pohang and Rotliegend reservoirs need fractures with lengths over 55 m. That is important because the permeability is related to the quantity of fluid that can be given for the reservoir and the capacity of transport of the fracture. In the case of the Pohang reservoir, notably, there is no analysis of FCD or dimensions of fracture design. In contrast, in the Rotliegend reservoir there is an analysis of geometry, but the simulation of the fracture is too conservative. *Table 6* shows the geometry of the fractures: in the design of Rotliegend reservoir the fracture length considered was 32 m, while in the Pohang reservoir X_f was 15 m. Consequently, the geometry of the fracture is important but it is not the only important parameter for geothermal reservoirs. In other words, the geometry has to be analyzed with the geothermal gradient because it provides a limit to the rate of fluid it is necessary to produce and bears on the profitability of the geothermal reservoir. For profitability, the geothermal theory should have a minimum geothermal gradient of 30 °C/km, assuming a 4 km reservoir with the rate of fluid production of 20 kg/s [10]. However, the design will be more successful if it resembles that of the reservoir geometry design indicated in *Table 5*.

Table 6

Main data of the geometry of the fracturing applied in the reservoirs

Pohang Reservoir			Rotliegend Reservoir		
W (width)	0.00006–0.00012	m	W (width)	0.0016	m
H (height)	30–150	m	H (height)	72	m
Xf (length of fracture)	15–75	m	Xf (length of fracture)	32–36	m

2.6 Recommendations for application to Ecuadorian reservoirs

Ecuador is a small country located in the west of South America. Of Ecuador's 11 prospective geothermal-energy sites, six are especially important: the Galápagos Rift, Galápagos Hot Spot, Northern Andes, Southern Andes, Coastal Fore-arc basin, and Oriente Foreland basin. This paper will analyze the geothermal resource located

in the northern half of the Andes Cordillera, considered Ecuador's best prospect [7]. The geothermal resource is located in extensive active quaternary volcanism. Within this area there are four high temperature plays, namely Chachimbiro, Chacana-Jamanco, Chacana-Cachiyacu and Tufiño-Chiles (there is another low temperature prospect in Chalpatán). A 1978 m well was drilled in Chachimbiro (PEC 1), which revealed basaltic andesite and andesite pyroclastic rock and a bottom temperature of 235 °C.

There are four main recommendations if hydraulic fracturing were to be applied in this play. (1) The fluid and equipment used for fracturing must be resistant to high temperatures. Packers, tools, and fluid – and especially the proppant used – must be able to withstand high temperatures (over 300 °C). (2) The play is located in a zone of active volcanism and the rock is not very malleable, so it is possible to find a lot of natural fractures. It is important to study the geomechanical (rock mechanical) properties for active tectonism, so as to avoid extremely disorganized fractures and find the best location for the wells. (3) The calculation of FCD, FOI and Geothermal Gradient is important in order to get productive fractures. (4) Finally, given the well's depth, it is possible that excessive fluid loss could occur through horizontal fractures in the reservoir. For that reason, the choice of well location must take into account the reservoir's horizontal stress directions.

3. CONCLUSIONS

The basement in the Pohang site in South Korea had a change of stress regime that caused hydro-shearing during the moment of applied hydraulic fracturing: subsequently, there were earthquakes and the project was put on hold. That example shows the importance of analyzing the stress regimes and their change over time when evaluating geothermal resources. The coefficient of fracture conductivity (FCD) and folds of increase (FOI) in the Pohang site revealed an extremely large fracture that could cause problems with earthquakes. It is also fundamentally important to analyze the temperature gradient in geothermal reservoirs, since the FCD, FOI and temperature gradient are complementary features. In the Rotliegend sedimentary reservoir a complete analysis was done, including calculations of the FCD, FOI and geothermal gradient, but in that case the simulation was too conservative. The sedimentary reservoir needed bigger fractures to get the optimum volume. Therefore, if the analysis joins the characteristics of a sedimentary reservoir with the necessity of bigger fluid rates, the simulation should be less conservative . However, the FCD values recommended – between 2 and 10 – must be verified in different kinds of geothermal reservoirs because these values are intended for conventional petroleum reservoirs.

The analysis of FCD and FOI in the Ecuadorian geothermal reservoirs is extremely important because the active tectonism in the place may have created different natural fractures in several directions. Consequently, it is recommended that calculations of the main stresses be updated before applying hydraulic fracturing. The high temperature of Ecuadorian geothermal plays will require high-specification hydraulic fracturing equipment.

ACKNOWLEDGMENTS

Franklin Gómez would like to recognize and express his sincerest gratitude to the **Politécnica Nacional University of Ecuador** for their sponsorship and assistance as he begins his doctoral studies at the University of Miskolc.

REFERENCES

[1] Schechter, R. (1992). *Oil Well Stimulation.* Englewood Cliff, N.J.: Prentice Hall.

[2] Augustin, M. A. (2015). *A Method of Fundamental Solutions in Poroelasticity to Model the Stress Field in Geothermal Reservoirs*. Technische Universität Kaiserslautern Birkhäuser.

[3] Watson, A. (2016). *Geothermal Engineering*. New York, Springer-Verlag.

[4] Rafiee, M., Soliman, M. Y., Pirayesh, E., Emami Meybodi, H. (2012). Geomechanical considerations in hydraulic fracturing designs. *Proceedings, SPE Canadian Unconventional Resources Conference*, October 30–November 1, 2012 Calgary, Alberta, Canada , Society of Petroleum Engineers, pp. 648–660. Paper Number: SPE-162637-MS.

[5] Smith, M., Montgomery, C. (2015). *Hydraulic Fracturing*. Boca Raton, London, New York, CRC Press.

[6] Zoback, M. D. (2009). *Reservoir Geomechanics*. New York, Cambridge University Press.

[7] Farkas, M. et al. (2021). Hydromechanical analysis of the second hydraulic stimulation in well PX-1 at the Pohang fractured geothermal reservoir, South Korea. *Journal of Geothermics*, 89, pp. 1–13.

[8] Hofmann, H. et al. (2019). First field application of cyclic soft stimulation at the Pohang Enhanced Geothermal System site in Korea. *Geophysical Journal International*, 217 (2), pp. 926–949.

[9] Sehyeok, P. et al. (2020). Observations and analyses of the first two hydraulic stimulations in the Pohang geothermal development site, South Korea. *Journal of Geothermics*, 88, pp. 1–19.

[10] Legarth, B. et al. (2005). Hydraulic fracturing in a sedimentary geothermal reservoir: Results and implications. *International Journal of Rock Mechanics and Mining Sciences*, 42, pp. 1028–1041.

[11] Moeck, I. et al. (2009). The stress regime in a Rotliegend reservoir of the Northeast German Basin. *International Journal of Earth Sciences*, 98 (7), pp.1643–1654.

[12] Beate, B, Urquizo, M., Lloret, A., (2015). Geothermal Country Update of Ecuador: 2010-2015. *Proceedings, World Geothermal Congress*, 19–25 April, Melbourne, Australia.

[13] Finger, J., Blankenship, D. (2010). *Handbook of Best Practices for Geothermal Drilling*. Sandia Corporation.

Geosciences and Engineering, Vol. 9, No. 14 (2021), pp. 29–42.
https://doi.org/10.33030/geosciences.2021.14.029

DETERMINING THE OPTIMUM CONCENTRATION OF PUMPKIN SEED SHELLS AS FILTRATION CONTROL ADDITIVE TO WATER-BASED MUD SYSTEM

HANI AL KHALAF * – NAGHAM AL HAJ MOHAMMED – GABRIELLA KOVÁCSNÉ FEDERER

Department of Petroleum Engineering
Faculty of Earth Sciences and Engineering, University of Miskolc
**hanipetro1988gmail.com*

Abstract: Filtrate loss within formations is one of the biggest problems during drilling operations. Therefore, many commercial chemical additives have been used to reduce fluid loss, such as carboxymethylcellulose (CMC) and polyanionic cellulose (PAC), which are expensive and are not environment-friendly substances. This study evaluates the usage of pumpkin seed shells (PSS), which is agricultural waste and at the same time an environment-friendly material, as an additive to the drilling fluid to reduce fluid loss. Six drilling fluid samples were formulated, adding PSS of 250 μm in size at different concentrations (1 wt%, 2 wt%, 3 wt%, 4 wt%, and 5 wt%). The effect of adding PSS on rheological properties and density was recorded and analyzed. Filtration was also studied by using an API LT LP press. The results of the study indicated that the addition of PSS to the drilling fluid has a clear effect on reducing fluid loss. The optimum concentration of PSS was 5 wt%.

Keywords: *Water-based mud, Drilling fluid, Lost circulation material, environmentally friendly additives, Filtrate loss*

1. INTRODUCTION

Oil is one of the most important economic resources for most countries in the world. Therefore, wells are frequently drilled to explore for new reservoirs of oil. Drilling operations are extremely complex and expensive operations. The drilling fluid used in drilling operations carries out many functions, which include the removal of cuttings from the well bottom to the surface, cooling and lubrication of the drilling bit, and stabilizing the wellbore by means of hydrostatic pressure exerted by the fluid column [1–3]. Drilling fluid is composed of liquid and solid phases, and certain additives are added to achieve the desirable properties. The additives affect important properties such as rheology, fluid loss, cake thickness, and density. The type and concentration of additives used in the drilling fluid are chosen on the basis of the properties that need to be modified. Depending on the type and concentration of the additives, some of the additives may increase the viscosity when added to the drilling fluid, while others might reduce the viscosity [4]. Hence, the success of drilling process relies on the selection of suitable material used in the drilling fluid with respect

to the prevailing conditions. During drilling it is certain that problems like pipe sticking, lost circulation, borehole stability, mud contamination, formation damage and hole cleaning will take place due to different geological conditions. Therefore, it is important to understand and anticipate the drilling problems, find the cause and plan the solution to reduce the cost of drilling and reach the target zone safely and successfully [5, 6]. Fluid loss is one of the most common problems that increases the cost and the total drilling time. Significant fluid loss into the formation can result in irreversible changes in the properties of the drilling fluid such as density, viscosity, and borehole instability [5, 7].

Fluid loss occurs as a result of the pressure difference between the drilling fluid column and the formations, which leads to the penetration of the liquid phase of the drilling fluid into the formations and the solid phase making a mud cake on the walls of the wellbore [8]. Thus, the properties of the drilling fluid must be modified to reduce the amount of fluid loss as well as to reduce the thickness of the mud cake forming on the wellbore [9].

Water-based drilling fluids are the most common type of drilling fluid used in well drilling due to their relatively low cost and environment friendly nature. Many materials have been used to control fluid loss and the rheological properties of drilling fluid, such as carboxymethylcellulose (CMC), starch, and xanthan gum (XC) [10–13]. These chemical materials are costly, harmful to the environment, and disintegrate at the high temperatures present in the well. Some of the additives are highly toxic and can harm health when used improperly during drilling operations. For these reasons, new additives are being tested which would be safe and comparatively affordable.

Researchers are focusing on finding low-cost, environment-friendly materials that reduce fluid loss and enhance the rheological properties of the drilling fluid. In the past various types of environment-friendly waste have been tested to reduce fluid loss, such as corn cobs, walnut shells, banana peels, rice husks, sawdust, and potato husks [17–21]. Pumpkin seed shells are an environmentally friendly waste material, and to date, no previous studies have been made on the evaluation of pumpkin seed shells as an additive in drilling fluid.

This study presents experimental work on pumpkin seed shells (PSS) as an additive to water-based bentonite drilling fluid and a measurement of its impact on many properties of drilling fluid, including rheology, density, fluid loss, and cake thickness.

2. EXPERIMENTAL PROCEDURE

All experimental measurements were done based on API-RP-13B-1 standards. The workflow of the experimental process is shown in *Figure 1*. The measurements included the rheological properties (plastic viscosity, apparent viscosity, production point, gel strength for 10 seconds, 1 minute, and 10 minutes), filtration properties (fluid loss for 30 minutes, cake thickening), and the density. The density was recorded with different concentrations of pumpkin seed shell powder added to a water-based drilling fluid.

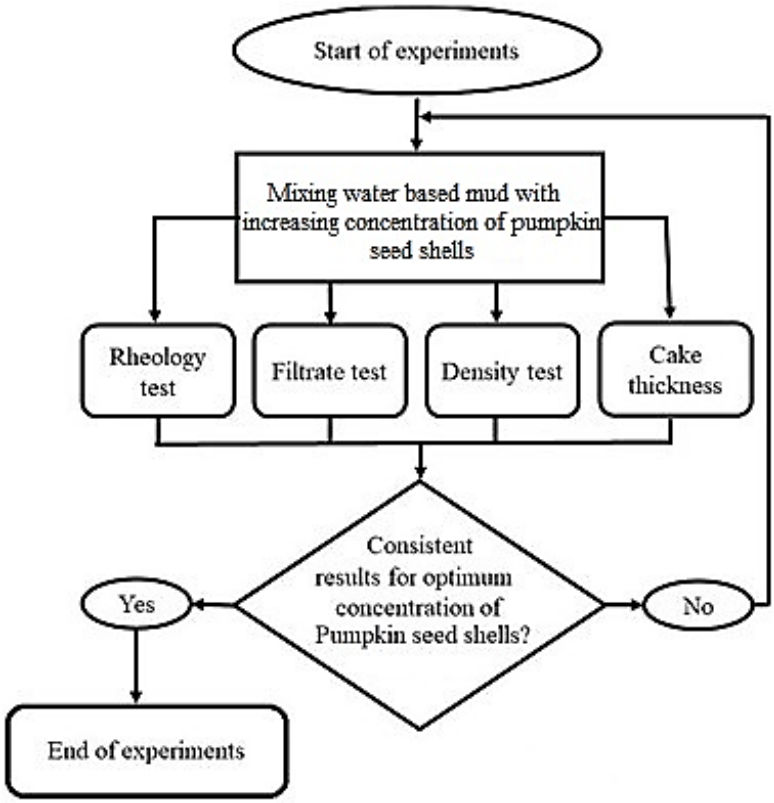

Figure 1. *Workflow of the experimental process*

2.1. Materials

In this article, the pumpkin seed shells (PSS) were the main materials used as an additive to water-based drilling fluid. After drying these peels for a week under the sun shines and then placing them in the oven at a 60 ºC temperature were grinded by an electric food grinder *Figure 2*. Then sieve them by mesh to the size less than 250 µm.

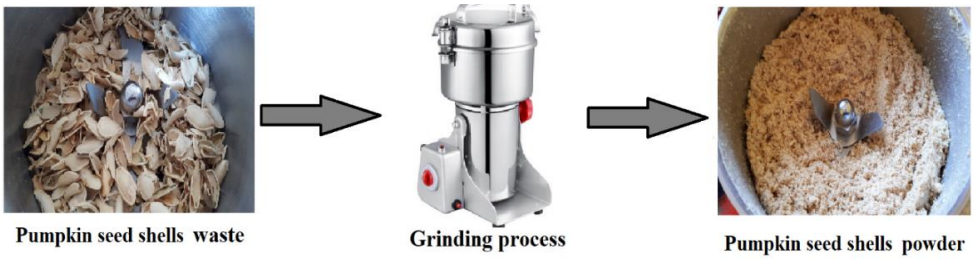

Figure 2. *Preparing pumpkin seed shell powder*

2.2. Preparation of the drilling fluid samples

Water-based drilling fluid was prepared with pumpkin seed shells as an additive in different concentrations by the weight of mud sample (1 wt%, 2 wt%, 3 wt%, 4 wt%, and 5 wt%). A single system of water-based drilling fluid consisting of water (base fluid) and bentonite (viscosifier agent) was used keeping in mind that this is strictly an index test for determining the effects of PSS in a base bentonite suspension. *Table 1* shows the formulation of the samples used in this study. Preparation was done by pouring 350 ml of water into a Hamilton Beach mixer, then adding 22.5 grams of bentonite and mixing for 20 minutes until the mixture was completely homogeneous. The drilling fluid was left to age for 24 hours to ensure the bentonite was hydrated in the water. Tests were conducted on six samples using different concentrations of PSS to determine their effect on the different properties of the drilling fluid and to determine the optimum concentration of the pumpkin seed shells.

Table 1

Mud formulation of water-based mud

Sample	**1**	**2**	**3**	**4**	**5**	**6**
Tap water (ml)	350	350	350	350	350	350
Bentonite (gr)	22.5	22.5	22.5	22.5	22.5	22.5
PSS (%wt)	–	1	2	3	4	5

2.3. Rheological testing

Figure 3 shows a multi-speed Fann 35 viscometer which was used to perform rheological tests that included measuring plastic viscosity (PV), apparent viscosity (AV), yield point (YP) and gel strength at 10 seconds, 1 minute and 10 minutes respectively. The device cup was filled with a designed volume of drilling fluid and then installed on the device after making sure that the clean and dry rotor was installed in the correct place. The viscometer was operated, and the readings were recorded at six different rotational speeds (600, 300, 200, 100, 6, and 3) [rpm], and this reading is it is the angular position of the torsion spring, and its unit is the degree of angular rotation. The plastic viscosity (PV) was calculated from the difference between reading at 600 [rpm] and reading at 300 [rpm] measured in [cp] unit. The apparent viscosity (AV) calculated by dividing the reading at 600 [rpm] by the number 2 measured in [cp] unit. As for the calculation of the yield point, it is the difference between the reading at 300 [rpm] and the plastic viscosity measured in [lb/100ft^2] unit. To measure the gel strength, the viscometer was turned on at 600 [rpm] for 10 seconds, then the viscometer was turned off for ten seconds. After that, the viscometer was restarted at 3 [rpm] and the maximum value that the viscometer index reached was recorded. This value indicates the gel strength, measured in [ml]. The process was repeated when the viscometer was stopped for 1 minute and for 10 minutes, each measured in [lb/100ft^2] unit.

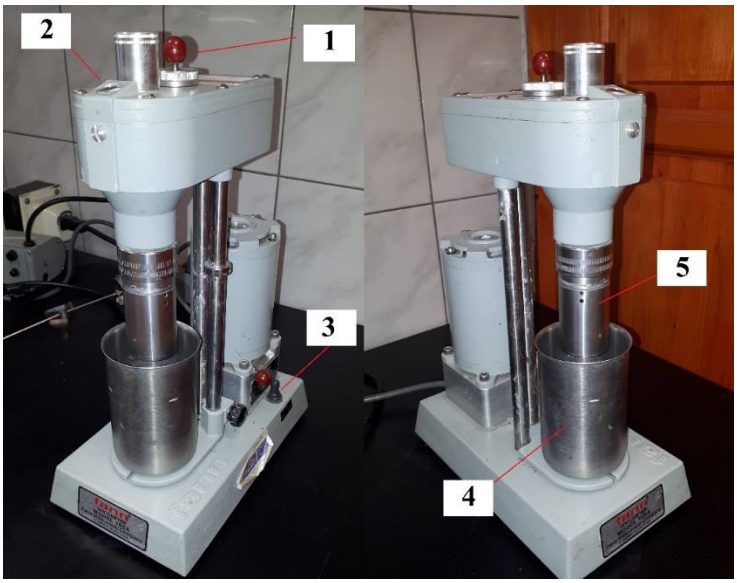

Figure 3. *Fann 35 Viscometer, Parts: 1. Gear shift knob, 2. Dial, 3. Motor speed switch, Sample cup, 5. Rotor*

2.4. Density testing

The density of the drilling fluid is measured using a mud balance *(Figure 4)*. The cup was filled with the drilling fluid to be measured, and a cup cover was placed which passes the drilling fluid from a hole in the middle of the cup cover to expel the excess amount of drilling fluid out of the cup. Once a balance was achieved between the cup of the device and the moving weight on the arm of the device, the density value was recorded from the ruler of the arm in ppg.

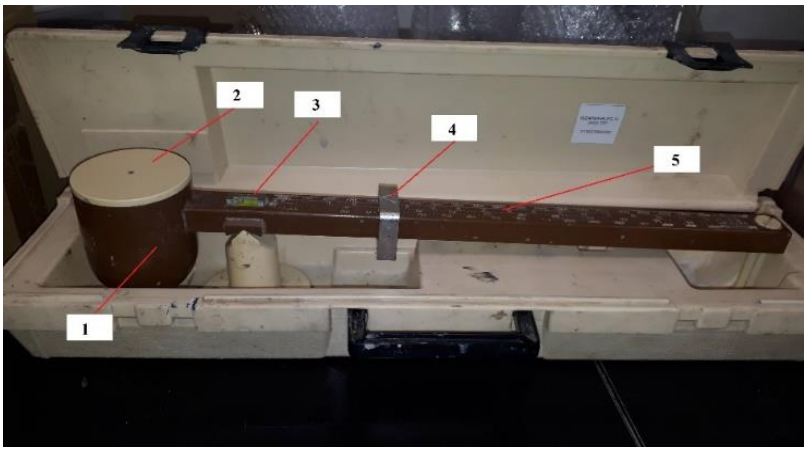

Figure 4. *Mud balance, Parts: 1. Cup, 2.cup cover, 3. bubble levelling, 4. moving weight, 5. Device arm*

2.5. Filtration properties measurement

API LT-LP press device was used to measure filtration properties *(Figure 5)*. The stainless-steel cell was filled with a sample of drilling fluid and the cover was tightly closed after making sure that the seal ring and filter paper are installed correctly. A pressure of 100 [psi] was applied on the cell and the filtrate was collected by a graduated cylinder placed below the cell and the amount of the filtrate was recorded at different times (1, 3, 5, 7.5, 10, 15, 20, 25, and 30 min) in ml. After that, the pressure was released, the cell was opened, the filter paper was taken out, and the thickness of the mud cake was measured on filter paper in three different areas, then the average value of the thickness was calculated in mm.

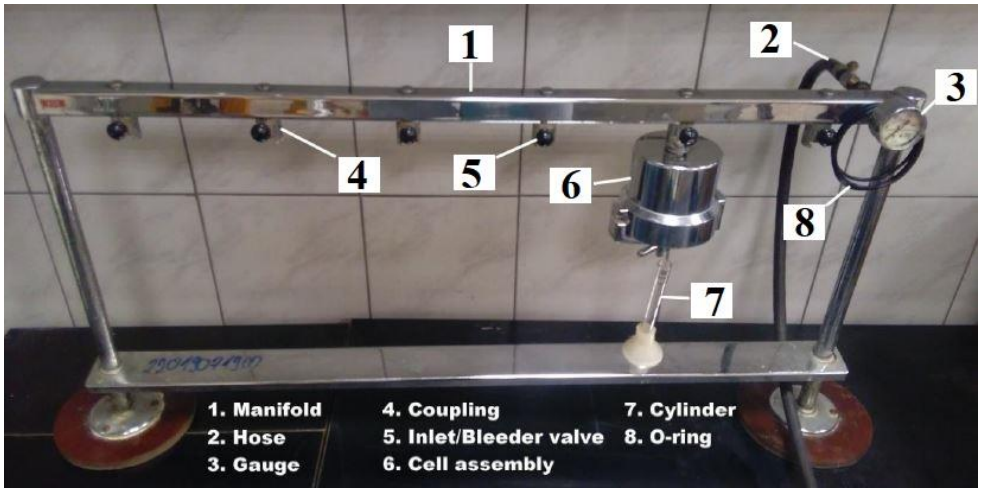

Figure 5
Multiple-unit filter press

3. RESULTS AND DISCUSSION

3.1. The effects of different concentrations of PSS on the rheology

To analyze the rheological properties of the drilling fluid, the samples were prepared by adding PSS. The concentrations which were used here are 1 wt%, 2 wt%, 3 wt%, 4 wt%, and 5 wt%. *Figure 6* represents the shear stress with shear rate. From *Figure 6* it is clear to say that the rheological model which best describes flow characteristics of tested muds is Bingham plastic fluids. An increase in PSS concentration led to increasing shear stress required to circulate the drilling fluid in the annulus. From analysing the results of the rheological test, it was found that increasing the concentration of PSS in the drilling fluid greatly improved the viscosity. *Figure 7* represents the plastic viscosity (PV) of drilling fluid with varying concentrations of PSS. It can be noticed that plastic viscosity increases with the concentration of PSS in the drilling fluid system until 4 wt% then decreases at 5 wt%, which means that using small

proportions of PSS can improve the viscosity significantly, thus increasing the effectiveness of cleaning the well and suspend cuttings and weighting additives. In case if the viscosity is undesirably high viscosity thinners can be added to the mud to compensate. *Figure 8* shows that the apparent viscosity increases with increased concentration of PSS in the drilling fluid system. The same is true for the yield point: its value increases with the increase in the concentration of PSS, as shown in *Figure 9*. The gel strength also shows a gradual increase with the increase in the concentration of PSS as shown in *Figure 10*. This increases the ability of the drilling fluid to suspend the cutting when the circulation is stopped.

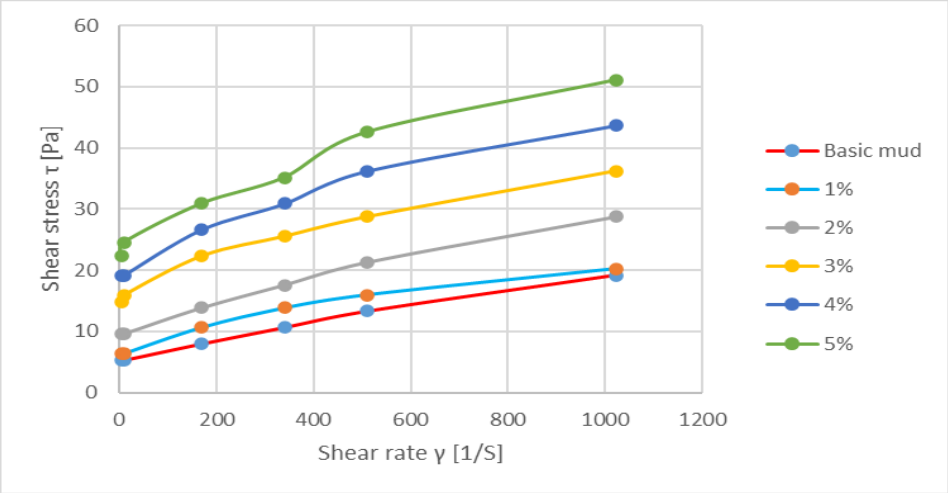

Figure 6. *Shear stress via. shear rate*

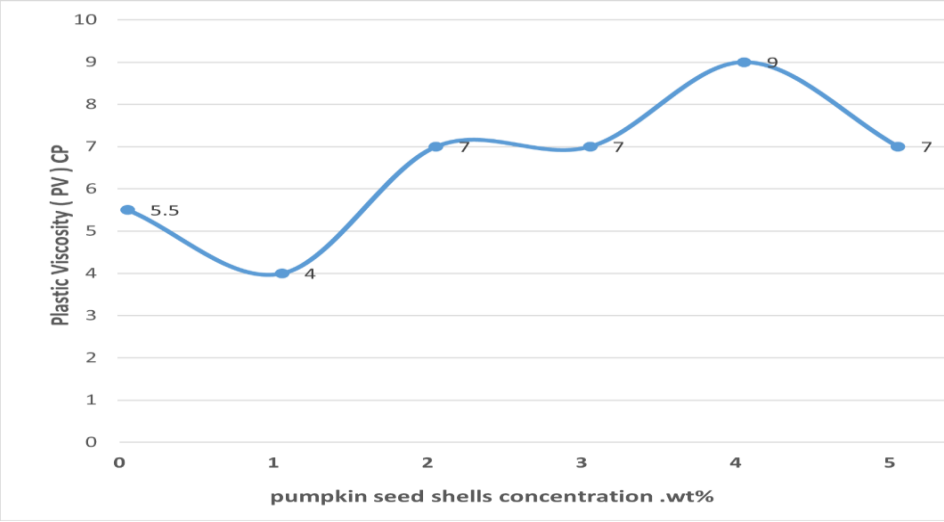

Figure 7. *Influence of PSS additive on plastic viscosity*

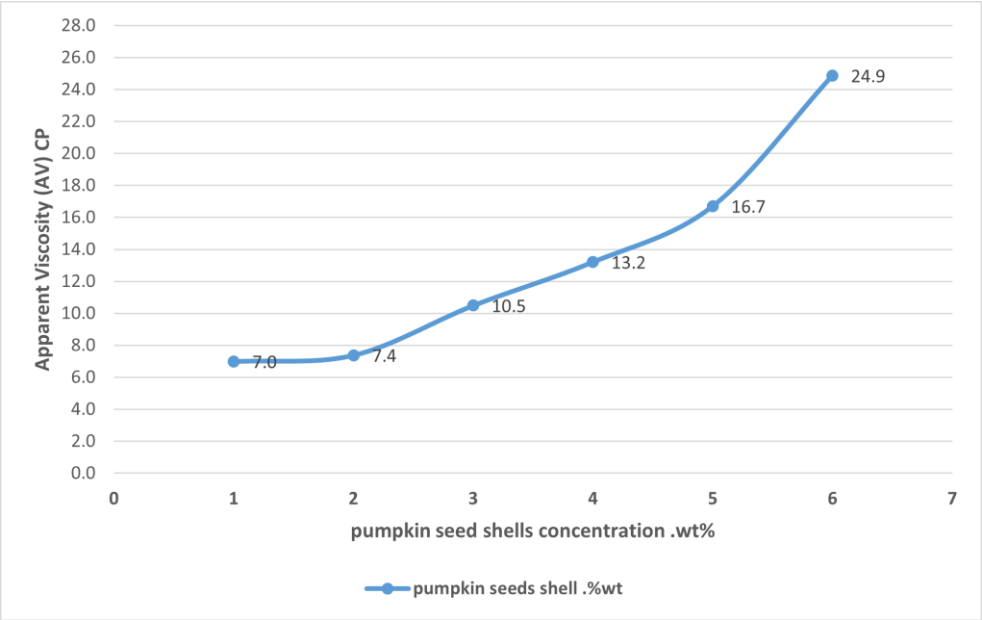

Figure 8. *Influence of PSS additive on apparent viscosity*

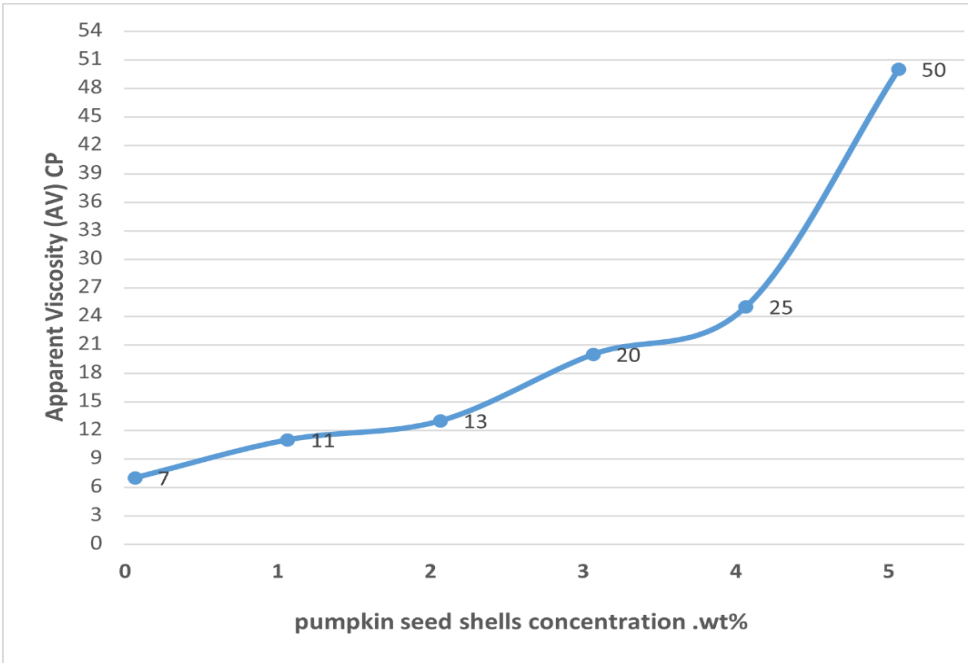

Figure 9. *Influence of PSS additive on yield point*

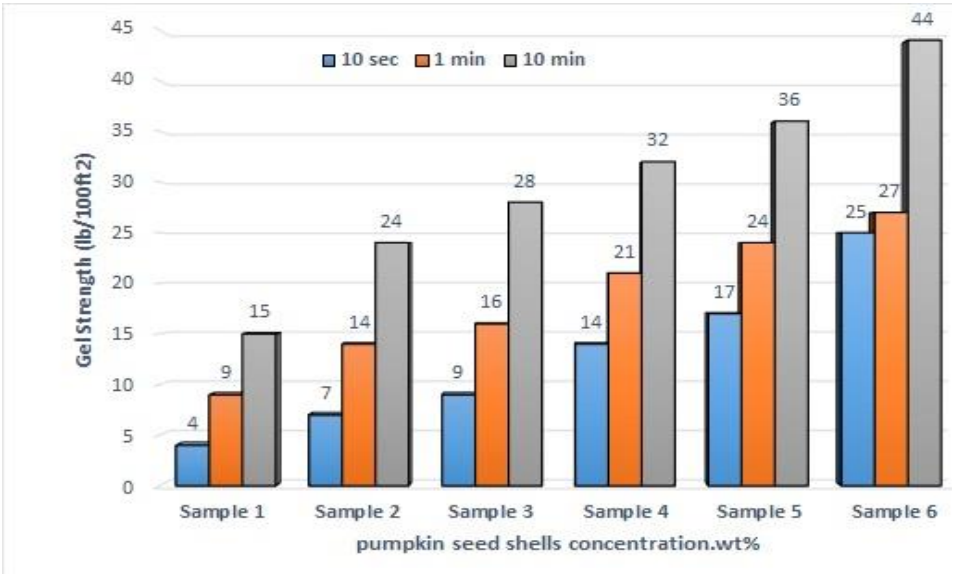

Figure 10. *Influence of PSS additive on gel strength*

3.2. The effects of different concentrations of PSS on the density

From *Figure 11*, it can be seen that there is no noticeable change in the density value after adding the PSS to the drilling fluid at different concentrations, which means that using the PSS as lost circulation material is a good option without exposing the well to the risk of breaking the formations by the extra weight of the drilling fluid.

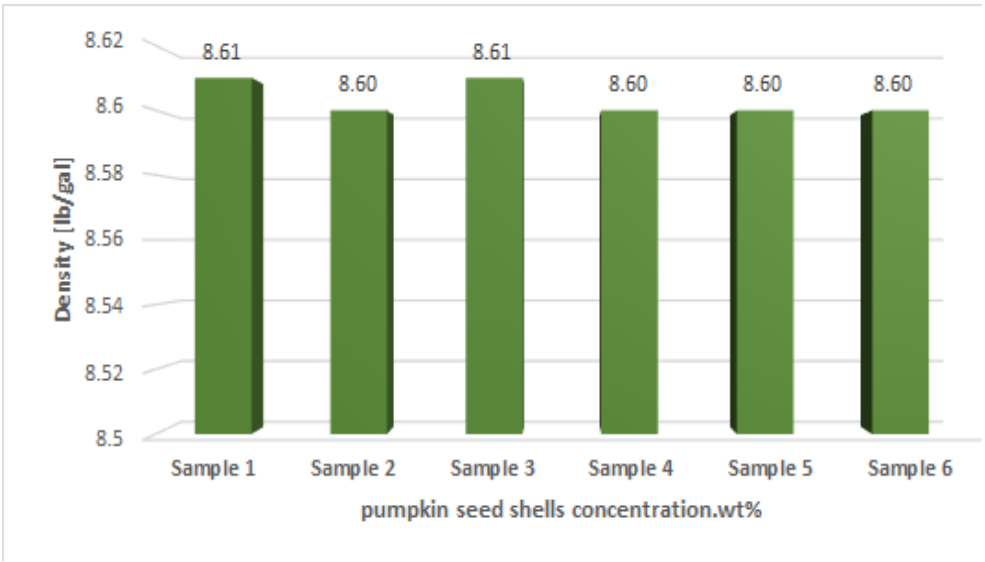

Figure 11. *Influence of PSS additive on density*

3.3. The effects of different concentrations of PSS on the filtration

Figure 11 presents the result of the filtration experiment using the API LT-LP press. The fluid loss test on all six samples was performed at room temperature. From the *Figure 12*, the effect of pumpkin seed shells on fluid loss property when added in different concentrations can be seen. As the concentration of the (PSS) increases, fluid loss continues to decrease. The volume of fluid loss with no added PSS (Sample 1-base mud) was 23.1 ml. From sample 2 it is shown that with the addition of 1 wt% of PSS the fluid loss was reduced to 19.6 ml. The lowest value of the fluid loss was for Sample 6, where the fluid loss decreased to 18.1 ml, which means that it decreased about ~22% from the original fluid loss value. Consequently, the addition of PSS reduces the contamination of the formations with the drilling fluid due to the low permeability of the mud cake, thus preserving the productivity of the production zones.

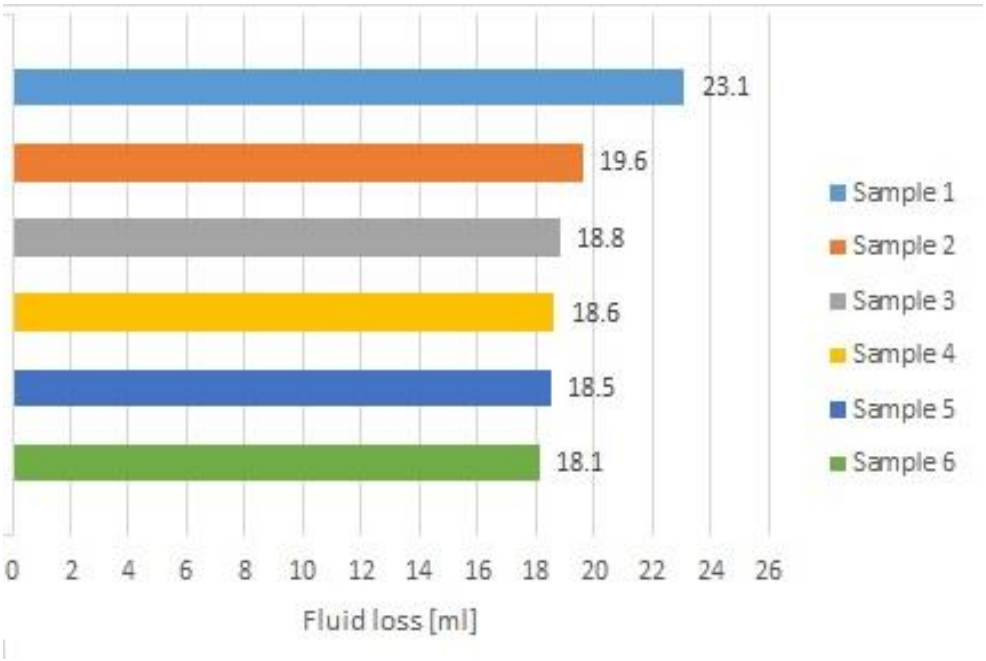

Figure 12
Effect of PSS additives on the filtration characteristics

Figure 13 shows that the cake thickness at 1 wt% remains the same as the sample with no PSS, at 1.9 mm. The thickness of the cake increases with further increase in concentration, reaching 2.3 mm. However, the cake thickness keeps growing with increasing PSS concentration, but the overall thickness grow is only 0,4 mm = 400 μm. The inserts in *Figure 14a* & *14b* shows the cake thickness of the original drilling fluid and after adding 5 wt% PSS.

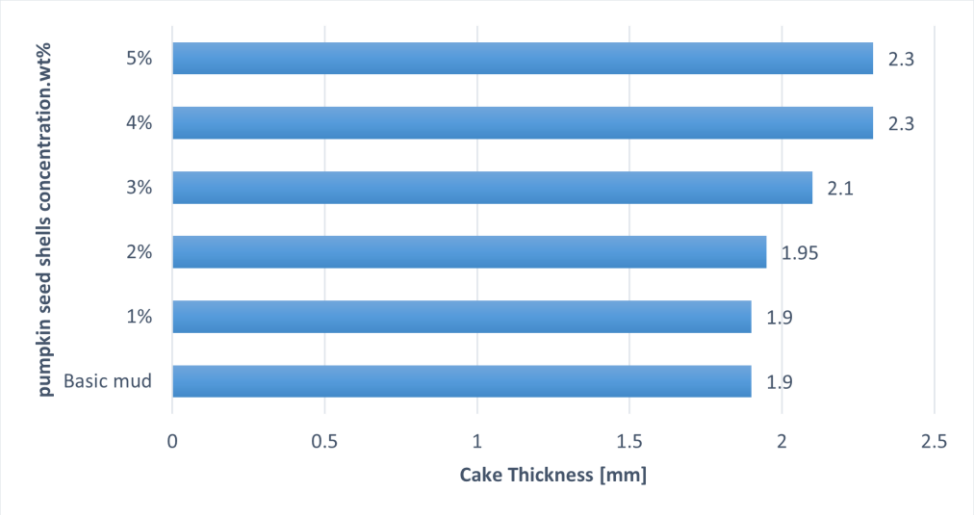

Figure 13. *The effect of PSS additive on the cake thickness*

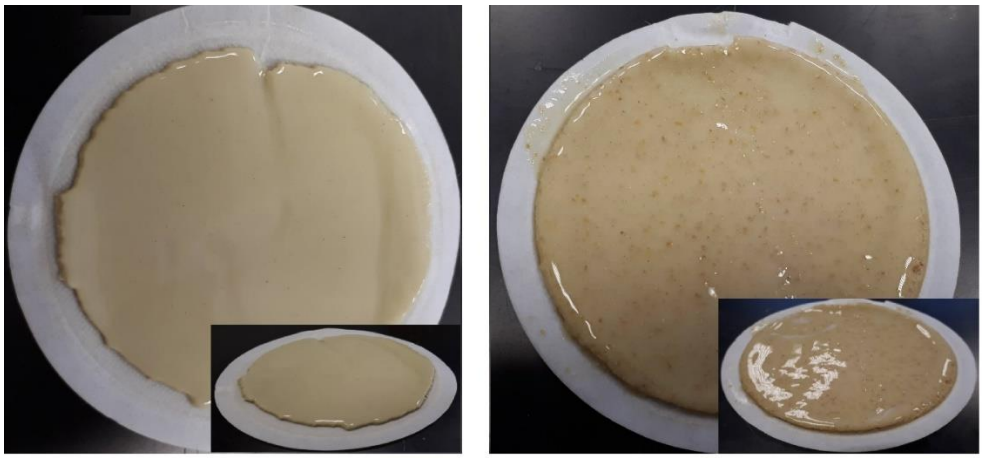

Figure 14. *The cake thickness of: (a) The original drilling fluid and (b) After adding 5 wt% of PSS*

4. CONCLUSION

A successful drilling operation requires minimizing fluid loss inside the formations. For this reason, many commercial materials such as carboxymethylcellulose (CMC) and polyanionic cellulose (PAC) have been used, which are very expensive and negatively affects the total cost of drilling in addition to their harmful environmental effects. In index study, pumpkin seed shells were used as an additive to control fluid

loss in the water-based drilling fluid. Through experiments, the following conclusions were drawn:

- Increasing concentration of the pumpkin seed shells (PSS) will positively affect the reduction of fluid loss, which means that in this study 5% was the optimum concentration of the PSS.
- Adding PSS gives a mud cake with acceptable thickness and low permeability.
- The addition of PSS has no significant effect on density and increases the plastic viscosity, apparent viscosity, yield point and gel strength. Thus, compared to the original fluid, adding PSS may has a good ability to increase the effectiveness of cleaning the well, reduce many drilling problems such as high torque, and increase the ability of the drilling fluid to carry the cuttings when circulation of the drilling fluid in the well is stopped.

ACKNOWLEDGEMENTS

The research was carried out at the University of Miskolc both as part of the project implemented in the framework of the Thematic Excellence Program funded by the Ministry of Innovation and Technology of Hungary (Grant Contract reg. nr.: NKFIH-846- 8/2019) and the project supported by the Ministry of Innovation and Technology of Hungary from the National Research, Development and Innovation Fund in line with the Grant Contract issued by the National Research, Development and Innovation Office (Grant Contract reg. nr.: TKP-17-1/PALY-2020).

REFERENCES

[1] Abdulkadir, A., Osawemwenze, L. A., Adogbo, G. M. (2013). Rheological and Filtration Properties of Kaolinite Based Drilling Mud. *International Journal of Scientific & Engineering Research*, 4 (7), pp. 2214–2220.

[2] Dhiman, A. S. (2012). *rheological properties & corrosion characteristics of drilling mud additives*. Halifax, Nova Scotia, p. 78.

[3] Elshreef, K., Lashin, A. (2016). Investigation of mud density and weighting materials effect on drilling fluid filter cake properties and formation damage. *Journal of African Earth Sciences*, 117, pp. 345–357. https://doi.org/10.1016/j.jafrearsci.2016.02.003.

[4] Amanullash, M. (2007). Screening and Evaluation of Some Environment-Friendly Mud Additives to Use in Water-Based Drilling Muds. *E&P Environmental and Safety Conference*, March 5–7, Galveston, Texas, U.S.A. https://doi.org/10.2118/98054-MS.

[5] Alsabagh, A. M., Abdou, M. I., Khalil, A. A., Ahmed, H. E., Aboulrous, A. A. (2014). Investigation of some locally water-soluble natural polymers as circulation loss control agents during oil fields drilling. *Egyptian Journal of Petroleum*, 23 (1), pp. 27–34, https://doi.org/10.1016/j.ejpe.2014.02.005.

[6] Kang, Y., You, L., Xu, X., Liao, Z. (2012). Prevention of Formation Damage Induced by Mud Lost in Deep Fractured Tight Gas Reservoir in Western Sichuan Basin. *Journal of Canadian Petroleum Technology*, 51 (1), pp. 46–51. https://doi.org/10.2118/131323-PA.

[7] Calçada, L. A., Neto, O. A. D., Magalhães, S. C., Scheid, C. M., Filho, M. N. B., Waldmann, A. T. A. (2015). Evaluation of suspension flow and particulate materials for control of fluid losses in drilling operation. *Journal of Petroleum Science and Engineering*, 131, pp. 1–10. https://doi.org/10.1016/j.petrol.2015.04.007.

[8] Warren, B. K., Smith, T. R., Ravi, K. M. (1993). Static and Dynamic Fluid-Loss Characteristics of Drilling Fluids in a Full-Scale Wellbore. *SPE Western Regional Meeting*, May 26–28, Anchorage, Alaska. https://doi.org/10.2118/26069-MS.

[9] Agwu, O. E., Akpabio, J. U. (2018). Using agro-waste materials as possible filter loss control agents in drilling muds: A review. *Journal of Petroleum Science and Engineering*, 163, pp. 185–198. https://doi.org/10.1016/j.petrol.2018.01.009.

[10] Blkoor, S. O., Ka, F. (2013). The Influence of XC-Polymer on Drilling Fluid Filter Cake Properties and Formation Damage. *Journal of Petroleum & Environmental Biotechnology*, 4 (5), https://doi.org/10.4172/2157-7463.1000157.

[11] Caenn, R., Darley, H. C. H., Gray, G. R. (2017). Chapter 5 – Water-Dispersible Polymers. In *Composition and Properties of Drilling and Completion Fluids*. Seventh Edition, Gulf Professional Publishing, pp. 135–150. https://doi.org/10.1016/B978-0-12-804751-4.00005-5.

[12] Dantas, A. P. T., Leite, R. S., Nascimento, R. C. a. M., Amorim, L. V. (2014). The influence of chemical additives in filtration control of inhibited drilling fluids. *Brazilian Journal of Petroleum and Gas*, 8 (3), pp. 97–108. https://doi.org/10.5419/bjpg2014-0009.

[13] Houwen, O. H. (1993). Chemical Characterization of CMC and Its Relationship to Drilling-Mud Rheology and Fluid Loss. *SPE Drilling and Completion*, 8 (03), pp. 157–164, https://doi.org/10.2118/20000-PA.

[14] Bourgoyne, A. T. (1986). Applied drilling engineering. *Society of Petroleum Engineers*, p. 502.

[15] Igwe, I. (2015). The Use of Periwinkle Shell Ash as Filtration Loss Control Agent in Water-Based Drilling Mud. *International Journal of Engineering Research and General Science*, 3 (6), pp. 375–381.

[16] Kosynkin, D. V., Ceriotti, G., Wilson, K. C., Lomeda, J. R., Scorsone, J. T., Patel, A. D., … Tour, J. M. (2011). Graphene oxide as a high-performance

fluid-loss-control additive in water-based drilling fluids. *ACS Applied Materials & Interfaces*, 4 (1), pp. 222–227, https://doi.org/10.1021/am2012799.

[17] Agwu, O. E., Akpabio, J. U., Archibong, G. W. (2019). Rice husk and saw dust as filter loss control agents for water-based muds. *Heliyon*, 5 (7), p. e02059. https://doi.org/10.1016/j.heliyon. 2019.e02059.

[18] Al-Hameedi, A. T., Alkinani, H. H., Dunn-Norman, S., Alkhamis, M. M., Al-Alwani, M. A., Mutar, R. A., Salem, E. (2020). Proposing a new biodegradable thinner and fluid loss control agent for water-based drilling fluid applications. *International Journal of Environmental Science and Technology*. https://doi.org/10.1007/s13762-020-02650-y.

[19] Al-Hameedi, A. T. T., Alkinani, H. H., Dunn-Norman, S., Salem, E., Knickerbocker, M. D., Alashwak, N. F., Al-Bazzaz, W. H. (2020). Laboratory Study of Environmentally Friendly Drilling Fluid Additives Banana Peel Powder for Modifying the Drilling Fluid Characteristics in Water-Based Muds. *International Petroleum Technology Conference*, 13–15 January, Dhahran, Saudi Arabia. https://doi.org/10.2523/iptc-19964-ms.

[20] Ashikwei, D., Marfo, S. (2016). Evaluation of the Suitability of Corn Cob Cellulose as a Viscosity Modifier in Water Based Drilling Fluid. *4th UMaT Biennial International Mining and Mineral Conference*, Tarkwa, Ghana, pp. MP 66–70.

[21] Iscan, A. G., Kok, M. V. (2007). Effects of Walnut Shells on the Rheological Properties of Water-Based Drilling Fluids. *Energy Sources, Part A: Recovery, Utilization, and Environmental Effects*, 29 (11), pp. 1061–1068. https://doi.org/10.1080/00908310600713982.

Geosciences and Engineering, Vol. 9, No. 14 (2021), pp. 43–59.
https://doi.org/10.33030/geosciences.2021.14.043

MODIFIED APPROACH FOR PROPPANT CONDUCTIVITY MEASUREMENT

PATRIK PUSZTAI[1, *] – PÉTER JÁNOS KORONCZ[2, 3]

[1]*Research Institute of Applied Earth Sciences, University of Miskolc*
[2]*Geochem Ltd.* [3]*Doctoral School of Earth Sciences, University of Pécs,*
[*]*patrpusztai@mol.hu*

Abstract: The main goal of this study is to combine two widely used standard proppant conductivity measurement methods in order to harvest some of their advantages in case of resin-coated proppants. The available literature was studied to determine which elements can be eliminated or modified for the measurement to simplify the method and shorten its length. The proposed measurement procedure provides as short a solution as possible while maintaining suitable accuracy. An additional object of the study is to investigate the effect of different flow rates through a propped pack and find the limit of non-Darcy flow. Since higher than recommended flow rates can be utilized, less complex differential pressure measurement devices can be used. Different evaluation methods have been tried out for improved solution.

Keywords: *proppant, conductivity, non-Darcy flow, evaluation method*

1. INTRODUCTION

In general, the purpose of proppant measurements is to obtain near-in-situ information about the permeability and conductivity of different proppants. Selecting a proppant with the right properties is one of the key aspects for well productivity and thus for the economy of a hydraulically fractured and propped reservoir [1]. In most cases, the proppant selection is based on measurements done under laboratory conditions. Although measurements have been made since the 1940s to investigate proppant behavior and the conductivity of hydraulic fracturing, there was no established standardized method until the end of the 1980s [2]. The first standardized measurement method was introduced by the American Petroleum Institute in 1989 under the name of "Recommended Practices for Evaluating Short Term Proppant Pack Conductivity" and with the identification number of API RP 61 [3]. As the measurement method involved a high degree of uncertainty, a modified measurement method and equipment for it began to spread in the industry [4]. This modified method became the standard in the industry and in 2006 it was established by the International Organization for Standardization as ISO 13503-5 [5]. In 2008 this standard was adopted by the American Petroleum Institute under the name of "Measuring the Long-term Conductivity of Proppants" and with the identification number of API RP 19D [6]. The main differences between API RP 61 and API RP 19D are summarized in *Table 1*.

It is important to note that significant differences can be found in the literature between measurements performed under the same conditions with API RP 19D, so the measurement uncertainty is high. In general, the variance between measurements is ±20%, although variance of more than 80% can be found in the literature as well [7]. During our investigation, we set a target to create a modified measurement method with which the results can be duplicated within the average range of ±20% and with a sufficiently high correlation coefficient. At the same time we attempt to reduce the measurement time as much as possible, since one measurement series with the API RP 19D standard requires more than 250 hours, not including preparation.

2. EXPERIMENTAL PROCEDURE

In order to modify the current processes, first we needed to study the literature and compare the already available methods. The main differences between API RP 61 and API RP 19D conductivity measurement methods are represented in the table below.

Table 1

Main differences between API RP 61 and API RP 19D measurement standards [7]

	API RP 61	API RP 19D
Circulated fluid	Deionized water	2% KCL solution
Closure body	Stainless steel platens	Sandstone core
Temperature	75 °F (~24 °C)	150–250 °F (~66–121 °C)
Time under closure stress	0.25 hours	50 hours

The first suggestion to use 1 to 2% potassium chloride (KCl) water instead of demineralized water appeared in the literature in 1986 [8]. The main assumption was that the water phase probably can be simulated better by this solution. As the effect of this has not been investigated extensively, during our modified method first demineralized water was used; in later studies, the effect of the usage of KCl solution will be analyzed.

The effect of proppant embedment on proppant conductivity is significant and its effect is more obvious under a certain closure value [13]. As 10,000 psi is the final closure stress during our measurements, this effect cannot be disregarded. To obtain more realistic conductivity values consolidated sandstone is used in our modified approach.

Most of the literature suggests higher than ambient temperature during conductivity measurement [2, 5, 6, 8, 9, 12]. The reason behind this is that in case of short loading times the temperature does not have a significant effect on the conductivities, but in case of significantly longer loading times the temperature is important, as stress-intensified corrosion may occur, weakening the grains and increasing the degree of crushing [12]. The investigated proppant in this study has a very low fine value after the ISO 13503-2 crush test. The value of the crush test in case of the

investigated proppant is equal to 3.13 wt% at 10,000 psi (~690 bar), which can be considered as low [10]. As the standardized crush test specifies ambient temperature [11] during, measurement, a temperature of 75 °F (~24 °C) was implemented in our modified approach, which is a considerable simplification of the method and further investigation may be necessary.

Three main factors have been identified that can cause variations in the measurement results under the same conditions in case of API RP 19D [1]:

- Variation in pack width: this can be caused by the initial packing arrangement, which is carried through during the different closure stresses and affects the rearrangement and the compression properties;
- Secondary changes in pack width: the main causes are the proppant rearrangement under different loads, grain crushing, and grain embedment (also other parameters like roundness and sphericity of the proppant grains have an impact on these parameters);
- Variations in permeability: caused by the initial proppant arrangement.

To achieve the same initial and during measurement conditions in the above conditions, API RP 19D suggests a relatively long loading time for each closure stress (±50 h). Also, a significant decline can be identified in the conductivities if the proppant pack is under closure stress for a significant time period [14]. In order to adjust to this phenomenon as much as possible, the holding time of the first closure stress after the initial load was 70 hours during our measurement. After that, to reduce the total time (compared to API RP 19D), permeabilities and conductivities were determined after 24 hours at each closure stress. The most important measurement parameters are given in *Table 2*, in which the values recommended by the two standards are also indicated in the last two columns as a comparison.

Table 2

The most important measurement parameters applied in the modified approach

	Modified approach	**API RP 61 (1989)**	**API RP 19D (2008)**
Temperature	75 °F (24 °C)	75 °F (24 °C)	250 °F (121 °C)
Fluid medium	demineralized water	demineralized water	2% KCl solution
Closure body	Kővágószőlős sandstone	stainless steel	Ohio sandstone
Initial load	310 psi	–	1,000 psi
Duration of initial load	1 hour	–	12–24 hours
Closure stresses	4,000 psi 6,000 psi 8,000 psi 1,0000 psi	1,000 psi 2,000 psi 3,000 psi 4,000 psi 5,000 psi 6,000 psi 7,000 psi 8,000 psi	2,000 psi 4,000 psi 6,000 psi 8,000 psi 10,000 psi

	Modified approach	API RP 61 (1989)	API RP 19D (2008)
		9,000 psi 10,000 psi 11,000 psi 12,000 psi 13,000 psi 14,000 psi	
Loading rate	Initial to 4,000 psi 725 psi/min, then 260 psi/min	–	100 psi/min ± 5%
Duration of closure stresses	At 4,000 psi 70 hours, then 24 hours	0.25 hours	50 hours ± 2 hours

The measurement was carried out by an equipment introduced in the ISO 13503-5 (API RP 19D) standard [22]. A schematic diagram of the experimental setup is shown in *Figure 1*.

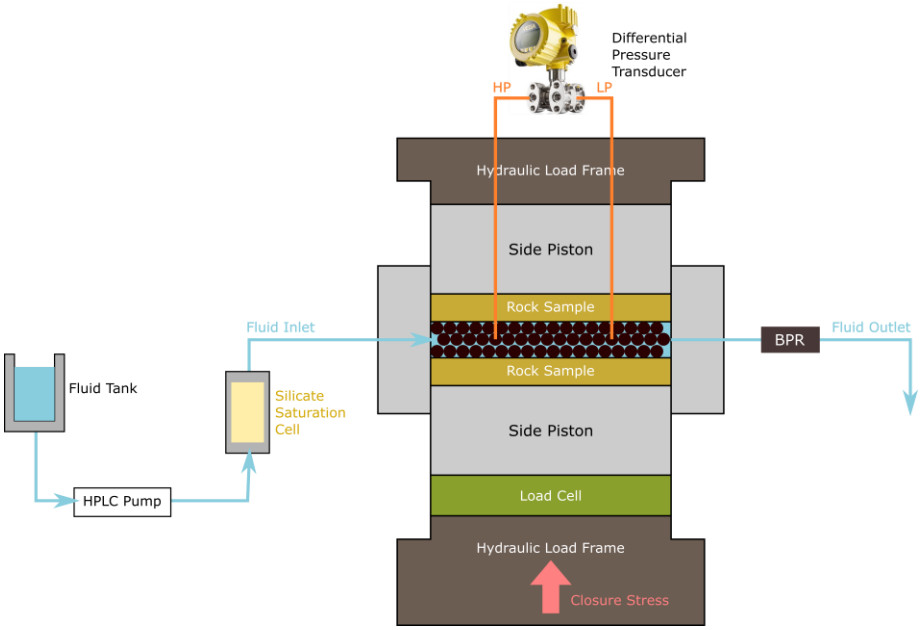

Figure 1

Schematic of experimental setup for proppant conductivity measurements

Pulsation-free constant flow rate was supported by a chromatographic pump with a built-in pulsation dampener unit. The injected fluid was passed through a silica saturation cell and filtered by a 0.5-micron sintered stainless-steel filter before entering the test cell. Proppant was placed into a proppant conductivity cell between two sandstone wafers from the Kővágószőlős Formation (detrital complex of the Upper Permian of the Mecsek mountains, Hungary). Closure stress was supported within +/– 1% of the setpoint value by a hydraulic load frame with a maximal loading ca-

pacity of 667 kN. Pressure drop between the pressure ports was measured with a differential pressure transducer with a resolution of 0.001 kPa. Pore pressure was set up by a back pressure regulator (BPR). The width of the proppant pack was measured with two laser distance sensors. Initial zero pack width was measured without the proppant pack. Pressure, temperature and distance parameters were collected and stored by a computer.

Other preparations for the measurements have been implemented as API RP 19D states, such as the presetting of the sandstone core with high-temperature silicone (RTV) in order to avoid any leakage at the sides of the core or the loading of proppant in the cell. The loading of proppant in the cell is a critical factor to reach nearly identical results. For example, recent studies proved that proppant loading with the application of vibration can significantly reduce the conductivity variations [15, 16]. This method has not been used during our measurements as it is not yet accepted by the ISO and our results indicate that the conductivities can be in an acceptable range without the utilization of any vibration techniques.

In order to be able to examine the effect of time, the data were recorded continuously during the measurement. Instead of the minimum flow rate of 2 ml/min specified in the standard, a flow rate of 2.6 ml/min was used and at the end of the loading cycles, four volumetric flow rates were applied instead of five recommended by the API RP 19D (2.6 ml/min; 3.1 ml/min; 3.6 ml/min; 4 ml/min), which determined the final permeability values.

The following standard equations were used to determine the permeability and conductivity values [5].

$$k = \frac{\mu \times Q \times L}{100 \times w \times (\Delta P) \times W_f} \tag{1}$$

$$C = \frac{\mu \times Q \times L}{100 \times w \times (\Delta P)} \tag{2}$$

where k is the permeability expressed in Darcy; C is the conductivity expressed in Darcy-meter; μ is the dynamic viscosity of the fluid expressed in cP; Q is the applied flow rate expressed in cm^3/s; L is the distance between the pressure ports expressed in cm; ΔP is the pressure drop (pressure upstream minus pressure downstream) expressed in kPa w is the cell width expressed in cm; and W_f is the proppant pack width expressed in cm.

3. RESULTS

The total duration of the measurement was 150 hours, which can be identified in *Figure 2*. Data were continuously recorded during the measurement, so it can be seen in the figure how the permeability values changing with time and under dif-

ferent applied loads. The different closure stress effects can be easily recognized, as the permeability values show a significant drop when greater pressures are applied to them.

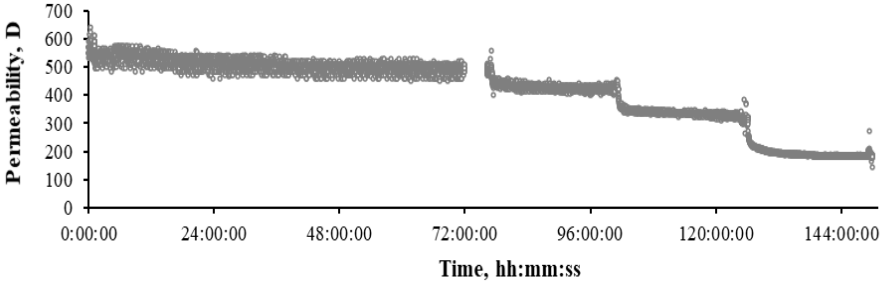

Figure 2. *Permeability values during the whole measurement*

The data recording took place every 5 seconds during the measurement, so more than 10,500 permeability values are calculated and presented in the figure above. Since the API RP 19D standard proposes that permeability values (at different flow rates) are to be determined at the end of the different closure stresses, the average of the values recorded at each flow rate serves as a starting point. The standard does not provide any evaluation method for this, so we propose that the average of the measured values (at each flow rate) be represented on a graph where the abscissa is the $\Delta P/L$ and the ordinate is the Q/A (or $Q/(w \times W_f)$). Interpolating a linear function on these data points, we can determine the permeability values from the slope of the line by the following equation.

$$k = slope \times \mu \times 1\,000 \tag{3}$$

where the slope can be found from the fitted line and is a dimensionless parameter. This method (later also referred to as *4-point measurement*) can be used efficiently, as it helps to eliminate the small irregularities from the result. We also tested the effect of applying more than four flow rates and basically negligible differences can be identified (see *Figure 5*), so it can be stated that the applied four flow rates are adequate to determine the final permeability values. With this approach we can slightly reduce the total measurement time without sacrificing perceptible degradation in accuracy. As can be seen from *Figure 3*, the r-squared values are very close to 1, which indicates that our regression model works well and only limited variance can be detected in the measurement. This was also reinforced by the application of a pulsation dampener in the system that helps to reduce the shocks caused by the increase in flow rates. The results clearly show that at higher applied loads the permeabilities decrease as the slope of the corresponding lines decreases. This is in line with the literature and also it is intuitive, since at higher applied loads the proppant pack is more compressed, so smaller channels are available for the fluids

to flow through and thus the differential pressure will increase; based on *Equation (1)*, with increasing ΔP the permeability values should decrease proportionally.

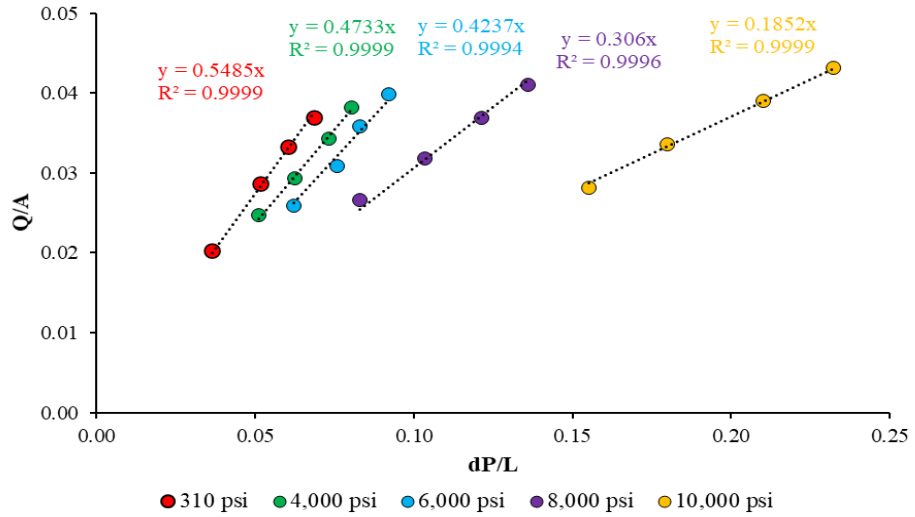

Figure 3. *Determination of permeabilities at different closure stresses*

By adding together, the permeabilities calculated from the presented slopes, the final permeabilty vs. closure stress graph can be determined. As data were registered during the complete measurement process the variations can be determined from the maximum and minimum points at each closure stress *(Figure 2)*. This is presented by a grey stripe in *Figure 4*, while the permeability values from the 4-point measurements are shown with a red line.

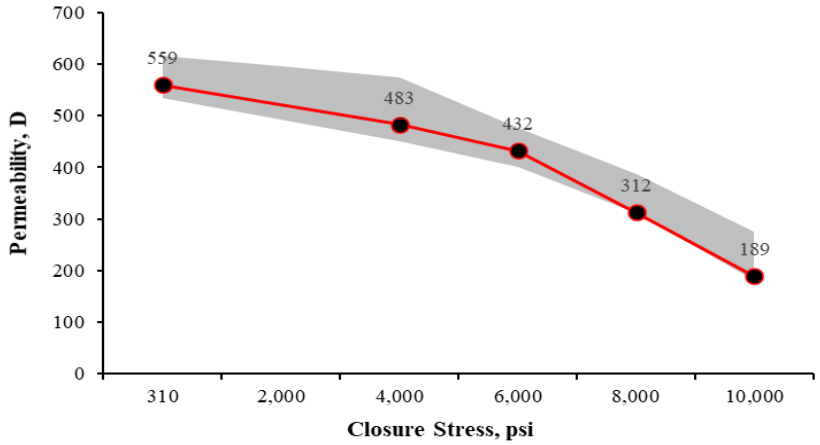

Figure 4. *Result of 4-point measurements and the variance of permeabilities during the whole measurement*

It has been previously stated that measurements can differ from each other despite the fact that the same circumstances are created. Based on the literature this variance is around 20% [1], which was confirmed by our results, although at the highest closure stresses the variance is +46%/–4%. This can be explained by the fact that at high closure stresses the proppant grains are crushed and the effect of embedment is enhanced [2]. With the combination of these two effects a significant permeability performance decline can be identified at the early stages. These results are collected in *Table 3*.

Table 3

Results obtained during 4-point measurements and maximum and minimum permeabilities obtained during the whole measurement (with percentage deviations)

Closure stress, psi	310	2,000	4,000	6,000	8,000	10,000
Max. permeablity from average, Darcy	616	596	575	476	387	275
Difference, %	10	14	19	10	24	46
Min. permeability from average, Darcy	534	492	450	400	310	181
Difference, %	–5	–6	–7	–7	–1	–4
4-point measurement permeability, Darcy	559	521	483	432	312	189

The ISO RP 19D standard specifies low flow rates during measurement to avoid the build-up of turbulent flows. In case of turbulent flow, it is necessary to correct the laboratory values with a non-Darcy coefficient [17]. In practice, this would occur in such a way that the points belonging to the higher flow rates in *Figure 3* would not fit properly after a given limit to the line but would have a slower slope [18]. During our measurement an experiment was conducted to investigate the effect of non-Darcy flow. For this reason, at the highest applied closure stress (10,000 psi) the flow rates were increased intermittently up to 50 ml/min. The closing stress of 10,000 psi was chosen because in this case the smallest channels are formed; thus, the appearance of non-Darcy flow is the most likely due to the higher Reynolds number [19]. Based on the equation proposed by Ergun in 1952 the Reynolds number region in this experiment is between 0.01 and 1 [20]. Results can be found in *Figure 5*.

To be able to identify the turbulent effect two lines were interpolated independently on the upper and lower part of the measurement points. The interpolated lines fit accurately on the points (each with a more than 0.999 r-squared value) and although the linear line fitted on the higher flow rates has a slightly lower slope, there is no significant difference between the slopes of the two interpolated lines. There is only a 2.7% difference between the slopes of the two fitted lines, so it can be stated that even at a volumetric flux of 0.541 cm/sec (that belongs to 50 ml/min of flow rate) no significant turbulent flow develops, which would justify the deter-

mination and use of the non-Darcy component. Using this result, higher than recommended flow rates can be used in the future, which consequently generates a higher pressure difference and thus makes the detections more accurate and less sensitive to small pulsation fluctuations.

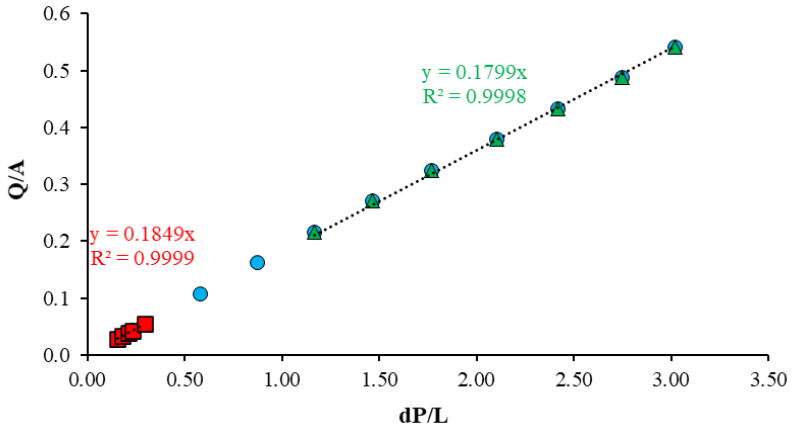

Figure 5
Experimental investigation of non-Darcy flow

Since several studies suggest the application of long closure stresses (API RP 19D also specifies this), it was worth investigating in detail whether a significant change is indeed observed over time. The *Figure 6* shows the absolute deviation of the calculated values over the entire measurement to the 4-point measurement permeabilities.

Based on the values obtained for the nearly 8,500 measuring points, it cannot be clearly concluded that even the 24-hour closing stress we use is necessary. At the closing stresses of 4,000 psi and 8,000 psi it is clear that continuously decreasing permeability values were measured; however, the values at 6,000 psi show different results. The results obtained at the 10,000 psi closing stress show that a significant decrease in permeability occurs in the first period, but this cannot be observed in the later period. This is presumably caused by the high pressures as the proppant grains crush and deform. Because of the fragmentation of the proppant grains into smaller pieces, the permeability can decrease suddenly (smaller pieces block the channels) but after a relatively short time these fragments become arranged.

In order to obtain a comparable result between our modified measurement and the results performed with the API RP 19D measurement, the technical data sheet of the tested proppant was compared with the values obtained by our measurements. *Figure 7* presents two acquired data series presented with different approaches, namely the results obtained by the 4-point measurement and results obtained by averaging the permeability values over each loading time *(Average of total measurement)*.

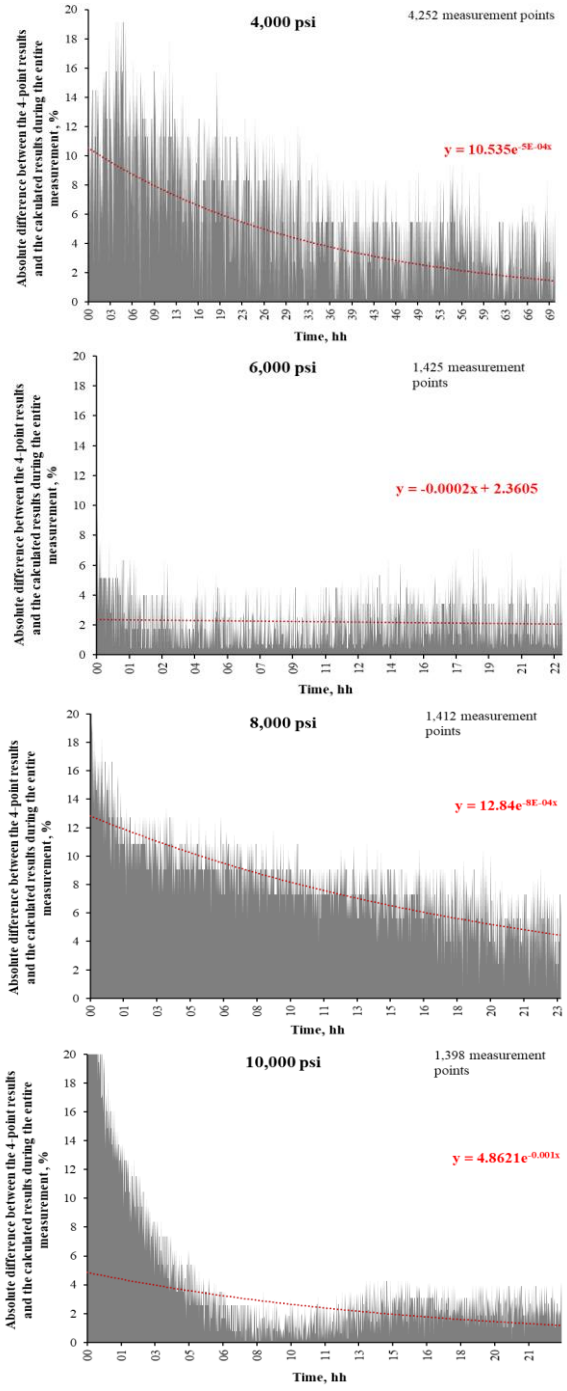

Figure 6
Effect of time on the permeability

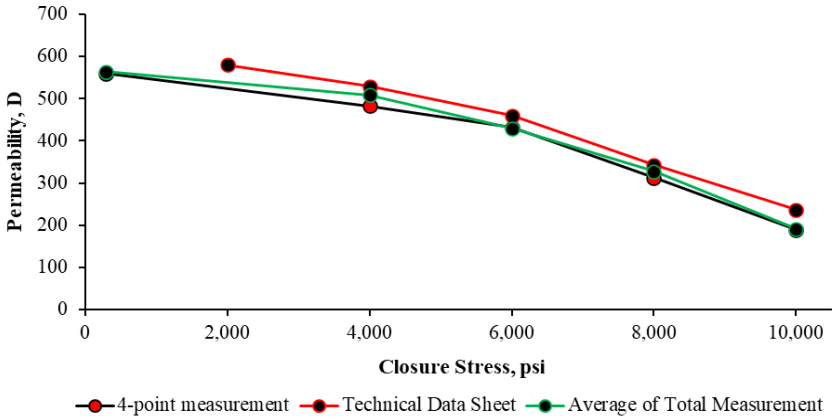

Figure 7

Comparison of the permeabilities with the proppant's technical data sheet

It can be seen from the figure that although there is a visible difference between the obtained results and the values indicated in the technical data sheet, but the trends of the lines are similar and the variance is between the range that the literature mentions. Also, no notable difference exists between the results obtained by the 4-point measurement and the average values recorded during the entire measurement. In this way the application of the 5-point measurement method proposed by the API RP19D is not necessarily essential to produce reliable results. The correlation coefficients and r-squared values are presented in *Table 4*.

Table 4

Statistical comparison of the two different evaluation methods compared to the permeability values indicated in the technical data sheet

	Correlation coefficient, –	r^2, –
4-point measurement	0.9975	0.995
Average of total measurement	0.9979	0.996

It has been found that there is a significant correlation between the obtained results and the results specified in the technical data sheet (where the data were obtained by the API RP 19D standard). This confirms that the modified measurement method can be used to test the permeability of resin-coated proppants. An interesting result is that the permeabilities calculated from the average of the whole measurement series provide a slightly better result, so both methods can be considered adequate. However, it is still suggested to use multi-point measurements since the measurement error due to the nonlinearity of the devices (pressure transducer, A/D converter, pump) can be eliminated.

The proppants were loaded into the measuring cell as specified in the API RP 19D standard. The goal is to achieve almost identical conditions with this method, but there is an obvious difference between the results obtained and the fracture widths calculated from the values specified in the technical data sheets. This can be

explained by the variation in the initial packing arrangement of the proppants [1]. The results can be seen in *Figure 8*.

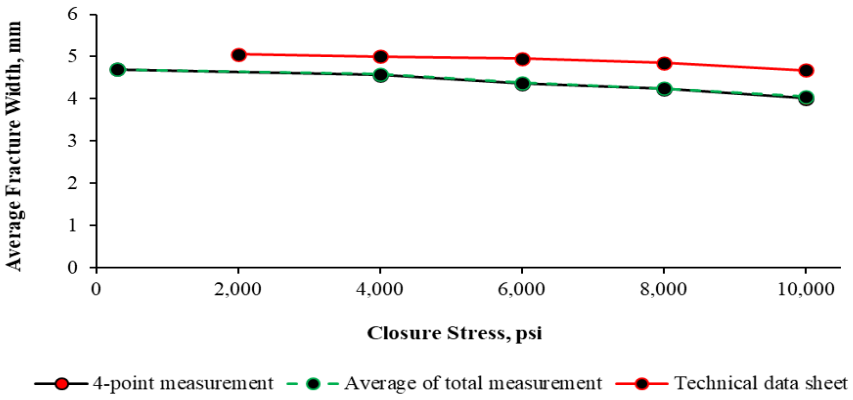

Figure 8
Comparison of the fracture width with the proppant's technical data sheet

Table 5
Statistical comparison of the two different evaluation method compared to the fracture width values calculated from the technical data sheet

	Correlation coefficient, -	r^2, -
4-point measurement	0.9698	0.941
Average of total measurement	0.9660	0.933

Although there is a significant correlation between the obtained results with high r-squared values, the differences can still be seen. The usage of the vibrational filling technique should be investigated in later studies to reach more accurate results. As the fracture width has a direct effect on the conductivity values (see *Equation 2*) it was assumed that the results will be slightly less accurate than in the case of permeabilities. This was confirmed by the results shown in *Figure 9* and *Table 6*.

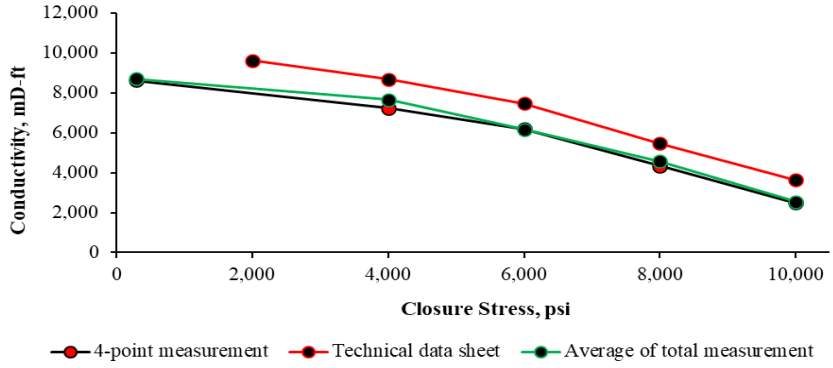

Figure 9. *Comparison of the conductivity with the proppant's technical data sheet*

Table 6

Statistical comparison of the two different evaluation method compared to the conductivity values indicated in the technical data sheet

	Correlation coefficient, –	r^2, –
4-point measurement	0.9974	0.995
Average of total measurement	0.9977	0.995

From the results it was found that the modified approach can be used within a suitable accuracy to determine the performance of different proppant packs. Also, no significant difference can be identified between the two offered evaluation methods.

Due to the continuous data recording, it is possible to study the distribution of permeability data and create a histogram. Since most of the results are assumed to be around a certain value, it is possible to fit a Gaussian curve on the acquired histogram. *Equation (4)* was used for this purpose.

$$f(x) = a \times \exp\left(-\frac{(x-b)^2}{2\times c^2}\right) \tag{4}$$

In the first step, the permeability values were determined at the same intervals and the number of occurrences within each interval was determined. The histograms can then be plotted *(Figure 10)*. Using *Equation (4)*, a curve can be fitted to the histogram, and then the calculated and measured r-squared values can be maximized by changing the parameters. For this optimization, the general reduced gradient method (GRG) was used, which is one of the most popular optimization methods for nonlinear problems [21]. Here only the results are presented without the calculation steps.

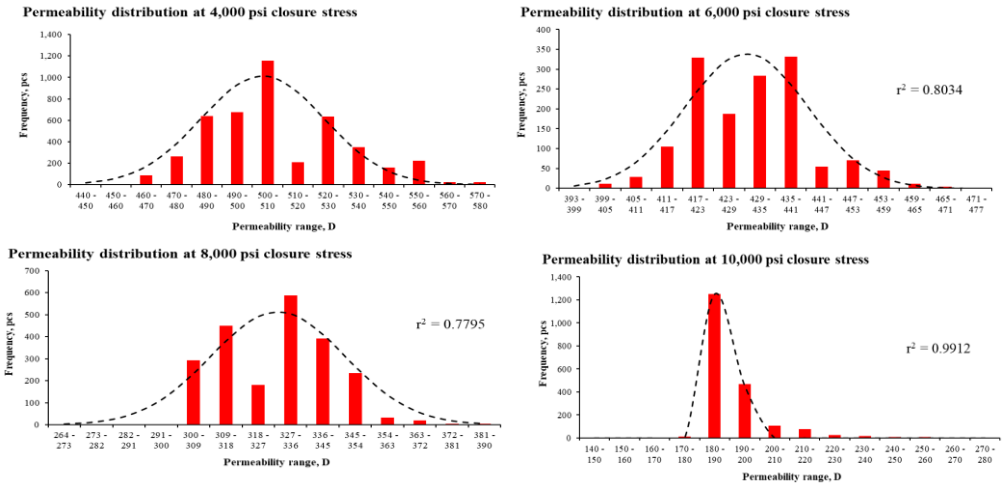

Figure 10. *Distribution of permeability values during the entire measurement*

The maximum of each function obtained gives the most likely accuracy of permeabilities. They can be determined by the derivative of the functions, but an easier way is that the *b* in the *Equation (4)* also determines the maximum value of the functions. *Table 7* represents the results obtained from the Gauss distribution functions and also from the other two proposed methods (4-point measurement, average of total measurements).

Table 7

Comparison of results based on Gaussian distribution

Closure stresses, psi	4,000	6,000	8,000	10,000
Gauss distribution, D	515	427	328	185
4-point measurement, D	483	432	312	189
Average of total measurement, D	509	429	328	191
Technical data sheet, D	529	460	343	237

The results obtained with each evaluation method are given in the table. The method based on the Gaussian distribution gives almost the same results as the other methods, especially the method based on the average of total measurement. Based on this, it is found that all of the methods can be applied with sufficient accuracy in the evaluation of proppant permeability results.

4. SUMMARY

The most important results from the study are summarized below:

1) The modified measurement approach may be used to measure the permeability and thus the conductivity of resin-coated ceramic proppants within the accuracy that can be reached by the standard method. It should be mentioned that further experiments are necessary to validate the results;
2) The applied method can be used to perform a series of measurements in less than half the time specified in the API RP 19D standard;
3) Based on the obtained results, the applied temperature has no significant effect on the permeability of resin-coated ceramic proppants. Further measurements are required to confirm this statement;
4) Volumetric flux can be increased up to 0.541 cm/sec without the occurrence of non-Darcy flow, resulting in higher pressure differences that are easier and more accurate to detect;
5) There is no significant difference between the result of the proposed evaluation methods. The evaluation method of 4-point measurement, the average of total measurement, or the Gauss distribution method provides nearly the same results.

The future plans of the research are summarized below:

1) It is necessary to perform measurement with several types of proppant in order to present more statistically representative results;

2) Sensitivity analysis should be required to further reduce the measurement time without deteriorating the results;
3) It is necessary to examine the modification of additional measurement parameters (such as temperature, proppant loading, fluid type) in order to achieve values even closer to the results acquired with the API RP 19D standard method.

ACKNOWLEDGEMENT

The authors acknowledge funding from GEOCHEM Ltd. and Mecsekérc Plc.

REFERENCES

[1] Barree, R. D., Cox, S. A., Barree, V. L., Conway, M. W. (2003). *Realistic Assessment of Proppant Pack Conductivity for Material Selection.* Paper presented at the SPE Annual Technical Conference and Exhibition, Denver, Colorado, Society of Petroleum Engineers, SPE 84306-MS. https://doi.org/10.2118/84306-MS.

[2] Liang, F., Sayed, M., Al-Muntasheri, G., Chang, F. F. (2015). *Overview of Existing Proppant Technologies and Challenges.* Paper presented at the SPE Middle East Oil & Gas Show and Conference, Manama, Bahrain, Society of Petroleum Engineers, SPE-172763-MS, https://doi.org/10.2118/172763-MS.

[3] API RP 61 (1989). *Recommended Practices for Evaluating Short Term Proppant Pack Conductivity.* Washington, DC, API.

[4] Penny, G. S. (1987). *An Evaluation of the Effects of Environmental Conditions and Fracturing Fluids Upon the Long-Term Conductivity of Proppants*. Paper presented at the SPE Annual Technical Conference and Exhibition, Dallas, Texas, Society of Petroleum Engineers, SPE-16900-MS. https://doi.org/10.2118/16900-MS.

[5] ISO 13503-5:2006: E (2006). *Procedures for measuring the long-term conductivity of proppants.* Petroleum and natural gas industries – Completion fluids and materials – Part 5, Geneva, Switzerland, ISO.

[6] API RP 19D (2008). *Measuring the Long-Term Conductivity of Proppants.* Washington, DC, API.

[7] Richard, S., Schrader, S., Schrader, R., Ereaux, B. (2019). *Improved Methods of Measuring Proppant Conductivity*. Paper presented at the SPE Western Regional Meeting, San Jose, California, USA, Society of Petroleum Engineers, SPE-195368-MS, https://doi.org/10.2118/195368-MS.

[8] McDaniel, B. W. (1986). *Conductivity Testing of Proppants at High Temperature*. Paper presented at the SPE California Regional Meeting, Oakland, Society of Petroleum Engineers, SPE-15067-MS. https://doi.org/10.2118/15067-MS.

[9] Abhinav, M., Chandra, S. R., Sondergeld, C. H. (2018). Proppant-Conductivity Testing Under Simulated Reservoir Conditions: Impact of Crushing, Embedment, and Diagenesis on Long-Term Production in Shales. *SPE Journal*, Volume 23, Issue 04, pp. 1304–1315, Society of Petroleum Engineers, SPE-191124-PA, https://doi.org/10.2118/191124-PA.

[10] Palisch, T. T., Duenckel, J. R., Chapman, M. A., Woolfolk, S., Vincent, M. C. (2010). How To Use and Misuse Proppant Crush Tests: Exposing the Top 10 Myths. *SPE Production & Operation*, Volume 25, Issue 3, pp. 345–354. https://doi.org/10.2118/119242-PA.

[11] ISO 13503-2:2006: E (2006). *Measurement of properties of proppants used in hydraulic fracturing and gravel-packing operations.* Petroleum and natural gas industries – Completion fluids and materials – Part 2, Geneva, Switzerland, ISO.

[12] McDaniel, B. W. (1987). *Realistic Fracture Conductivities of Proppants as a Function of Reservoir Temperature*. Paper presented at the SPE/DOE Joint Symposium on Low Permeability Reservoirs, Denver, Colorado, Society of Petroleum Engineers, SPE/DOE 16453, https://doi.org/10.2118/16453-MS.

[13] Qingzhi, W., Schicheng, Z., Lei, W., Yongshan, L., Xianping, L. (2007). The effect of proppant embedment upon the long-term conductivity of fractures. *Journal of Petroleum Science and Engineering*, Volume 55, Issues 3–4, pp. 221–227, https://doi.org/10.1016/j.petrol.2006.08.010.

[14] Much, M. G., Penny, G. S. (1987). *Long-term Performance of Proppants Under Stimulated Reservoir Conditions*. Paper presented at the SPE/DOE Joint Symposium on Low Permeability Reservoirs, Denver, Colorado, Society of Petroleum Engineers, SPE-16415-MS, https://doi.org/10.2118/16415-MS.

[15] Ramlan, A. S., Zin, R. M., Bakar, N. F. A., Othman, N. H. (2021). Recent progress on proppant laboratory testing method: Characterisation. *Journal of Petroleum Science and Engineering*, Volume 205. https://doi.org/10.1016/j.petrol.2021.108871.

[16] Blair, K. (2015). *Modifying Fracture Conductivity Testing Procedures.* Montana Tech of the University of Montana, Graduate Theses & Non-Theses, Paper 60.

[17] Forchheimer, P. (1901). *Wasserbewegung durch Boden*, Zeitschrift des Vereins deutscher, Ing. 45.

[18] Milton-Tayler, D. (1993). *Realistic Fracture Conductivities of Propped Hydraulic Fractures*. Paper presented at the SPE Annual Technical Conference and Exhibition, Houston, Texas, Society of Petroleum Engineers, SPE-26602-MS, https://doi.org/10.2118/26602-MS.

[19] Reynolds, O. (1883). An experimental investigation of the circumstances which determine whether the motion of water shall be direct or sinuous, and of the law of resistance in parallel channels. *Philosophical Transactions of the Royal Society*, pp. 935–982, https://doi.org/10.1098/rstl.1883.0029.

[20] Ergun, S. (1952). Fluid flow through packed columns. *Chemical Engineering Progress*, 48, pp. 89–94.

[21] Chapra, S., Canale, R. (2009). *Numerical Methods for Engineers*. 6th edition, McGraw-Hill, New York, NY.

[22] Füvesi V., Vörös Cs., Bölkény I., Jobbik A., Fedor F., Hlatki M. (2015). Geotermikus kutak kiképzésének vizsgálatára alkalmas laboratóriumi berendezések és mérési módszerek fejlesztése. *Műszaki Földtudományi Közlemények*, Volume 85, Issue 1, pp. 48–54.

Geosciences and Engineering, Vol. 9, No. 14 (2021), pp. 60–77.
https://doi.org/10.33030/geosciences.2021.14.060

THE TOPICALITY OF GEONOMY

RÓBERT NÉMETH[1, *] – ZOLTÁN VERRASZTÓ[2]

[1]*ALFÖLD System House, Szolnok, Hungary*
[2]*Middle-Danube Regional Environmentl Authority, Budapest, Hungary*
[*]*alfoldgis@gmail.com*

Abstract: Elemér Szádeczky-Kardoss realized that the entire material and spiritual culture of mankind constitutes an interconnected system, which he named geonomy. He established environmental science, identifying the need for network research. With the use of geographic information systems (GIS), IT technology expands the possibilities of recognizing, interpreting, and examining transdisciplinary connections in their dynamic relationships in many areas. The starting point of environmental modeling is the fact that the processes to be studied take place in a common space – in the field of interpretation of the earth sciences this is the landscape, the space in which the natural, social and economic processes take place, so the study of sustainability is a spatial, multi-faceted decision-making task. We need to reconcile the goals of population preservation and of production with social, cultural and environmental stabilization and nature conservation tasks. The map based decision support we propose provides the exact possibility of multi-aspect decisions in a complex, spatial system. The key to solving this problem is the grouping of the "Big Data" data set, the structuring of the data groups and then the harmonization of the data layers.

Keywords: *environmental science, spatial, multidimensional decision, map decision support, harmonization of data layers*

1. MAPS AND GIS SYSTEMS

The previously unimaginable development of the IT technology toolkit with the use of GIS (geographic information systems) expands the possibilities of recognizing, interpreting, and examining transdisciplinary relationships in their dynamic relationships in many areas. It makes sense that the starting point for the application of dynamic GIS in thematic maps is an expediently structured database.

Although a handmade mining map made in Selmecbánya (Banská Štiavnica) (Mikoviny 1746) is known as the first "overlay map system", this method was soon forgotten. We first used it with István Klinghammer (1994) as a traditional static thematic map system, as an environmental decision support method. The transparent map sheets containing relevant environmental information can be overlapped, so that different combinations of these provide the opportunity to recognize the relationships between influencing factors and the affected variables and the consequences of environmental use in a given space, going beyond previous map representations that

only visualize relationships. A brief professional guide draws attention to the possibilities of these. A significant departure from the practice of previous map representations is that the measured data are represented at the measurement point, providing ample space for professional evaluation. (The significance of this is given by the fact that, for example, there can be many changes **between** two measuring points, even showing the same data, e.g. dilution from groundwater and further pollution, etc.!)

Under the guidance of Tamás Rapcsák, we performed the water quality modeling of the Soroksár Danube branch using mathematical methods developed as a support for multi-aspect decision making, where the results of model computations were made compatible with each other in thematic maps. (Balla et al. 1999)

In the preparation of an environmental impact study, the possibility of spatial confrontation of influencing factors and the affected using this method is of particular advantage. During the planning, the overlay system formed from the relevant thematic maps makes it possible to coordinate the needs and opportunities appearing in the same space – the preliminary environmental impact study of the South Buda-Rákospalota (4th) metro line has already proved this (2002).

GIS-based *environmental monitoring* covering the Ipoly catchment area (Miklós et al. 2014), proved that a database built on thematic maps and GIS systems based on traditional geological, hydrological, biological and soil maps can ensure the interpretation and examination of dynamic relationships.

Modeling including the dynamics of complex environmental systems allows development toward *environmental safety* applications (Balogh et al. 2015, Csikós et al. 2015]. By implication, this includes the examination of the effects of environmental elements endangering social facilities, as well as the modeling of the environmental consequences of possible accidents and breakdowns. The modeling of flood inundation for the Bódvár River and then the Hernád was already based on the dynamic modeling of GIS with special mathematical tools (Németh–Dobos 2015).

2. GEONOMY

In the obituary of the late Tamás Rapcsák (1947–2008), his colleagues draw attention as a novelty to the fact that "environmental decision-making tasks are essentially multi-faceted decision-making tasks, since environmental aspects such as water, air, noise, vibration, etc. should be taken into account, together with other social, economic and financial aspects. Multi-faceted environmental applications have also opened up new directions for development. GIS systems have proved to provide effective tools for collecting information related to the task of decision, displaying them on a map, and examining time-dependent dynamic relationships. Developments and applications related to multi-faceted decision support have also raised important theoretical and methodological issues." (1994)

There is no doubt that LANDSCAPE is the space in which all the activities of our lives take place. All of the natural, social and economic processes that are the inherent biological and/or social – and consequently also the economic – needs of our

existence take place in the landscape. The essence of this was already formulated by Pál Teleki (1917) a hundred years ago, and then the "geographical idea" was filled with exact earth science content by Elemér Szádeczky-Kardoss (1974). He recognized that the entire material and spiritual culture of mankind formed an interconnected system, which he referred to as **geonomy**. He laid the foundations for **environmental science** (Verrasztó 2019) and identified the need for network research today. "This is an impossible challenge for one person, but only one person can do it in a unified approach," praised posterity (Benkő F. 2003). Szádeczky-Kardoss's discovery was based on the discovery of the law of cycles: "Clay-phyllosilicate sedimentation provides the material connection between the solid earth and the mobile zone (hydro-, atmospheric-, lithosphere)… it is… one of the most important foundations of the specific development direction of the Earth… which constantly refreshes the surface used by life processes and ensures its ability to sustain life at all times… The pollution of civilization upsets this balance."

The last hundred years have been characterized by an incredible expansion of knowledge. The improvement of research tools and the proliferation of data and information require the deepening of specialization, which has also resulted in the disintegration of knowledge and the segregation of sciences. In opposition to this, he formulated the need for **synthesis**: "*Geonomy is not only the investigative unit of the earth sciences, but it also comprises the basic biological subject of the origin and inorganic determination of life. The real meaning of geonomy is not in the details, but in the study of the relationship between the details… According to the new results of geonomy, the Earth is a unified active system, each zone of which is connected to the others…*The world explored by physics and chemistry is not the whole of reality. Reality implies complexity." (emphasis added) (Szádeczky-Kardoss 1974) "Earth science research must be approached consciously from two sides: On the one hand, maintaining immersion and precision of the usual professional details, and on the other hand, introducing a generous approach to a synthesis of hitherto unimaginable size. The results of geonomy affect the totality of sciences and are important for the general approach and public education" (Dudich 2003).

The "hitherto unimaginable generous approach to synthesis" is made feasible by today's IT toolkit. At the same time, the synthesis must have a basic structure of systems science, and its scientific result must be the recognition and scientific foundation of network connections. As a practical benefit, we can use *environmental modeling* to base all decisions that affect ***sustainability*** in an exact *multi-criteria decision support system*.

3. SUSTAINABILITY

The real meaning of protecting the environment and nature is to ensure the **sustainability** of our social existence: a development process resp. an organizational principle that "meets the needs of the present without reducing the ability of future generations to meet their own needs". But what are the realistic needs of the present and the future?

The answer to this question would be based on a multitude of social decisions, the common problem of which is that they are ***value-based***. Not only do the diverse social evolutions of ethnic groups influence consumption habits, cultural differences, and different value choices, but our needs for the environment, our habits, our individual tastes, and family traditions also diversify the components and indicators of our wealth and well-being.

The specifics of society's environmental conflicts are, in fact, clashes of concepts of land usage. The expectations of interest groups and the differences of social needs are determinative factors in this, but the conflict of the needs, opportunities and interests of the past and the future is also concentrated in this.

What cannot be the subject of debate is ***natural sustainability*** – behind it are often still little-known but unquestionable natural laws, exact networks of relations, causal connections. We can examine the causes and effects in an exact way through their indicators, we interpret the relationships between the influencing factors and those affected – establishing the protection of our environment, recognizing the necessary and possible measures.

We cannot ignore the fact that many people demand the protection of the environment as **resource protection**. This is undoubtedly a rational concept – at the same time we need to see that a resource is a changing need, a concept that changes in space and time. The demand for flint of our Stone Age ancestors was then more important than energy carriers to us today! Ensuring the sustainability of our social groups and our diverse natural environment requires different resources!

Here we have to mention the concept of the so-called "ecological services" that is prevalent today – where we object in principle to the fact that it regards the satisfaction of value-driven social needs as the starting point as opposed to the unquestionable demand of adapting to natural conditions.

If we want to satisfy today's scientific needs in planning for the future and make use of the possibilities of research and planning provided by modern IT technology, the changing interpretations are out of place; we need an exact use of concepts in environmental protection, nature conservation and spatial planning; we need to interpret, study, and model sustainability for coming generations.

In order to achieve this, the expectations must be enforced not only more effectively than at present, but also with the requirements of systems science and multifaceted decisions, using IT tools in all regional and economic development concepts that determine the future, environmental use, landscape, the connection of society and its environment!

Today, the European Landscape Convention (Florence 2000) also defines further concepts of *environmental protection, environmental safety, environmental policy, nature protection, regional development and spatial planning* as international commitments (Verrasztó 2017, 2018). The synthesis of all these includes all the demands that we have to satisfy in the spirit of *geographical thought*, with the scientific need of *geonomy*, in order to protect the *unified environmental system* and to meet the need for sustainable development:

"The landscape…

…plays an important role of public interest in the cultural, ecological, environmental and social fields and acts as a resource to support economic activities, the protection, management and planning of which can create new jobs;

…promotes local cultural development and is an essential element of Europe's natural and cultural heritage;

…contributes to people's well-being and the strengthening of European identity;

…it is an equally important part of people's quality of life everywhere: in cities and villages, in degraded and pristine areas, in places that are considered particularly beautiful and places without such qualities," says the European Landscape Convention.

With the need for sustainability, the role and perception of the rural landscape, nature and the environment have undergone significant changes. In addition to the historical task of the rural area, other functions come to the fore. **The "countryside" is not only the scene of agriculture, but also a biological and social habitat.** The community that preserves traditions, the cohesion factors of society, the ecosystems are also functions of nature, environmental, and landscape protection that serve the interests of the community, that produce consumption and service as well as "public goods". If land use and other interventions are driven solely by the need for production, natural and social relations and living space functions will be jeopardized, but the economy cannot be without diversity either. Degradation of the environment leads to a decline in production and poses a serious threat to human living conditions.

Today, urbanization and industrial "development" are growing – in an unsustainable manner – in the same space at the expense of each other, and social and economic activity is growing at the expense of natural life, increasing human health risks and reducing biodiversity. A system of nature and environmental protection based on passive post-sanctioning is not indispensable either, but it is of doubtful efficiency in enforcing interests. The possibilities of our time with the application of IT technology (Verrasztó 2017, 2018) must create a demand for exact territorial planning, which, using *multi-aspect decision support*, establishes all the development concepts and land use needs that have to be coordinated in the shared space – in the landscape**.** Production goals must be coordinated with the increasingly important tasks of population retention, social, cultural and environmental stabilization, and nature conservation.

4. ENVIRONMENTAL MODELING

The insights of the last half century have led to the social need, political expectation and administrative enforcement of environmental protection (see environmental and nature protection legislation), but their practice has not kept pace with the demands and possibilities arising from the development of either science or technology. We have known for a hundred years from the Academic inauguration speech of chair holder Pál Teleki that the natural and social effects are congregated in the complicated, multi-complex system of the Earth. Geonomy concretized the

processes taking place on Earth. The effects of economic activity – its needs and consequences – are undoubtedly realized in those influenced by the natural and social processes. In examining these, we can surpass today's – very limited – practice if we can provide the possibility of exact environmental modeling, which in turn presupposes a number of things:

- the exact use of terms (environment, environmental data);
- exact examination of the territory (environment, landscape, river basin, region) ensuring the system control;
- clarification of spatial data relations (system of landscape factors, common social space, economic relations, etc.);
- definition of aspects of group formation (natural, social and economic components);
- awareness of the basic environmental condition;
- awareness of the process of changes (transport processes, historical and/or social changes, etc.);
- a database that provides the possibility of thematic, spatial, and temporal structuring.

As the starting point of environmental modeling – a tool for the spatial interpretation and examination of **sustainability** – we must see that the environment is a **dynamic system**, and the data set to be examined consists of several subsystems. The dynamics of the subsystems as well as the dimensions, units and properties of the data differ significantly. The change of many elements of change is *not* dynamic; however, natural, social and economic sustainability can only be interpreted by their interconnection based on their contexts and spatial relationships. The exact interpretation and examination of this complex system has so far encountered a number of obstacles.

In addition, a major shortcoming of current practice is that

- there is no social consensus on the environmental objectives and individuals with different life situations, different social groups have different environmental needs;
- there is no scientific consensus on the actual state of the environment;
- economic interests overshadow the territorial, spatial consequences, benefits, damages of the use of the environment;
- the groups involved in the decision-making process have very different demands and their advocacy capacity also differs significantly;
- the groups involved in the decision-making process do not have sufficient knowledge or depth of information about the real consequences of their decisions that are distant in space and time.

It should be noted that economists dealing with the topic point out that the results cannot be condensed into a single measure (as they are based on a variety of arguments) and therefore their generalizability is limited.; this is one of the major disadvantages of the multidisciplinary and participatory evaluation methods used so far.

On the other hand, we would like to point out that it is not even expressed as their demand:

- to study the natural systems in their complexity,
- to specify the factors of influence and those exposed to them,
- for professional consideration of the consequences exerted upon those subjected to them,
- to consider the consequences over time,
- to weigh the potential consequences, which again cannot be concentrated in a single measure,
- for evaluation of the non-generalizable, unique characteristics of the subsystems of the environmental-social system operating as a network.

The **map-based decision support method** we propose includes the demand and possibility of multi-criteria decision support, while it does not need to condense the result into a "single unit of measurement". An infinite number of variations of relationships, alternatives, and the consequences of their spatial and temporal changes can be examined by interconnecting data systems structured in thematic maps. The method is suitable for the exact examination of that spatial decision – the consequences of the decision – which explores the complex and dynamic system of natural, social and economic relations taking place in the *landscape as a given space – in its own system of context.* The key phrase is its *"own system of correlations"*, as the interactions between natural and social and closed inanimate and open living systems within their own systems, as well as their interactions with each other, but also their components, are different and require qualitative or quantitative assessment.

Obviously, the method's accuracy and professional depth depend on the current data upload. The advent of digital cartography, – the digital storage, management and processing of cartographic data – has made it possible to renew this traditional methodology as an essential interface for the operating system of spatial decisions. By its application we visualize what is being said in each field, and at the same time we create the interface for all the relevant factors with which we want to examine the spatial and temporal relationship.

The development of digital maps primarily requires an adequate amount and quality of data. The digital recording of spatial relationships is not necessarily related to cartographic activity; moreover, the purpose of data collection during the establishment of GIS systems is not primarily for cartographic use. Data collection can be independent of graphical methods and can lead to the construction of a database that in most cases contains the following types of data:

- a spatial reference system;
- qualitative and/or quantitative indicators;
- temporal aspects;
- a situation in an environmental relationship system.

The stored data are not characteristic of the map per se, as they are to some extent independent of scale, projection, sectioning, etc., while the ***background maps*** provide an illustration of the relationship with geographical factors, the indispensable visualization. It is advisable to use different systems for maps of different scales – and consequently with different information content – but its selection should be significantly influenced by the specific case-specific objective to be defined, the thematic content to be represented and examined and its target system.

The **map-based decision support** solution we have proposed and developed is suitable for placing the demand and possibility of *multi-aspect decisions* on an exact basis. It presents an alternative with advanages to the previously used social decision-making practice since the ***factors of influence and those exposed to them*** can be linked quite exactly in space and time to a **given, specific land use** – represented and separated in thematic maps, using surface symbols – with the assumed, envisioned and modeled land uses – even up to their sustaining capacity, projecting into the future to the sustainability of the natural, social, and economic components.

"As an interpretive geophysicist, I was faced with the fact that there are plenty of application programs around the world that deal with data collection (which is understandable), yet there are very few projects that focus on geological interpretation of data (which is less understandable). Interestingly, this problem arose as early as 1967 during the debate on plate tectonics theory, formulated by JT Wilson in this way: 'They immersed themselves to such a degree in improving technical procedures, accumulating data, and designing a computer system for storing information as to forget that other sciences have made their problems easy to understand by formulating new principles' " – thus, in fact, coming closer to solving the problem…

Magnetic data providing national coverage are now available in almost all countries, which, in addition to examining the oceanic crust, also provide important information for the study of the old continental crust, which bears the results of several rock formation cycles; in that case, however, the magnetic data must be converted into geological information in an adequate and prudent manner. (Kiss J. 2014).

It would have been difficult to characterize more clearly the situation surrounding the demand for ***environmental data*** than it is done in this quote. The INSPIRE directive sets out a number of forward-looking requirements for the collection, management and access of spatial data, but its interpretation, system concept and harmonization of data layers only ensure the expected result based on real data connections. The root of the problem is definitely a systems science question: How do we group our data, how do we draw **system boundaries**? In fact, this is also the gist leading to network research: In a narrower sense, how do we group our data in order to examine environmental protection and, more broadly, sustainability; what do we consider to be the organizing principles of group training?

All science should have as the starting point the study of the **niche**. In the life sciences, this is a space defined by several dimensions of resources within which the life functions and survival of a population become possible, but it is by definition determined by a multitude of physical, chemical, and biological components. We

know that biotic factors are also influenced by a number of abiotic components, which are also separated by differences in research methods, dimensions and units of measurement between traditional, segregated disciplines. We can only overcome this with a new research methodology that favors the examination of spatial relationships, considering the data demands of group formation derived from a unified system concept as a guiding principle.

Meeting the social and economic needs of our society no longer affects only the natural foundations of our environment. We need to examine the interactivities and the processes that take place in the factors that determine our living space, touching on many fields of social and economic sciences too. The INSPIRE EU directive creates a need to use the tools and possibilities of our information society to examine our deeper knowledge of the complex conditions of society and its environment in order to preserve the life chances of future generations with as much orderly information as possible. The key to solving this problem is the **harmonization of data layers** provided by this system. The database organized into thematic maps is suitable for basing all decisions that affect ***sustainability*** by *building a multi-criteria decision support system* using real physical, chemical and biological relationships. (Balla K. et al.1999) The starting point of *exact environmental modeling* is that the relationships and processes to be examined take place in a **common space** – this is the **landscape** in the field of interpretation of the earth sciences. (Verrasztó 1979, 2017)

Consequently, we formulate the following objectives for the implementation of environmental modeling:

- The biologically, physically and/or chemically related processes are connected or can be connectable to each other, their spatial relationships should be examinable;
- Influencing factors and those affected can be examined, evaluated and collided together;
- Information and data sets arising from legal obligations (e.g. knowledge of the state of the environment) can be examined in coherent data systems;
- Both spatial and temporal changes can be examined;
- The causal relationships of the indications observed in the individual environmental characteristics should be examinable;
- The GIS system to be developed should be able to satisfy the needs of decision support of official decisions requiring, using and generating spatial data;
- The GIS system to be developed should be a uniform basis for the requirements of the EU regulations on the details of the field;
- The GIS system to be developed should be able to provide information to the widest possible circles of society about the state of the environment and its changes;
- The GIS system to be developed should be able to establish all the social decisions that promote the adaptation of the society to the environmental conditions or to its changes.

We saw all the objectives set out above as achievable by starting from the following premises:

- We start from the basic premise that "**environment = landscape**", so we consider the relationship system of landscape-forming factors as a governing principle in the system of physical/chemical/biological relations of influencing factors and the affected, incorporating into this system the effects generated by society as well;
- We strive to adapt to the system the widest possible range of information and/or data on the widest possible range of influencing factors, the affected and indicators;
- In addition to the nature and boundaries of protected areas that can be clearly and easily depicted on a map, we ensure the possibility of incorporating into our system the protected species and groups by elaborating their characteristic ecological needs;
- By matching the projection, raster and vector data of the basic elements of the information system to be developed, we ensure not only the territorial, but also the real spatial precision to ensure the examination of the real spatial relationships;
- We want to supply exact information to decision-makers by accepting and integrating the spatial needs, data, information and expectations arising from all the regulations and interests pertaining to all of the sectors;
- In order to support the different decision-making problems of decision-makers, the system must be able to manage different influencing factors, those affected, environmental factors and indicators together and in a selectively targeted way, in a map-based system and in a dynamic manner.

The complex spatial approach of DGIS is priority-free; the system implements the fullest possible unity of the used environmental information (maps, related descriptive data), so the system is able to give exact information to the decision-maker by displaying the spatial demand, data, information and expectations arising from the special examination methods, limit values, international obligation, regulation, and sectorial enforcement.

The query, analysis, and evaluation system developed in recent years is an efficient DGIS tool optimized for complex problem management. It is suitable for the comprehensive assessment of the state of the environment, for the modeling of possibilities and risks, for the exploration of hidden connections and values, and for the preparation for emergencies. Thus, in addition to a perceptible increase in efficiency (safety), not only can significant cost reductions be achieved, but *the known and important, characteristic data and known potential changes of the relevant factors of the entire environmental system can be integrated into a unified decision support system. This can support the specific demands of data and information of each decision level or competence with exact data, without compromising the examining need and possibility of the unity of the system.*

5. THE NEED AND POSSIBILITY OF INVESTIGATION OF DYNAMIC PROCESSES, ENVIRONMENTAL PROTECTION AND ENVIRONMENTAL SAFETY

Although industrial accidents in different parts of the world can be the result of technical failures, for example the one that took place at the chemical plant near the well-known Seveso or at Chernobyl, their consequences can be examined in the same way as the effects of either the eruption of the Eyjafjallajökull volcano in Iceland in 2010 or the accident at the Fukushima nuclear power plant. Not only is their interpretation and examination in the whole environmental system justified, but without the exact modeling of interactions all this is unthinkable. It follows from the scientific interpretation of the environment, the earth science logic of the concept of the environment, and the requirements of the European Landscape Convention, that the study of environmental safety must be based on a structured analysis of risks, analyzing

- the chances of natural risks in a given area;
- what is endangered by hazards of natural origin and how;
- additional hazards the future damage will generate.

In current practice, primarily due to the practice of social division of labor, there is a sharp separation between the tasks of *environmental protection*, the system of social and administrative rules, and the tasks of *disaster protection* [disaster managment] (environmental safety?). In complex systems, it would be no less important to examine:

- how (industrial) accidents (can) affect social and environmental systems;
- how environmental disasters (can) affect social and environmental systems;
- the physical, chemical and/or biological processes that they (can) generate;
- how we can prepare for prevention;
- how we can prepare for the defense;
- how we can prepare for remediation.

Safety as a need for a state free of danger often appears in relation to natural disasters. Approaching from this aspect, the possibility of disasters occurring, prediction of their consequences and forecasting play a role. In our opinion and suggestion, the method for this is also the **tool system of environmental modeling,** with special regard to *the possibilities of map-based decision support and the application of dynamic GIS.*

Starting points for the application of the multi-criteria decision support method (Balla K. et al. 1999):

1) Formulation of the goals as accurately as possible, verbally, in the decision-making forum responsible for solving the problem;
2) Identification of characteristics relevant to the objectives, relevant disciplines and decision-making levels as well;
3) Identification and investigation of environmental conflicts for *all* natural, social and economic relations and all concerned parts;
4) Examining the current situation in terms of goals, including
   - designation of the examination of the necessary parameters;
   - spatial delimitation of conflicts that can be identified with each field study;

- the scale and dimension of the factors to be examined;
- identification of external effects,;
- modeling of the dynamic processes to be studied (eg hydrological relationships, transport processes, ecological services, etc.);

5) Identification of control points and possible action plans and measures;
6) Modeling, including the study of mechanisms of action and the numerical forecast of characteristics for the given scenarios; in this context
   a) selection of possible propagation models for testing, and
   b) selection of relationships between relevant natural and social models;
7) The applicability of the models and the forecast of the impact of possible packages of measures;
8) Evaluation and comparison in the responsible decision-making forum of the packages of measures considering technical and economic aspects.

Naturally, in the case of significant changes, one can return to the same measures. The information system must therefore be able to meet the following demands:

- clear formulation of objectives;
- spatial and temporal documentation of the location of the influencing factor;
- identification of the mechanism of action of the influencing factor;
- possibility of spatial and temporal investigation of the influencing factor transport processes;
- spatial and temporal documentation of the location of the affected;
- identification of the mechanism of action of the affected;
- the possibility of spatial and temporal examination of the affected transport processes.

The database of the information system meeting the above requirements is expediently arranged in thematic maps. The structuring of the "Big Data" data set includes the possibility to evaluate the data components of the information obtained in any way possible, ie the data from either remote sensing or direct measurements, structured in a unified system, in their **context**. The possibilities of thematic cartography also ensure that the location, quantity and/or quality of the object or phenomenon characterized by the data is represented by a suitably selected point, line or surface symbol to interpret the relationship between each data set. Temporal changes are made possible by the mapping of successive state characteristics.

NATURAL PROCESSES – mainly PHYSICAL and/or CHEMICAL PARAMETERS – SPATIAL and TIME physical relationships (eg pressure differences and pressure and temperature differences, a significant part of which are due to eg level differences, where many dynamic factors are also important, but the "static state" characteristic of the "moment of time" characteristic of the basic state is decisive).

The most important elements of the dynamic changes of **SOCIAL COHESION**, typically in SPATIAL and TIME, were the research is focused on **cultural, religious, linguistic and historical** aspects, which are embodied in **traditions, folk traditions, legends, folk music and material folk art**. In essence, this is the "gene of society" (A. Faust 2020). The concept of **the COMMON SOCIAL SPACE** fills the objective

space of the LANDSCAPE that can be studied by natural sciences as well, in which the past, the evolution and the present of a **multitude of common actions, beliefs and constructions** provide the points of connection, the possibilities of group formation.

ECONOMIC COHESION is characterized by SPATIAL and TEMPORAL relationships and changes, partly by static and partly by dynamic spatial- and temporal factors. Arguably, the **group organizing principles** of these are the **historical relations**, the **natural and social resources**, the **political-, institutional-, logistical relations**, the **resources of raw materials** and the **division of labor**. We can clearly see that all of these change in space and time. A good example is the transport problems in today's Slovakia, which result from the fact that the historical administrative units and borders influenced by the topography were "reshaped" with "one-sided" decisions satisfying current political needs.

Animation has long been known in modeling dynamically changing factors, even when evaluating natural, social, or even economic processes. Animation is essentially a visualization that provides the ability to structure data on demand. This can be based on historical maps to examine the **basic state** and environmental needs. We suggest that, where available, this should refer to environmental status characteristics recorded in Military Surveys. We are aware of the urbanization, infrastructural, industrial and technological changes that have taken place in the environment since then, and the environmental consequences of all this are everywhere around us. Consequently, all the *influencing factors* that we experience in the *consequences* related to the basic state in the present environmental state can be examined in an exact way.

Animation is excellent for illustrating the spatial interconnection of data characterizing known processes and temporal changes, such as

- propagation of flood and inland waters resp. atmospheric phenomena (direction, speed)
- spread of pollutants in water or air (direction, speed)
- dangerous or endangered factors, risks of objects.

As a result of significant methodological development, the method of modeling beyond the possibilities of animation was implemented to forecast the disaster management risks of Bódva and then Hernád.

As already mentioned, our starting point for the environmental baseline is the map of military survey. We consider the connection – in a system – of environmental indicators as well as of the influencing factors and the affected to be the methodological basis of our development. In the current practice, the lack of this complicates such modeling of the natural processes taking place in the affected area – e.g. flood events resp. their possible technical details and/or accidents, e.g. the rupture of an embankment – that allows for specific local, on stop, and/or individual decisions.

The theoretical basis of the model is the spatial study of the determining physical factors – positional energy, compressive energy and kinetic energy – in the GIS system together but separately. The amount of water flowing from cell to cell is calculated. The flow rate of water is obtained by multiplying the velocity by the cross section. If the cross-section is taken as the total surface of one side of the entire water

column, the outflow velocity must be averaged, since at the top of the water column it will be 0 m/s and maximum at the bottom.

The input parameters are essentially physical data that characterizes a cell. The dimensions of the cells determine the accuracy of the model. In the system we developed (Bódva and Hernád) we calculated the pressure of 1 m^2 cells, which results in 75% accuracy in the model. If we were to increase this to decimeter accuracy, we could expect 90% accuracy – but slowing down computer capacity would make this impossible.

For other natural-science-based landscape forming factors we can ensure, for example, the harmonization of the system by animating the ecological changes of the living world over time.

In order to study the relationship between natural, social and economic processes in the landscape with the demand of systems science, the structuring of data systems and group formation is of special importance. We suggest that this should be done on thematic maps, drawing particular attention to the fact that data generated by statistical methods often obscure the point.

This solution also makes it possible to coordinate technical interventions for flood protection with the requirements of the ecological criteria set out in the Water Framework Directive. In addition, we modeled scenarios for the expected events that would take place in the floodplain on the saved side, requiring disaster management interventions. The multi-aspect study of dynamic processes in the same space satisfies specific practical demands.

It must be taken into account that the water of streams, springs, and canals connected to the river and flowing into it will rise with its water level. Flooding can result not only from the main river but also from its tributaries. We also have to reckon with phenomena originating outside the river that affect the change in water volume. Prolonged, heavy rain can raise the water level in the floodplain by several centimeters, and sinks can turn into karst springs. Previous significant rain soaking the otherwise dry area can prevent the body of water entering the area from infiltrating the soil. High heat can increase evaporation. Strong, stormy winds can affect the speed and direction of water flow, so we have to take into account the weather factors as well.

The basic condition of the logistics modeling that is part of the project is the accurate knowledge of the natural factors, since in case of a rupture of the embankment, the water flowing to the protected area (here: saved side) flows to the lower areas and in the bays. In addition to topographic factors, the flow rate is affected by a number of factors. For example, infiltration and/or runoff conditions, surface conditions, undergrowth, bushes, forest strips, roads, embankments, drainage channels, caves, sinks, springs, soil characteristics, meteorological conditions, e.g. rain, freezing, water saturation, etc.

The speed of the flood wave flowing through the field depends on the conditions of the soil surface, the height and density of the vegetation, and the amount of sediment brought together. In settlements, structures such as buildings, cellars, roadside ditches, temporary barriers, or dams also affect the flow rate, they can change the amount of water absorbed. The situation is different in the field, where

there may be a few centimeters of cultivated plants or one and a half meters of dense vegetation. These can vary from month to month – however, it is essential to take into account the location and needs of the protected objects or objects to be protected – this is how the task of environmental safety and environmental and nature conservation are linked.

As we can see, the essential expectation of the logistics model is the knowledge of the landscape-forming factors that determine the spatial processes taking place in the environment. The accuracy of the 4D model depends on their exactness. Monitoring flood processes requires the existence of a harmonized, spatial database covering the entire river basin, the creation and harmonization of which was a key part of the project. (Balogh et al. 2015, 2017; Németh et al. 2015) The input parameters are essentially physical data that characterize a cell. The dimensions of the cells determine the accuracy of the model. In the system we developed (Bódva and Hernád) we calculated the pressure of 1 m^2 cells, which results in 75% accuracy in the model. If we were to increase this to decimeter accuracy, we could expect 90% accuracy – but slowing down computer capacity would make this impossible.

Our aim with this GIS system was to monitor the flooding situations and their potential consequences during the expected flood events in the Bódva and then Hernád river basin districts, including the modeling of the local, ad hoc and specific consequences of possible embankment ruptures. This is the basis for defining the necessary and possible tasks of disaster management, for making the necessary and possible decisions minute by minute. With the successful implementation, we have significantly contributed to the application of modern IT solutions in environmental security tasks requiring multi-faceted decisions, thus increasing the efficiency of protection tasks, as well as facilitating practical efforts to unify the European Information Space (INSPIRE) through cross-border cooperation.

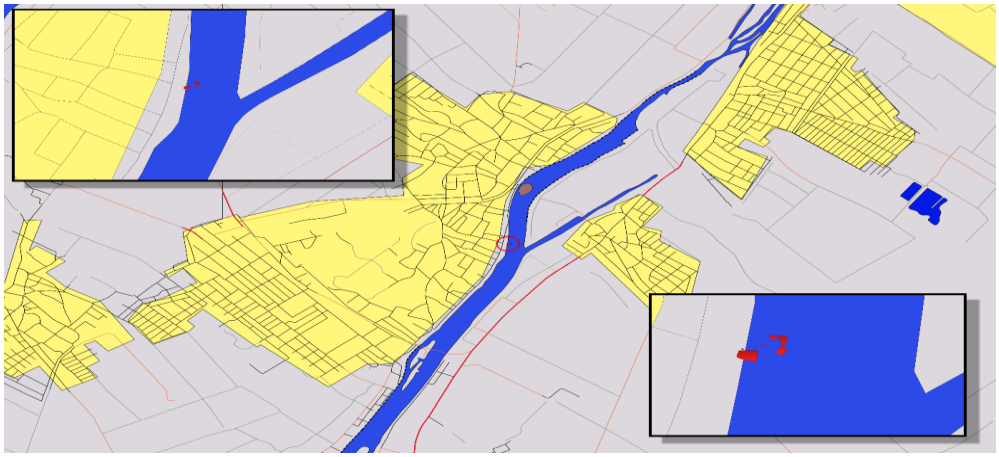

Map 1. *Szigetszentmiklós and the strictly protected floating bog endangered by pollution (using the Fishing Map of the Ráckeve Danube Anglers' Association and the habitat map of the Danube-Ipoly National Park Directorate)*

To the south from Budapest, on Csepel Island (at Szigetszentmiklós), the damage control of one of the most significant environmental pollution events of recent years and the search for those responsible are still in progress at the time of writing these lines. Thousands of liters of used oil spilled on the island, close to the shore, severely damaging the extremely valuable wildlife of the Ráckeve Danube Branch regulated by sluice from both upstream and downstream.

This outline map visualizes the location of the pollutant, but also shows that when loaded with appropriate data (e.g. oil-using industrial activity) it could help to identify potential culprits. Additional logistical information is essential for planning damage control, hydro-geological information can highlight the vulnerability of groundwater and plotting the flow conditions of the river can help by modeling the spread of the contaminant.

6. CONCLUSION

Our biological and social existence takes place in a space from which we draw our resources and in which we place our wastes of various consistence. The technical possibilities of our time involve the treatment of waste that does not decompose naturally or only in an extremely long time, and the population explosion and the needs of our urbanized society result in huge amounts of foreign substances. "Overshoot Day" warns society year after year of the unsustainability of the current natural, social and economic way of life.

The changing interpretation of the concepts and the different approaches of different disciplines consist the methodological obstacle both to the control of the processes taking place in the landscape as a space and to the exact examination, modeling and planning of sustainability.

According to our proposal, the geological landscape – in practice a river basin – can be defined as a spatial unit suitable for system control, in which we build the "Big Data" data set into the thematic overlay map system, laying the foundations for a dynamic application of GIS and spatial multi-criteria decision support system and application data upload.

As early as 1974, before Lovelock's GAIA theory, Elemér Szádeczky-Kardoss recognized and formulated the taxonomic connections of the unified operation of the Earth, and the application of the spatial multi-criteria decision support system and dynamic GIS ensures its practice and the joint modeling of natural, social and economic components of sustainability.

REFERENCES

[1] Balla, K., Kéri, G., Németh, E., Rapcsák, T., Sági, Z., Tóth, T., Verrasztó, Z. (1999). Water quality modeling of the Ráckeve (Soroksári) Danube branch using multi-criteria decision methods. *Szigma*, 30, pp. 135–159.

[2] Mikoviny, S. (1732). Selmecbánya's topgraphics map. Epistola de methodo concinendarum mapparum Hungariae, Pozsony, p. 76, 3.

[3] Balogh, I., Benkhard, Á., Csikós, A., Lipták, A., Németh, R., Verrasztó, Z. (2015). GIS decision support system for the Bódva catchment area. *Protection Disaster Management Review*, June 2015, 4, pp. 10–12.

[4] FAUST JNNÖ Conference presentation (2020).). *Annual General Meeting Closing Conference* – Presentation Budapest, 6 June 2020.

[5] Németh, R., Verrasztó, Z. Csikós, A. (2015). Flood GIS decision metodology for the Bódva catchment area. *HUSK Bódva flood model project final conference* – presentation, Miskolc, 18 September 2015

[6] Csikós, A., Gercsák, G., Márton, M., Németh, R., Verrasztó Z. (2015). Map decision support: case study for the Bódva catchment area. *Geodesy and Cartography*, 2015/7–8., pp. 22–27.

[7] E. Dudich (ed.) (2003). *GEONOMY after the turn of the millennium*. Hungarian Academy of Sciences Subcommittee on Geography, Budapest, pp. 1–199.

[8] Kiss, J. (2014). Plate tectonics, volcanism and the map of the Carpathian-Pannonian region geomagnetic anomaly. *Hungarian Geophysics*, 55/2, pp. 51–81.

[9] Klinghammer, I., Verrasztó, Z. (1994). *Environmental characteristics of the Ráckeve resort area (thematic atlas)*. KDV Environmental Inspectorate – Department of Cartography, Eötvös Loránd University, Budapest, p. 28.

[10] Miklós, L., Németh, R., Verrasztó, Z. (2014). Application of GIS in studying the drainage basin of the Ipoly river. *Scientific Annals of the Danube Delta Institute*, Tulcea, Romania (20), pp. 109–128.

[11] Németh, R., Dobos, E. (2015). Flood Model for the Bódva Catchment. *Landscape and Environment*, 9 (1), pp. 12–26.

[12] Rapcsák, T., Verrasztó, Z. (2002). Decision and environmental modeling. *Experts of Economic Modeling: Conference*, Balatonfüred, pp. 37–38.

[13] Rapcsák, T. (2009). Multipurpose decision support. *Applied Mathematical Journals*, 26, pp. 129–142.

[14] Zádeczky-Kardoss, E. (1974). *Geonomy*. Geochemical Research Laboratory of the Hungarian Academy of Sciences, pp. 1–192.

[15] Teleki, P. (1917). *The History of Geographical Thought*. MTA chair inauguration speech, Budapest. 1917.

[16] Verrasztó, Z. (1979). Land formation and the geological aspects of environmental protection. *Symposium Changes of the geological environment under the influence of man´s activity*, IAEG Nation group, Krakow–Sandomierz–Belchatow–Plock–Warszawa, pp. 135–141.

[17] Verrasztó, Z. (2017). Holistic environmental modeling using cartographic, GIS and remote sensing methods. *Rs & Gis - Journal of Remote Sensing Technologies and GIS*, 7 (1), pp. 490–516.

[18] Verrasztó, Z. (2018). Geonomy – Currentism and Environmental Modeling. *XIV. Environmental Science Conference*, Gödöllő, Apr. 2018. 5–7, pp. 369–373.

[19] Verrasztó, Z. (2019). Environmental science – from geographical thought to geonomy. *Geographical Bulletin*, 3, pp. 67–76.

Geosciences and Engineering, Vol. 9, No. 14 (2021), pp. 78–80.
https://doi.org/10.33030/geosciences.2021.14.078

AUTHORS' COMMENT TO
THE TOPICALITY OF GEONOMY paper by

RÓBERT NÉMETH[1, *] – ZOLTÁN VERRASZTÓ[2]

[1]*ALFÖLD System House, Szolnok, Hungary*
[2]*Middle-Danube Regional Environmentl Authority, Budapest, Hungary*
[*]*alfoldgis@gmail.com*

Dear Editor,

We received your reviewer's opinion regarding our article "The Topicality of Geonomy", on the basis of which we formulate our answer as follows:

Today, in practically all natural sciences (and even beyond!), there is – quite rightly so – a system of environmental relations, crosstalk, and demand, but these were (are) not built into a scientifically formulated environmental system approach. It is mandatory to ensure the publicity of environmental data in all EU Member States – however, the concept of ENVIRONMENT is undefined, and the nature of environmental data is the basis for legal disputes. The significance of this is crystallized in the application of IT technology: without an exact definition, digital data management is unsolvable; we cannot ensure the expectations formulated in the INSPIRE directive with a variable interpretation. Exact data interpretation is the basis for the management and organization of environmental data and for group formation, which is indispensable in network research – environmental modeling in our practical use.

As we have pointed out, in practically all natural sciences there is a scientific crosstalk, demand oriented towards environmental relations, but these were (are) not built into a scientifically formulated environmental system approach. Although this leads to great new discoveries in the relevant natural and social sciences, if the results of these cognitions and recognitions were (are) not integrated into the system approach to the unified environment, they remain unknown in environmental protection, while they exist on the periphery within their own field of science. But the need for integrative knowledge a unified scientific approach, a systemic basis is absent – which was already formulated by chairholder Pál Teleki in his Academic Inaugaration speech "The History of Geographical Thought" in 1917. The sciences have been segregated since then – in the ingenious wording of Konrad Lorenz, "we know more and more about less and less – until eventually we will know everything about nothing". In addition to its historical value, Szádeczky's GEONOMY can provide this as the basis of environmental science. That is why it is important to build on this. There is no literature on this outside of Hungary.

As for the significance of the scientific history of geonomy, it is important to mention that Elemér Szádeczky-Kardoss's scientific concept – which has since been forgotten – preceded the recognition and formulation of a unified system by Lovelock's well-known GAIA theory, and that the (Hungarian Academy of Sciences) (MTA) set up a special committee for its actualization in 2003. In addition, Professor Szádeczky built his scientific basis in Miskolc, another reason why it would be important to prove its relevance in your publication.

The reviewer's opinion also expresses the criticism that we did not rely on the extremely extensive international literature on GIS technology, nor did we refer to it in our paper.

Regarding this, similarly to the above, we need to point out that we are aware of and strive to gain knowledge of the results of this technology, and consequently we see that they are primarily aimed at solving and illuminating problems of application techniques. They ignore all the foundations of professional philosophy without which progress in the interpretation and modeling of the dynamic environmental SYSTEM cannot be made. (What is the environment? What are the environmental data and how are they related to each other?) Therefore, it was of great importance that we were able to publish the methodology of data collection and data sorting in Geodesy and Cartography, proving its functionality with practical, disaster management results. We also think it is important to mention here that this specific disaster management application for the Bódva river basin was also the result of our joint work with the University of Miskolc.

This method and system is suitable for fully satisfying the different data management needs and expectations of different disciplines with the possibility and need to study the processes and relationships taking place in the same space – the importance of which is well proved by the work of Hungarian researchers, notably of Tamás Rapcsák.

Please allow us to add a few words about a major figure in this area, Tamás Rapcsák (1947–2008). References given here can be found in the publication list attached to the obituary of Tamás Rapcsák that appeared in *Alkalmazott Matematikai Lapok* [Volume 26 (2009), pp. 129–142], available at aml.math.bme.hu/wp-content /uploads/2014/03/26-Rapcsak.pdf. In addition to working on decision support and expert systems and contributing to theoretical and methodological research work on spatial decision problems, Tamás Rapcsák was also happy to take part in working on applications. He was also involved in engineering sizing [27], production planning [32, 34] and transport optimization [58, 59, 65] projects. However, his most successful field of application is considered to be applications related to decision support systems.

Research in the field of decision support and expert systems began at the SZTAKI (Institute for Computer Science and Control) Operations Research Department of the Hungarian Academy of Sciences in the second half of the 1980s [45]. This research work continued on the WINGDSS system later developed by the Department of Operations Research and Decision Systems, which he led [46, 48, 55, 56, 57]. The software and the methodology behind it can be applied in decision

situations where a group of decision makers has to evaluate and rank several alternatives according to several aspects. Rapcsák led several application projects in which the developed methodology and software were also used. The range of applications is wide, from supporting decision-making in government and enterprise tendering [47, 51, 70, 82, 84, 103] to modeling and solving complex multi-faceted environmental and spatial problems [64, 74, 75, 76, 78, 83, 85, 90, 98, 101, 115].

In connection with multi-faceted environmental and spatial decision-making tasks, the name of Zoltán Verrasztó (Central Danube Valley Environmental Inspectorate) must be mentioned, who provided the professional background in many joint projects. He and Tamás Rapcsák recognized that environmental decision-making tasks are essentially multi-faceted decision-making tasks, as environmental aspects such as water, air, noise, vibration, etc. should be taken into account, among other social, economic and financial aspects. Multi-faceted environmental applications have also opened up new directions for development. GIS systems have been shown to be an effective tool for collecting information for the decision task, displaying it on a map, and examining time-dependent dynamic relationships. Developments and applications related to multi-faceted decision support have also raised important theoretical and methodological issues.

Together with Tamás Mészáros, Rapcsák developed an effective sensitivity test method [66, 102]. He co-authored an important article with Saul Gass (University of Maryland) on the synthesis of group decisions [71] and the application of singular value resolution in the AHP methodology [96]. Together with his student Sándor Bozóki, they investigated the inconsistency of pairwise comparison matrices [110].

With the above information, we hope to prove that the methodology we recommend for environmental modeling is an innovation based on Szádeczky's system approach – based on the concept of geonomy – and utilizes the possibility of GIS technology to study relationships in real space, which has no international literature.

Geosciences and Engineering, Vol. 9, No. 14 (2021), pp. 81–95.
https://doi.org/10.33030/geosciences.2021.14.081

DEVELOPMENT OF UNDERWATER SURFACE MEASUREMENT – MULTIBEAM SONAR

ZOLTÁN EKE[1, 2] – ISTVÁN HAVASI[2, *]

[1]*System Design Department, Bay Zoltán Applied Research Public Benefit Nonprofit Ltd.,*
[2]*Institute of Geophysics and Geo-Information Science (IGGIS), Department of Geodesy and Mine Surveying, University of Miskolc, gbmhi@uni-miskolc.hu*
[*]*gbmhi@uni-miskolc.hu*

Abstract: This study was written in the title theme as a result of the cooperation between the staff of the departments of the two scientific institutions mentioned above. Its first author is also a PhD student of the IGGIS. This year the Bay Zoltán Applied Research Public Benefit Nonprofit Ltd. has purchased a Norbit-iWBMSe multibeam ultrasonic system. The primary purpose of this paper is to describe a multibeam ultrasonic system (Norbit-iWBMSe) and to examine its useful application for mine surveying purposes, particularly for measurements used in underwater mining situations, such as the official determination of the amount of the extracted mineral resources, which also serves as the basis for determining the payable annual mining rent. In our study, first, we will briefly review the new surveying technologies which have appeared in Hungarian mine surveying recently and are likely to be used more and more in the future. Then we will deal with the history of underwater topographic mapping. Afterwards the multibeam sonar survey device and its advantages will be discussed, and two waterbed surveying examples from our own practice will be shown. Finally, the legal background of mining volume computation will be briefly described. Furthermore, it is important to highlight the role of multibeam sonar in mining exploitation process.

Keywords: *new surveying technologies, mine surveying, volume computation, history of bathymetry, single-beam sonar, multibeam sonar, mining volume computation, relevant legislation*

1. CHANGES IN MINE SURVEYING TECHNOLOGY

It is known that the extraction of mineral raw materials, and even mining planning, must be based on reliable and accurate spatial data. These are provided by mine surveyors for each mining company and mining entrepreneur. Their most important tasks include but are not limited to the accurate survey of the excavated areas, the precise determination of the quantity (stocks) of various materials, the representation of the surface and underground spatial position on the various mine maps, mining plans, etc.

Today, new opportunities and challenges are arising in mine surveying, as several new survey methods are being applied and systematized [1]. What are these? Ground-based laser scanning; UAV (drone)-based aerial laser scanning and aerial photogrammetry; ultrasonic measurements; and USV (Unmanned Surface Vehicle)

sonar systems, that is to say, "vehicles" for unmanned aerial or waterborne transport to which sensors or devices using various surveying technologies can be installed. Terrestrial Laser Scanning (TLS) is an alternative which automatically produces a large amount of spatial information (a dense 3D point cloud) relative to the location of the scanner. Consequently, the method is suitable for determining the spatial changes characterizing the progress of mining activity over time, thus for calculating volumes, as well as for studying movements and deformations in a mine, and for documenting unfortunate accidents. Although the investment price of TLS is steadily decreasing, it is still quite high. Recently, more and more mining companies have also started to use UAV-based aerial photogrammetry. These aircraft (drones) have state-of-the-art digital cameras which allow high-resolution aerial photography. By processing these digital images, several valuable survey products (e.g. orthophoto map, point clouds, 3D models, etc.) can be produced. Thus, this measuring procedure can also facilitate the performance of mining and mine surveying tasks, such as exploration; surveying stockpiles, or tracking time-varying processes. Combining UAV with LIDAR (Light Detection and Ranging) can also support the implementation of several mining monitoring activities (e.g., environmental, mining, etc.). In connection with technologies based on unmanned aerial vehicles, however, it is necessary to mention the dependence on weather, the relatively high cost of LIDAR equipment, the environmental and other constraints associated with the application, and the required expertise. Portable laser scanners are much more affordable and can be a solution mainly to facilitate certain tasks of underground mine surveying (e.g. surveying inaccessible areas).

2. DEVELOPMENTAL HISTORY OF WATER DEPTH MEASUREMENT AND SINGLE-BEAM SONAR

Water depth measurement, known also by the Greek word bathymetry, means the measurement and mapping of the surface under different waters (e.g., the seabeds, lakes, and riverbeds). Products from this survey include, for example, depth lines connecting points of the same depth, a depth-coloured bed map, or a bottom-bed Digital Terrain Model. These can then be used for a number of purposes, including safer water, underwater transport, or underwater mining, which is the most interesting to us now, and the computation of mineral raw material stocks using time-varying bed surfaces associated with it.

Mapping of the Hungarian surface waters dates back to the 18th century. In the second half of it, regulation of our larger rivers (the Danube and the Tisza) began, and this was accompanied by remarkable mapping results. Studying the change in our water network was formerly – and still is today – an important research theme. As for the technological development of riverbed survey and water depth measurement concretely, it is important to examine the method of determining the spatial location of the survey points related to the route of a watercraft moving above the surface to be mapped (e.g. surveying with a total station, RTK GPS technique) and the depth surveying procedure adapted to these points. Let us focus now on the

latter. In the past, a rope/wire loaded with plummets/weights was used for this purpose. In this method, the accuracy of the measurement was significantly affected by currents and vessel movement. This was later replaced by the fish radar. Today, either a sonar device is used for this task, which is mounted under/next to a boat, or a LIDAR sensor may be installed on a device flying above the water (mostly on a drone). The sonar records the created sound wave(s), while LIDAR records the reflection of light from the bed. Here we only deal with the sonar approach.

The depth measured with a sonar can be calculated by the following formula:

$$\mathbf{D} = \frac{\mathbf{1}}{\mathbf{2}}\mathbf{v} \cdot \mathbf{t}$$

where *v* is the propagation velocity and *t* is the travel time.

The use of single-beam sonar (SONAR Mite SPX in this example) for bed surveying is described in [2]. In this we gain a detailed insight into the riverbed survey of Lake Bánki, which is 60 km from Budapest and has an average depth of almost 4 m. The measuring system used here consisted of 3 main units. These were a single-beam sonar (transmitter and main unit), a RTK GPS receiver and a data acquisition unit (portable PC), to which the former two were connected. Among the technical data of the sonar measuring instrument, it is worth mentioning its small size and weight, easy handling, the measuring limit up to 75 m, and the approximately 20 cm depth measurement accuracy.

Before starting the measurement, the instrument was fixed to the side of a boat, making sure that its probe was a few centimeters below the water level (taking into account any tilting of the water craft). Considering the progress of the measurement and the nearly regular survey grid, parallel lines at intervals of 4 m on a land office map were designated to measure the depth of the inner part of the lake, and this was supplemented by a survey of parts close to the shore. As the nature of the water of the lake to be measured (in this case it was fresh water) and its temperature affect the velocity of the sound waves, this was taken into account by the surveyors with a correction factor.

When processing the survey data, the y, x and z coordinates of each survey point measured by RTK; the water depth obtained with the sonar; the depth offset value (RTK-GPS-sonar distance) and the average water level correction were taken into account. Further evaluation was then performed in a GIS environment (Quantum GIS), providing visualizations such as a Triangulated Irregular Network (TIN) model (treating the lake shore as 0 depth), a depth-line diagram, or a layer-colored bed map.

The brief description of measuring the mining lake bed with a modern single-beam sonar [2] is relevant further highlight the new possibilities and benefits associated with the multi-beam sonar, which is the backbone of our study.

3. INTRODUCTION OF NORBIT-IWBMSE MULTIBEAM SONAR, PRACTICAL APPLICATION EXAMPLES

In the field concerned (in this case: mining), the multibeam sonar surveying tool is suitable for the efficient solution of a wide range of problems that arise, coupled with significant measuring capacity and flexibility. Bay Zoltán Applied Research Public Benefit Nonprofit Ltd. is one of the first Hungarian service providers to have this modern sonar system. Accordingly, we consider it important to provide convincing information about the surveying instrument, as well as to describe the essential characteristics of surveys carried out with it. In the present study, comparing this multi-beam ultrasonic measuring device with the sonar ones already common in practice, its most important features will be highlighted. These are the following [3], [4]:

1. guaranteed high surveying accuracy;
2. efficiency;
   a. high measurement resolution, huge amount of data (point cloud) (15,000 points/sec is possible), fast surveying, shorter measuring time, less vehicle revolutions than with single-beam sonar, with significantly higher measuring accuracy,
   b. a significant number of parameters which can be adjusted according to the purpose of the measurement,
3. mobility.

More detailed information on these features is provided below.

1. Units of the multibeam survey system which ensure guaranteed measuring accuracy:

- the sonar system also includes two GPS antennas capable of receiving RTK corrections and an integrated GPS receiver;
- the inertial unit (acceleration sensors, angular velocity meters) for elimination of factors influencing surveying accuracy on water (rotation about the spatial axis X, Y, Z, namely rocking of the boat “rotation in place” back and forth, right and left, and the change in height due to waves;
- the unit for determining the speed of sound propagation (sound speed meter) for determination and correction of different physical parameters (temperature, water pressure, speed of sound) necessarily resulting from the depth of the water column above the riverbed (water depth) in the water medium to be measured, as an external unit, and an additional one integrated in the sonar body so that the shape of the emitted measuring signal corresponds to the surveying parameters;
- the Sonar Interface Unit (SIU) collects sonar, inertial unit, sonic speed meter data, calculates depth surveying data, and automatically performs corrections;
- special software to control the measurement and perform data processing, to define the surveying parameters appropriate to the purpose of the planned measurement (simple bed survey; detailed, high-density bed survey or inves-

tigation of a pipeline, possibly sunken objects such as hull search for a vessel), and to edit and convert surveying data (point cloud, up to a few cm^2 resolution).

2. Efficiency
- In contrast to the single-beam devices accepted and used in practice in Hungary (which only work with one test signal at a time), this measuring system works simultaneously with up to 512 test signals/separate radii in a fan-like arrangement;
- With the help of a large number of emitted test signals, it has a very wide measuring zone, even in the lateral direction, so that the coastal strip of surface waters can be surveyed, which is often an areas that a boat can only reach with great difficulty or not at all. Thus, no other (terrestrial) surveying method is required to determine the coastal strip;
- After starting the parameterized measurement, no operator intervention is required, as the measurement and correction are taken into account automatically;
- The survey speed is high. It is capable of emitting the test signal at a maximum frequency of 60 Hz for all 512 signal sources. This frequency may even change automatically depending on the water depth; therefore the sonar system is able to provide the highest expected measuring resolution without intervention. The frequency of the emitted signal can be adjusted between 200 kHz and 700 kHz, and the practical depth measuring range is from 1 m to 250 m;
- By changing the surveying parameters on the sonar units, it is possible to improve the device according to the purpose of the measurement, so the required time for surveying, the measured amount of data and, in this connection, the amount of post-work in the office can be optimized.

3. Mobility
- Despite the multiple units which ensure the required surveying accuracy, the device is characterized by compact size and weight;
- The measuring device can be mounted on the vast majority of boats and smaller vessels used in practice, so it is not necessary to transport it fixed to a boat, since it can be mounted on a watercraft available at the survey location.

The excellent signal processing sonar and the state-of-the-art GNSS which form the basis of the depth surveying and navigation systems, and the inertial system complementary to the RTK, result in reliable depth measurement and driving stability. With a multibeam sonar, a large number of bed points are measured in a short time, so that a much more accurate model of the river/lake bed topography can be produced.

The survey diagram which can be associated with the measuring device and its parameters can be seen in *Figure 1*.

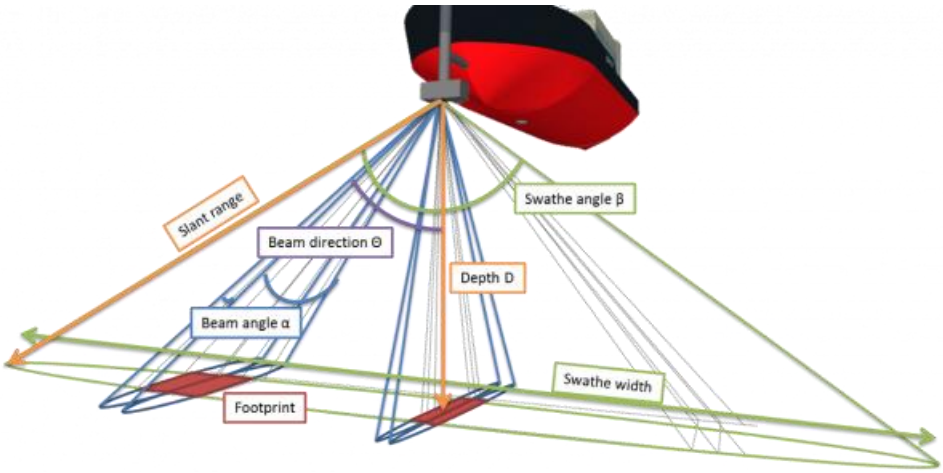

Figure 1
The multibeam sonar (survey diagram + parameters)
https://www.hydro-international.com

Here the above parameters supplemented with some explanations are briefly overviewed:

Depth – *the measured data*,
Slant range – the maximum of line-of-sight distance along a slant direction between the vessel and the area to be measured,
Swathe angle – the width of the measuring band, the angular range of the receiving angles of the sensors (hydrophones),
Swathe width – section of the receiving angle range of the sensors formed with the bed bottom (sensing band of the sonar),
Beam direction – the orientation and location of the signal sources (usually at the same distance or with equal angular deviation, but there are other options as well),
Beam angle – the angle of narrowing of the emitted signals (it can be 512 at the same time), the extent of this largely determines the horizontal resolution of the sonar,
Footprint – the common part of the cross-section of the measuring signals with the river or lakebed (blue ellipses) and the cross-section of the sensor receiving angle with the just-mentioned bed (larger green ellipse): the red rectangles. This is the horizontal resolution of the sonar. As a result, we get just one depth data from an area of a red rectangle.

The width of the described sonar measuring band/adjustable angle range of the receiving angles of the sensors: 5° to 210°; depth measuring range: 0.2 m to 275 m and the angle range of the resolution for the standard operating frequency (400 kHz) is 0.9° to 1.9°. The specified operating temperature range is –4 °C to +40 °C.
In the following, we briefly describe the main units of the multi-beam sonar system, which is the subject of our study, and the preparation of the measuring device

mounted on the boat *(Figure 2)* for the bed survey, which we illustrate with several photos *(Figures 2–11)* thereby making it even more understandable.

Figure 2
The multibeam ultrasonic measuring installed for bed survey

The survey equipment includes the following:

- 2 GPS antennas, which are placed on the support frame during the measurement,
- a sonar head *(Figure 4)*, which is also mounted on the frame (this frame must be attached to the boat),
- an interface unit (with interface, a GPS unit for receiving RTK correction, and an integrated inertial unit),
- a mobile hotspot, a telephone for internet connection,
- a sound speed meter,
- a control laptop with the necessary software,
- the powered battery and an inverter.

Several of the system components listed above can be seen in *Figure 3*.

Figure 3
The sonar instrument and its accessories in the carrying case

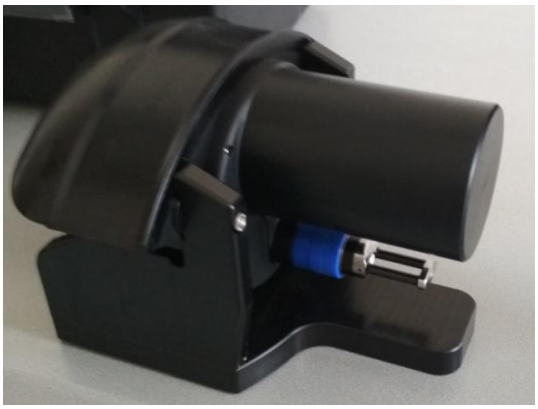

Figure 4
The Norbit-iWBMSe sonar head unit

A very important instrumental unit of this ultrasonic measuring system is the *interface unit*, which can be seen in *Figure 5.*

Figure 5
The Sonar Interface Unit (SIU) with the connecting cables

The sonar (bottom left), two GPS antennas: Ant1 and Ant2 (top left), the Ethernet connector for communication with the control computer, and the power cable are connected to the interface unit shown in *Figure 5*. This ultrasonic system unit connects to the multi-beam sonar unit and GPS antennas, performs the NTRIP correction processing, and handles the integrated inertial unit. A schema of the complete system is shown in *Figure 6.*

Before starting the bed survey, we also have to deal with the role of the sonar control software *(Norbit Graphic User Interface)* in the measurement preparation and the initialization of the inertial unit.

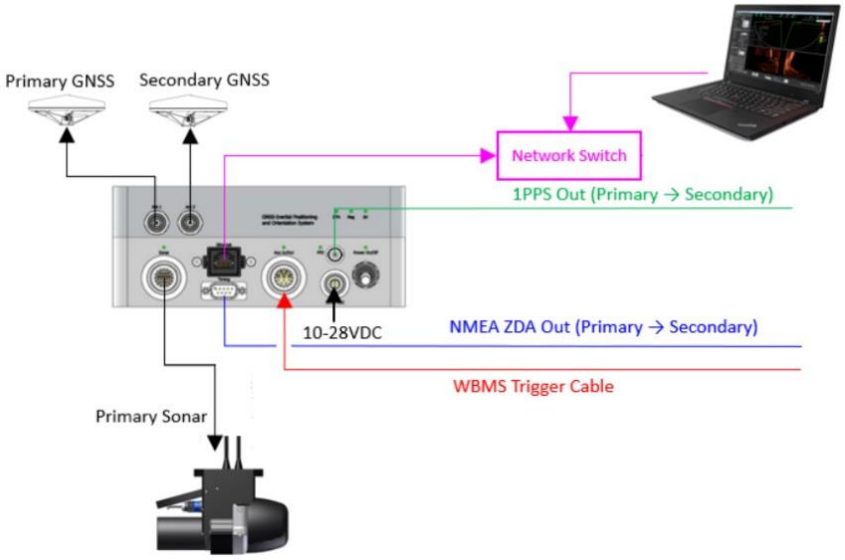

Figure 6
The schema of the sonar system

The sonar is set up and parameterized on a graphical interface, which was created by the manufacturer specifically for the given device. In this software, we can modify the measuring parameters within the range of the survey device, according to the purpose of the measurement and the existing conditions. Once the cable connections and power supply are ready, the ethernet connection between the sonar and the computer controlling it must be set up, and then the frame parameters (antenna distances from each other and the sonar) can be specified *(Figure 7)*, but the RTK correction setting is primary *(Figure 8)*.

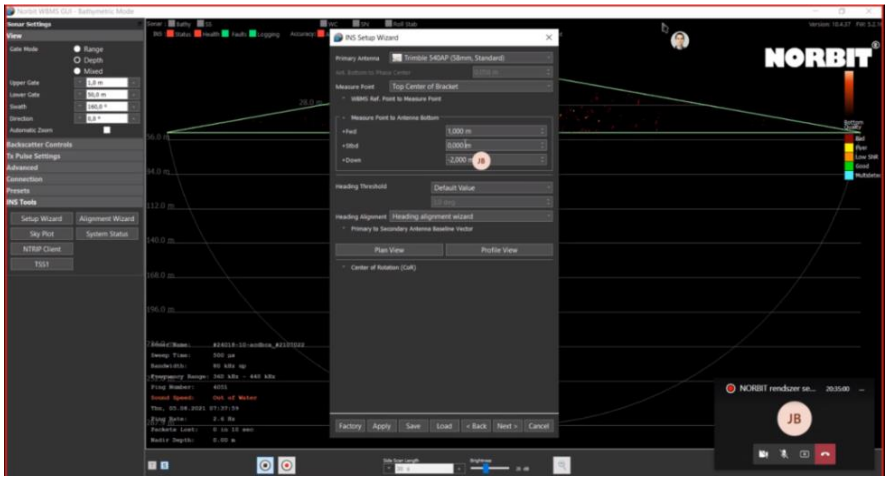

Figure 7. *Setting the frame parameters*

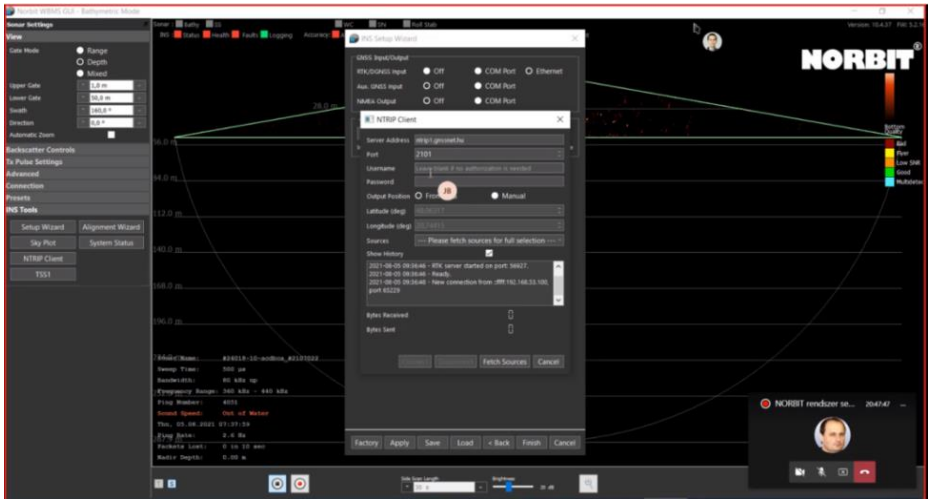

Figure 8
Setting the RTK correction

Then we can set the survey parameters, the most important of which are the depth range to be tested; the opening angle of the sonar "umbrella"; the angle of rotation; the survey frequency; the number of measuring pulses, their geometric arrangement; and the signal strength *(Figures 9–11).*

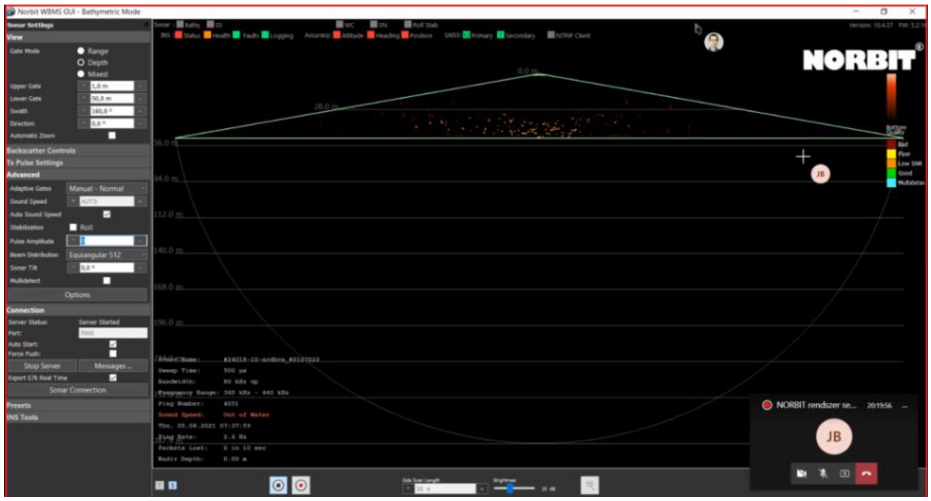

Figure 9
Survey image of the connected sonar in control application

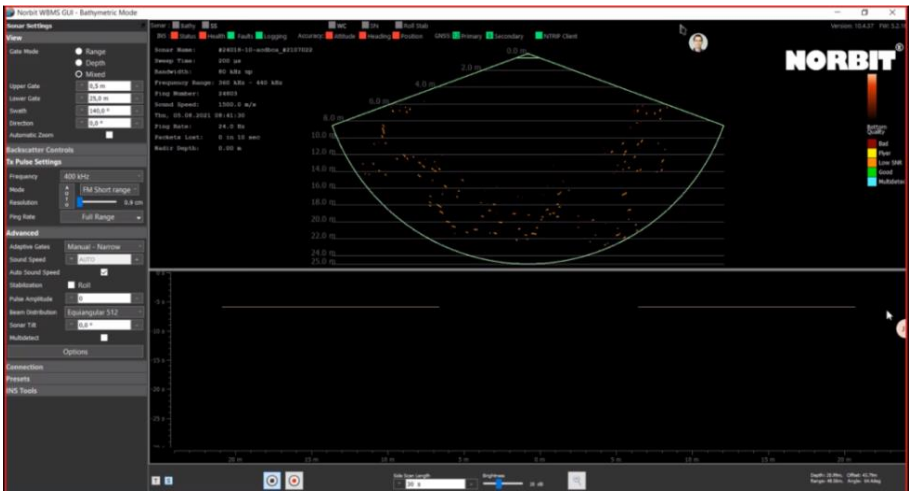

Figure 10
Survey image of the connected sonar in control application with a smaller "umbrella" opening

Figure 11
Measured image of the connected sonar with a rotated "umbrella" in control application

The next step is *to start with the parameterized system* and then *initialize the inertial unit (Figure 12)*. In the latter, the so-called laid-out octagonal shapes must be traversed continuously by the boat until the inertial unit is ready for surveying. Then it is necessary to travel back and forth in one or two test sections. After that, the actual survey can begin.

Figure 12. *The process of initializing the inertial unit*

Figures 13–15 illustrate our own demo measurements (two survey samples) performed with the multibeam ultrasonic measuring system. One of them was made on a stretch of the Danube River, and the other was a lakebed survey of a gravel mine. In the latter, our goal was to describe the raw material to be extracted and to gain an overview of the mining exploitation process.

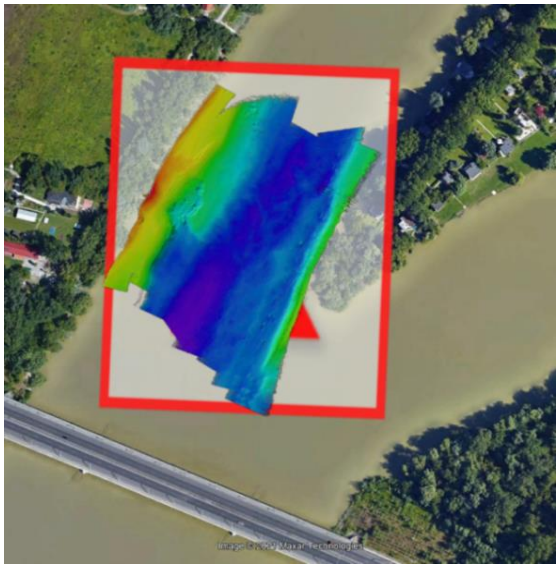

Figure 13. *Survey site of a section of the Danube*

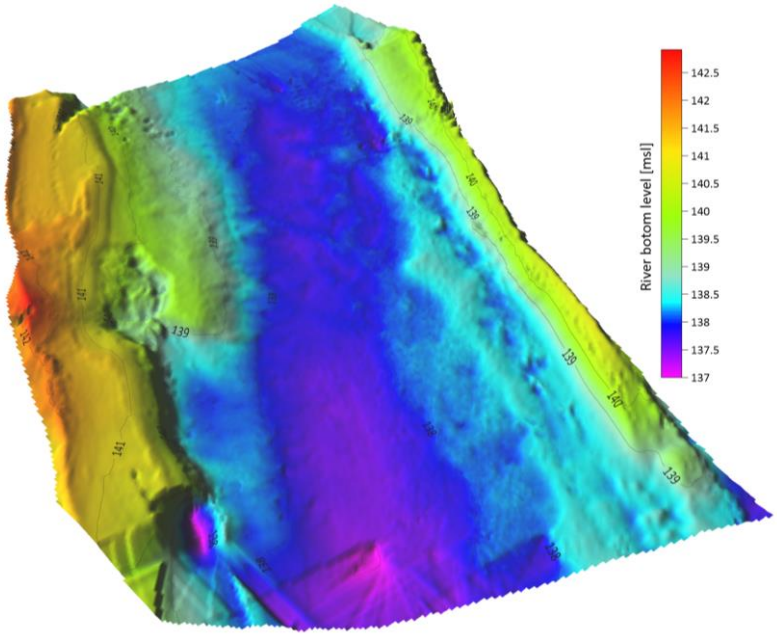

Figure 14. *3D model of the surveyed Danube section (40cm resolution)*

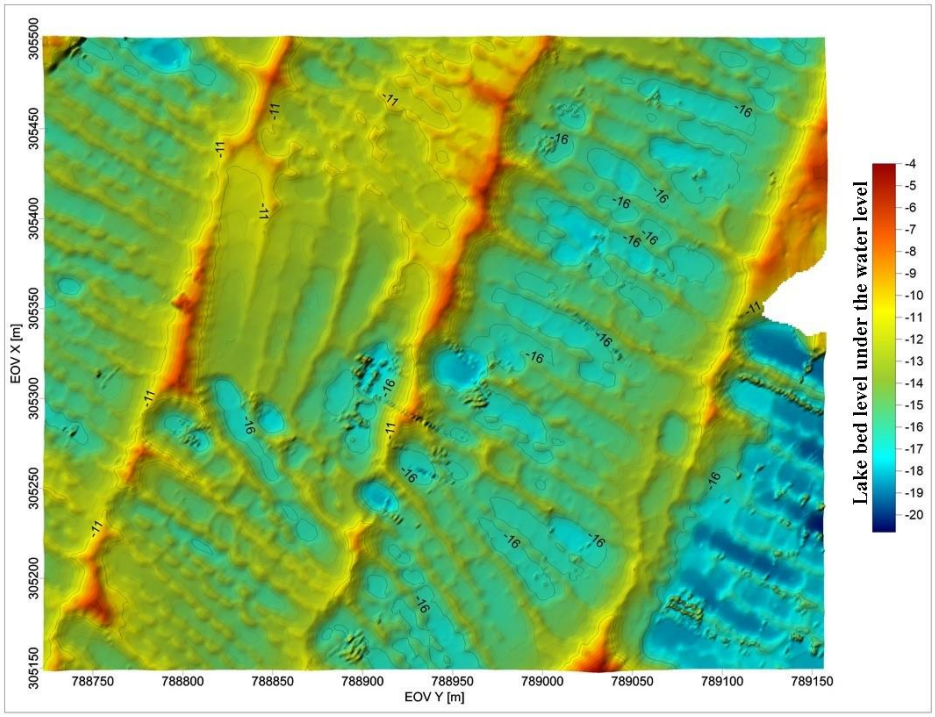

Figure 15. *3D model of a lake bed in a gravel mine*

4. THE LEGAL REQUIREMENTS FOR THE VOLUME COMPUTATION IN MINING

This professional group of problems is regulated by a Hungarian government decree [5] on determining the specific value of mineral resources and geothermal energy and the method of calculating value. Paragraph 2 (Section 2) of this Decree regulates the case of the payment of annual mining rent in the case of solid mineral raw materials, including the following:

"Paragraph 2 (Section 2): The licensee extracting the mineral raw material with the other official permit is obliged to determine the quantity of the extracted mineral raw material by mine surveying (geodetic) methods or in another suitable manner. The method and result of the determination must be substantiated."

"Within 60 days after completing the extraction of the raw material, the licensee is obliged to determine the change in the quantity of the mineral raw material by geodetic calculation (volume computation), and send a report about it to the Mining Authority."

"Paragraph 2 (Section 3): The mining entrepreneur is obliged to determine the amount of extracted mineral raw materials by mine surveying (geodetic) methods. In the case of underground mining, the extracted quantity can also be determined by weighing. The change must be indicated on the mining map. The change in the quantity of the mineral raw material for the current year must be determined by a calculation based on geodetic measurements (volume computation). The result of the determination must be certified."

In addition to the legal background, we would also like to highlight the 3–5% accuracy requirement imposed on this mine surveying task in Hungarian mining practice.

It is important to note that the application of the title "surveying device" in mining for the surveys of mining lake beds – one of which was briefly described above –, is justified not only for the sake of the afore-mentioned legal requirements. This is because periodic measurements, depending on the progress of production, can increase the efficiency of extraction by providing an accurate picture of the bed shape. Thus, it will be possible to identify raw material formations whose extraction has been unintentionally delayed. As a result, the mineral raw material can be extracted with higher efficiency in a mine, and the state receives an annual mining rent considering a larger extracted share of the available theoretical stock.

5. CONCLUSIONS

In our study, after a brief description of today's changing state-of-the-art mine surveying technologies we have reviewed the development history of water depth measurement in Hungary in detail. Subsequently, based on a study [2], we overviewed the single-beam ultrasonic measuring device based on the example of bed surveying of a mining lake. Then we described the iWBMSe multibeam sonar sys-

tem in detail, emphasizing its application benefits in surveying mining lake beds. Afterwards we discussed the preparation for use of this survey system and illustrated two of our own practical examples as well. Finally we dealt briefly with the legal regulation of mining volume computation and mentioned benefits of using the multibeam echosounder system in the mining process.

ACKNOWLEDGEMENTS

The authors express their gratitude for the support provided for the preparation of this study to the managers of Bay Zoltán Applied Research Public Benefit Nonprofit Ltd.

REFERENCES

[1] van Wegen, W. (2018). Surveying in mining sector: An Overview of Geospatial Methods in Mining Engineering. *GIM International*, January 12. https://www.gim-international.com/content/article/surveying-in-the-mining-sector.

[2] Galli, Cs. (2017). *Water depth mapping with modern tools*. BSc Thesis, Eötvös Loránd University, Budapest.

[3] https://www.hydro-international.com

[4] www.norbit.com

[5] Hungarian Government Decree No. 54/2008. (III. 20.) on the determination of the specific value of mineral resources and geothermal energy and the method of calculating value.

Geosciences and Engineering, Vol. 9, No. 14 (2021), pp. 96–115.
https://doi.org/10.33030/geosciences.2021.14.096

INVESTIGATION OF GAS FLOW MODELS IN CASE OF MICRO- AND NANOPORE SIZE RESERVOIRS

PATRIK PUSZTAI[1, *] – ANITA JOBBIK[1]

[1]*Research Institute of Applied Earth Sciences, University of Miskolc*
[*]*patrpusztai@mol.hu*

Abstract: Conventional continuum-flow equations, such as the well-known Darcy's law, greatly underestimate the fluid-flow rate when applied to micro and nanopore-bearing reservoirs. This paper concentrates on the collection, interpretation and presentation of different flow models which can be used in such conditions. They are utilized on core samples which originated in a Hungarian reservoir under extreme pressure and temperature (over 1,100 bar and 200 °C). As only limited literature is available which can describe the exact flow behavior of natural gas in these conditions, comparison of the different models under these conditions can provide information for a wider understanding of these types of reservoirs.

Several factors influence gas production from these unconventional formations, so the creation of an adequate material balance equation was necessary to describe pressure depletion and original gas in-place. Integration of this novel material balance equation with the different flow models results in a calculation algorithm which enables investigation of the reservoir behavior during production. Finally, the adaptability of this model to real production data is investigated.

Keywords: *fluid flow, nanopore, natural gas, material balance*

1. INTRODUCTION

The growing requirement for energy and the decreasing quantity of fossil fuels areforcing engineers to find alternative solutions. This phenomenon is valid in the case of hydrocarbons too, where the role of unconventional reservoirs is becoming more significant. Natural gas production from these types of reservoirs has been developed remarkably in the past few decades thanks to technological advancement.

These types of reservoirs (tight gas, shale gas) usually have a pore size distribution in the range of micro- to nanometers and the reservoirs are placed in extreme conditions, which influence the equations describing the gas flow and the material balance equations. Appropriate description and modeling of these mechanisms are indispensable for economic exploitation of unconventional natural gas reservoirs.

2. MATERIAL BALANCE EQUATION

Investigation of the multiple mechanisms which characterize the tight and shale gas reservoirs is necessary. Shale gas reservoirs are organic-rich, fine-grained reservoirs in which the pore space can be classified into three main categories: porous in

organic matter, interparticle pore system in the organic matrix, and open fractures (induced by hydraulic fracture stimulation and natural fractures). Natural gas (mainly methane) in shale gas reservoirs is generally believed to be stored as either free or adsorbed gas, although solution gas within pore fluids and bitumen may also be important [1]. There are multiple mechanisms for gas storage in organic-rich shales including [2]:

1. Adsorption upon internal surface area;
2. Conventional (compressed gas) storage in natural and hydraulic (induced) fractures;
3. Conventional storage in matrix porosity (organic and inorganic);
4. Solution in formation water;
5. Absorption (solution) in organic matter.

This paper concentrates on the 1st, 3rd and 4th mechanisms, as later the investigated formation is not considered to be fractured and the effect of absorption is neglected in this study. The total organic content (TOC) has a near linear relationship with the total gas content of shale reservoirs [3].

In the following two subsection the explanation of the 1st and 4th mechanisms are detailed, as they can be investigated in different ways.

2.1. Adsorption

The matrix systems of shale reservoirs (also coalbed methane – CBM) have immense capacity for methane storage. The mechanism by which this occurs is called adsorption. In adsorption, molecules of gas become attached to the surface of coal or to organic material in shale (which is obviously proportional to the total carbon content of the formation). Nearly all of the gas stored by adsorption to shale exists in a condensed, near liquid state. In order to simulate gas production in shale gas reservoirs, an accurate model of gas adsorption is very important. There are two different types of adsorption: chemical adsorption and physical adsorption. This paper deals with only physical adsorption as it is more relevant in reservoir engineering.

The expression of adsorption isotherm must be introduced, as the temperatures of reservoirs are assumed to be constant in this paper. It is assumed that at a given temperature the volume of adsorbed gas is only pressure dependent in the case of a given gas component and a given adsorbent [4].

This paper suggests the use of the so-called Langmuir isotherm, which is one of the most commonly applied adsorption models for shale gas reservoirs. It is based on the assumption that there is a dynamic equilibrium at constant temperature and pressure between adsorbed and non-adsorbed gas. Also, it is assumed that there is only a single layer of molecules covering the solid surface. The Langmuir isotherm has two fitting parameters: Langmuir volume (V_L) and Langmuir pressure (P_L). The typical formulation of a Langmuir isotherm is shown in *Equation (1)*, where V is the adsorbed gas volume at pressure p, V_L is the Langmuir volume or the maximum

gas volume of adsorption at infinite pressure, and P_L is the Langmuir pressure, which is the pressure corresponding to one-half Langmuir volume [5].

$$V = \frac{V_L \times p}{P_L + p} \tag{1}$$

In *Equation (1)* the V_L [sm^3/ton] and P_L [bar] values are determined in laboratory tests and their values are proportional to temperature, adsorbent material, and adsorbed material. *Figure 1* shows the Langmuir isotherm of the investigated reservoir in this paper (detailed later).

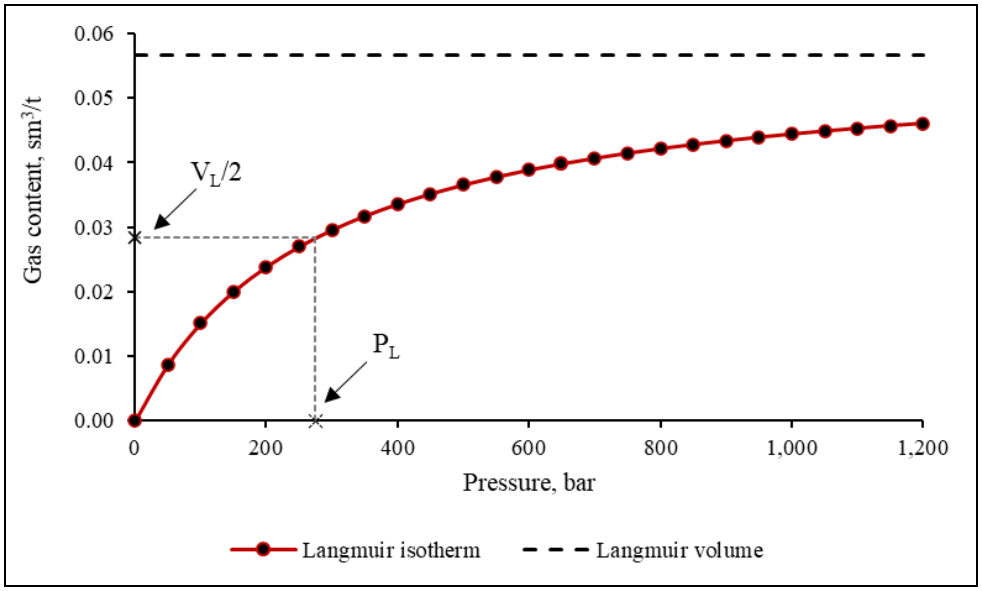

Figure 1
Langmuir isotherm of the investigated reservoir at P_L = 275 bar and V_L = 0.057 sm^3/t

2.2. Solution in formation water

As is known, normally natural gas cannot dissolve in water effectively, although under high pressure and temperature the volume which dissolves in water can reach significant amounts. Since the investigated reservoirs are under extreme conditions and the measured connate water saturation of the core samples was significant, it is clear that natural gas coming out from the solution must be taken into account. Solution depends on pressure, temperature, and salinity values. The solution is less effective if the salt content of the formation water is high. As natural gases mostly consist of methane, the calculation of methane solubility can provide adequate results. Blount and Price in 1982 developed two correlations for calculating the me-

thane solubility in formation water [6]. This work uses the correlation which provides a lower standard deviation value, *Equation (2).*

$$\log_e CH_4 = -1.4053 - 0.002332 \times T + 6.3 \times 10^{-6} \times T^2 - 0.004038 \times S - 7.579 \times 10^{-6} \times P + 0.5013 \times \log_e P + 3.235 \times 10^{-4} \times T \times \log_2 P \quad (2)$$

where standard deviation of residuals is 0.0706 and multiple R is 0.9943, T is the formation temperature [°F], P is the formation pressure [psi], and S is the formation salinity [grams/liter]. CH_4 is in standard cubic feet [sft^3] per petroleum barrel at 25 °C and atmospheric pressure. The validation of this correlation is 160 °F–464 °F (71 °C–240 °C) temperature and 3,500 psi–22,500 psi (241 bar–1,551 bar) pressure.

Methane solubility is greater with increasing pressure and temperature. Also, it is greater with decreasing salinity values, as is indicated by *Equation (2)*.

2.3. Derivation of pressure drop calculation

Material balance equations are one of the most powerful tools for a reservoir engineer to model the reservoir behavior and approximate the original gas in place. The main concept in generating the material balance equation is simply a volumetric balance, which states that the algebraic sum of volume changes of gas in reservoir and the gas produced must be zero. The reservoir temperature is assumed to be constant. In this study a material balance equation was necessary which deals with the fact of several different mechanisms. Because of the reservoir conditions a closed reservoir is assumed (in the case of tight, compact reservoir this assumption is acceptable) where the gas expansion, formation water expansion and formation rock expansion are the basic mechanisms. As a great deal of unconventional gas reservoirs are shale gas types, dealing with adsorption is indispensable. Because of the great pressures and temperatures the dissolution of natural gas in the connate formation water is necessary (also since the measured connate water saturation of the core samples was extremely high). Due to these phenomena the following connection is stated in this paper where the volumes are identified under reservoir conditions.

$$\begin{aligned} &Cumulative\ gas\ production\ [m^3] \\ &\quad = Gas\ expansion\ [m^3] + Rock\ and\ water\ expansion\ [m^3] + Desorption\ [m^3] \\ &\quad + Release\ from\ formation\ water\ [m^3] \end{aligned} \quad (3)$$

It is evident that due to the mechanisms taken into account the pressure depletion is not as high for all mechanisms as in the case of only a closed reservoir without desorption or release of natural gas from formation water. This statement is visualized in *Figure 2.*

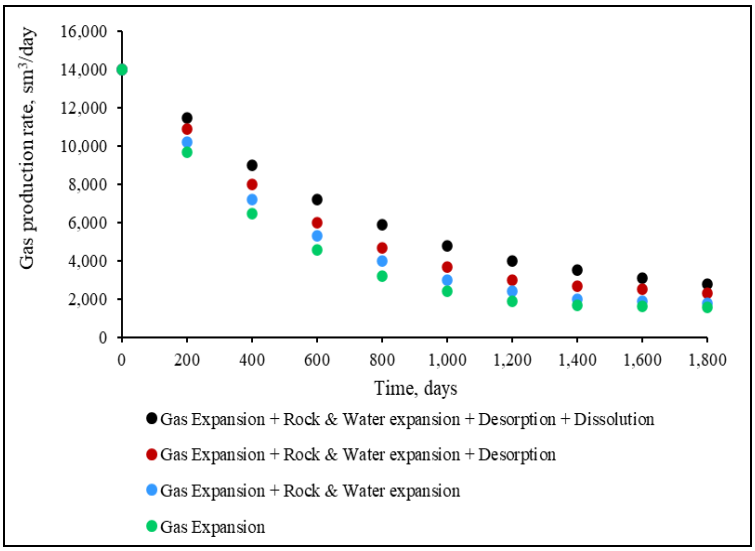

Figure 2
Behavoir of different material balances during production

Identification of the different parts of this connection can be seen in the following equations, where the Langmuir isotherm *(Equation 1)* was used for the desorbed gas volume calculation and *Equation (2)* was used for calculation of the release dissolved gas volume. Gas expansion and formation water and rock expansion calculation were calculated by clear equations.

$$Cumulative\ gas\ production\ [m^3] = G_p \times B_g \tag{4}$$

$$Gas\ expansion\ [m^3] = G_f \times (B_g - B_{gi}) = A \times h \times \Phi_{ci} \times (1 - S_{wi}) \times \left(\frac{B_g}{B_{gi}} - 1\right) \tag{5}$$

$$Rock\ and\ water\ expansion\ [m^3] = G_f \times B_{gi} \times \frac{S_{wi} \times c_w + c_f}{1 - S_{wi}} \times (p_i - p)$$
$$= A \times h \times \Phi_{ci} \times B_{gi} \times (S_{wi} \times c_w + c_f) * (p_i - p) \tag{6}$$

$$Desorption\ [m^3] = G_a \times \frac{1}{G_{ci}} \times B_g \times \left(\frac{V_L \times p_i}{P_L + p_i} - \frac{V_L \times p}{P_L + p}\right) = A \times h \times \rho_{bi} \times B_{gi} \times \left(\frac{V_L \times p_i}{P_L + p_i} - \frac{V_L \times p}{P_L + p}\right) \tag{7}$$

$$Release\ from\ formation\ water\ [m^3] = G_s \times B_g \times \frac{1}{V_{si}} \times \Delta V_s = A \times h \times \Phi_{ci} \times S_{wi} \times B_g \times \Delta V_s \tag{8}$$

Where the subscript $_i$ stands for values under initial reservoir conditions, G_p is the cumulative gas production under standard conditions [sm^3], G_f is the initial free gas volume under standard conditions [sm^3], G_a is the adsorbed gas volume under standard conditions [sm^3], G_s is the dissolved gas volume under standard conditions [sm^3], G_{ci} is the initial adsorbed gas content of the reservoir [sm^3/kg rock], V_{si}

is the initial dissolved gas content [sm^3/m^3], ΔV_s is the initial dissolved gas volume minus the dissolved gas volume under depleted reservoir pressure [sm^3/m^3], p_i is the initial pressure [Pa], A is the reservoir area [m^2], h is the reservoir height [m], B_{gi} is the initial formation volume factor [m^3/sm^3], B_g is the formation volume factor under depleted reservoir pressure [m^3/sm^3], Φ_{ci} is the corrected porosity [–], S_{wi} is the initial water saturation of the reservoir [–], V_L is the Langmuir volume [sm^3/kg], P_L is the Langmuir pressure [Pa], c_w is the water compressibility assumed to be equal to 45.8×10^{-11} [1/Pa], c_f is the formation compressibility [1/Pa] factor which can be calculated by Hall's correlation [7] who investigated 12 samples (7 limestones and 5 sandstones) to develop a c_f correlation, *Equation (9)*.

$$c_f = 1.86 \times 10^{-6} \times \Phi_m{}^{-0.415} \times \frac{1}{6{,}894.75729} \tag{9}$$

The use of corrected porosity is necessary because in this model the free gas volume is lower than when the adsorbed phase volume is ignored. The adsorbed gas is located on the surface of the pores, so it decreases the effective porosity. As the pressure decreases the adsorbed phase vaporizes (due to the Langmuir isotherm) and makes a vacant space that is instantly occupied by free gas. Thus, the pore volume available for free gas is allowed to increase as pore pressure decreases, in this case during production. Williams-Kovacs et al. [8] suggest a correction factor for this phenomenon presented in field unit, *Equation (10)*. It should be corrected with a Φ_{cm} term, suggested here, as the measured porosity (measured in laboratory conditions) is required in reservoir conditions, *Equation (11)*, suggested by Engler in 2010 [9].

$$\left(\frac{\Phi_{ac}}{\Phi_{cm}}\right) = \frac{\Phi_{cm} \times (1 - S_{wi}) - 1.318 \times 10^{-6} \times M \times \frac{\rho_b}{\rho_a} \times V_L \times \frac{p}{p + P_L}}{\Phi_{cm} \times (1 - S_{wi})} \tag{10}$$

$$\Phi_{cm} = \frac{e^{c_f \times (p_i - p_m)}}{\frac{1}{\Phi_m} - \left[1 - e^{c_f \times (p_i - p_m)}\right]} \tag{11}$$

where Φ_{ac} is the corrected porosity due to adsorbtion [–], Φ_{cm} is the corrected measured porosity [-], M is the gas molar mass [lb/lbmol], V_L is in [scf/t] and P_L is in psi, ρ_b/ρ_a is the reservoir bulk density over adsorbed phase density under initial conditions [–], where the adsorbed gas density is assumed to be equal to liquefied methane density, which is approximately 420 kg/m^3. Bulk density can be measured by laboratory circumstances (ρ_{bm}) and corrected by the formation compressibility under reservoir conditions, *Equation (12)*.

$$\rho_b = \rho_{bm} + \rho_{bm} \times c_f \times p_m \tag{12}$$

where p_m is the pressure during porosity measurement [Pa]. The initial corrected reservoir porosity is given by the following equation.

$$\Phi_{ci} = \Phi_{cm} \times \left(\frac{\Phi_{ac}}{\Phi_{cm}}\right) \tag{13}$$

Finally, the enhanced material balance equation suggested in this paper is presented below.

$$\begin{aligned} G_p \times B_g &= A \times h \times \Phi_{ci} \times (1 - S_{wi}) \times \left(\frac{B_g}{B_{gi}} - 1\right) + A \times h \times \Phi_{ci} \times B_{gi} \times (S_{wi} \times c_w + c_f) \times (p_i - p) \\ &+ A \times h \times \rho_{bi} \times B_g \times \left(\frac{V_L \times p_i}{P_L + p_i} - \frac{V_L \times p}{P_L \times p}\right) + A \times h \times \Phi_{ci} \times S_{wi} \times B_g \times \Delta V_s \end{aligned} \tag{14}$$

where B_g, B_{gi}, can be calculated by *Equation (15)* (in case of B_{gi} the equation is used by the initial deviation factor and with the initial reservoir pressure) and ΔV_s by the use of *Equation (2)* (where its value is equal to the volume under initial reservoir pressure minus the volume under depleted reservoir pressure).

$$B_g = \frac{P_{st} \times z \times T_i}{T_{st} \times p} \tag{15}$$

where P_{st} is the standard pressure (101,325 Pa), T_{st} is the standard temperature (298.15 K), z is the deviation factor of the gas under reservoir pressure [–]. The terms in ΔV_s are determined by SI units, so a C_1 correction factor is necessary to convert it back to psi and its value is 0.000145037738.

As pressure drop calculation is required to predict the gas production over several years this paper suggests a method based on the material balance equation presented above. *Equation (14)* is not a linear equation, so we suggested to solve the equation for depleted reservoir pressure (p) using Newton's method, which is an iterative calculation method. For this purpose, the function in *Equation (16)* is determined by rearrangement and simplification and the derivative of this function *(Equation 17)* is determined.

$$\begin{aligned} f(p) &= \frac{\beta 11}{p} + \beta 14 - \beta 3 \times p + \frac{\beta 13}{p} - \frac{\beta 4}{p} \times \frac{V_L \times p}{P_L \times p} + \frac{\beta 5}{p} \\ &\times \left[\beta 6 - e^{\beta 7 - \beta 8 \times (p \times C1) + \beta 9 \times \ln(p \times C1) + \beta 10 \times (p \times C1)}\right] - \frac{\beta 15}{p} \end{aligned} \tag{16}$$

$$\begin{aligned} f'(p) &= \frac{V_L \times \beta 4}{(p + P_L)^2} - \frac{\beta 5 \times \left(\frac{\beta 10}{p} + \frac{\beta 9}{p} - \beta 8 \times C1\right) \times e^{\beta 10 \times \ln(p \times C1) + \beta 9 \times \ln(p \times C1) - \beta 8 \times C1 \times p + \beta 7}}{p} \\ &- \frac{\beta 5 \times \left(\beta 6 - e^{\beta 10 \times \ln(p \times C1) + \beta 9 \times \ln(p \times C1) - \beta 8 \times C1 \times p + \beta 7}\right)}{p^2} + \frac{\beta 15}{p^2} - \frac{\beta 13}{p^2} - \frac{\beta 11}{p^2} - \beta 3 \end{aligned} \tag{17}$$

To find the solution a starting p_0 value should be chosen that is less than the initial formation pressure (assumed to be less by 1 bar). Then with *Equation (18)* the calculation of a new p value should be done. The procedure has to be continued until the difference between p_n and p_{n-1} is acceptably small.

$$p_n = p_{n-1} - \frac{f(p)}{f'(p)} \tag{18}$$

However, the deviation factor and the cumulative gas production also depend on the reservoir pressure (p). So after finding an acceptable p_n value the whole procedure should be recalculated with the recalculation of the deviation factor (z) and G_p (gas production rate calculations with different apparent permeability values – detailed in a later section) which now should be calculated with the new p_n pressure instead of the assumed p_0 pressure. So, the whole procedure is a double iteration method, as can be easily understood with the flow chart in *Figure 3.*

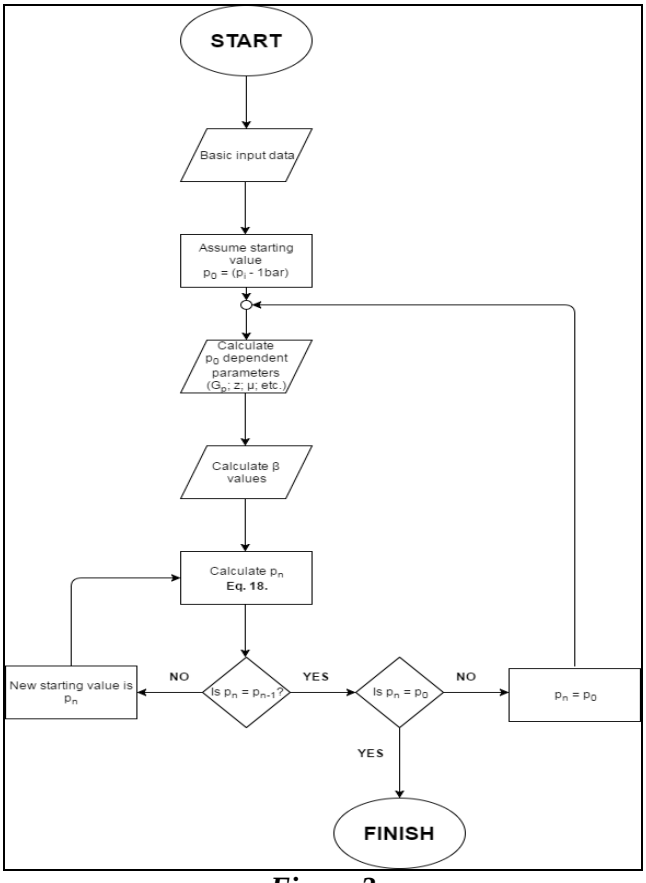

Figure 3

Algorithm flow chart for pressure drop calculation

The first step is to identify the constant values that are the basic input parameters during the calculations, including measured porosity, reservoir area, absolute permeability, reservoir height, Langmuir pressure and temperature, initial reservoir pressure and reservoir temperature, average pore radius, produced gas specific gravity, etc. Then if the calculation is the first iteration, we have to choose a starting depleted reservoir pressure where a 1 bar depletion from initial reservoir pressure is a good assumption in most cases. Otherwise, if the iteration is not the first one, we have to use the previously calculated depleted pressure (p_n). The next step is the calculation of the pressure dependent parameters (where the depleted pressure is necessary), such as the apparent permeability, gas deviation factor, and the cumulative gas production (where we have to identify the required time step). Then we need to calculate the initial values (corrected initial porosity, formation compressibility, initial reservoir bulk density etc.) and the β parameters that are necessary for *Equations (16)* and *(17).* Next the calculation of *Equation (18)* is necessary, where the starting pressure is the assumed depleted pressure (in the first iteration) or the depleted pressure determined in the previous iteration step. Then we have to determine if the resulted pressure is close enough to the starting pressure. If not, we must recalculate *Equation (18)* with the previously determined pressure (this iteration proceeds until two consecutive calculated pressures are close enough). If we get an acceptable value for depleted pressure, we need to determine if this pressure is close enough for the initial assumed (or previously determined pressure by the previous iteration process). If yes, we are finished with this process; if not, we have to attach back the calculated depleted pressure (after basic input data) and continue the whole process until we get a suitable depleted reservoir pressure.

The disadvantage of this method is the huge computational quantity, but it has a great advantage as most of the influential mechanisms are contained in the calculation. *Figure 2* shows how different material balances behave with different mechanisms accounted in them. The data used in them are listed in *Table 2*, except V_L is assumed to be equal to 10 sft^3/t and the reservoir is assumed horizontally fractured with 40 m fracture half-length and 10 stages, and the basic Darcy's model was used. The production rate does not drop as significantly in the case of material balance equation (MBE), which accounts for all of the detailed mechanisms as in case of other MBE (which take into account less mechanisms) because of the release of the dissolved natural gas in the connate water and desorbed gas during pressure depletion. All of the MBE can be reached with the presented model by neglecting the unnecessary terms, as can be seen in *Figure 2.*

3. GAS FLOW MODELS

The Darcy equation, which was derived from the Navier-Stokes equation based on continuum theory, has been used for more than 150 years to linearly relate fluid-flow rate and pressure gradient across a porous system. The linearity of the Darcy equation makes it easy and practical to use in reservoir engineering analysis and

numerical reservoir simulations. Darcy's equation correctly models the flow behavior at macrometrical and micrometrical scale where the main forces interacting are viscous. However, physics of fluid flow in shale and tight reservoirs cannot be predicted from standard flow or mass transfer models because of the presence of nanopores, ranging in size from one to hundreds of nanometers. Conventional continuum flow equations, such as Darcy's law, greatly underestimate the flow rate when applied to nanopore-bearing reservoirs [10].

This phenomenon can be described by the fact that with decreasing pore sizes the interacting forces between the pore walls and gas molecules are become significant than those between gas molecules (which is typical in viscous Darcy's flow). As this effect becomes more significant the flow will alter increasingly from the Darcy's flow. Also, when the pore sizes are small enough (comparable to molecule size) the main driving force becomes the concentration difference (diffusion) instead of the pressure difference.

To specify the magnitude of the alteration from Darcy type flow, different flow regimes are introduced. But before the characterization of the flow regimes, introduction of new expressions such as mean free path and Knudsen number are essential.

3.1. Mean free path

In a closed system, the molecules are constantly colliding with each other as they are not geometrical points. The average distance between the collisions is the mean free path [11]. A good visualization is given in *Figure 4*, where the molecule diameter is presented by d [m], so the collision area A [m^2] can be calculated by *Equation (19)*.

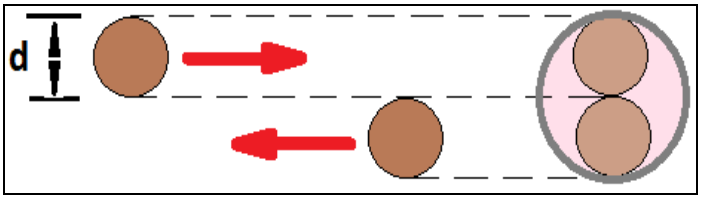

Figure 4. *Visualization of the mean free path*

$$A = d^2 \times \pi \tag{19}$$

In time the collision area will sweep out a cylindrical volume where n number of molecules is presented (treated as point masses). The molecules move with a constant speed along straight lines so the mean free path, λ [m] can be calculated as the length of the path divided by the number of collisions (volume of the cylinder, V [m^3] times the number of molecules per unit volume n), *Equation (20)*.

$$\lambda = \frac{l}{V \times n} = \frac{\bar{v} \times t}{\bar{v} \times t \times d^2 \times \pi \times n} = \frac{1}{d^2 \times \pi \times n} \tag{20}$$

The problem with this expression is that the average molecular velocity is used, but the target molecules are also moving, so the frequency of collisions depends upon the average relative velocity of the randomly moving molecules. The magnitude of the relative velocity is the square root of the scalar product of the velocity with itself *(Equation 21)*. The number of molecules per volume can be given by Avogadro's number, N_A (6.022×10^{23} mol^{-1}) and the ideal gas law. The ratio of the universal gas constant, R [8.314 J/(mol × K)] and Avogadro's number is the Boltzmann number, K_B (1.38×10^{-23} J/K). Finally, the corrected mean free path equation is given by *Equation (22)*.

$$\bar{v}_{rel} = \sqrt{2} \times \bar{v} \tag{21}$$

$$\lambda = \frac{R \times T}{\sqrt{2} \times d^2 \times \pi \times N_A \times p} = \frac{K_B \times T}{\sqrt{2} \times d^2 \times \pi \times p} \tag{22}$$

It is evident that the mean free path is proportional to pressure because at higher pressure, a greater amount of gas molecules can be present in a unit volume, so collisions between the molecules will be more common and decrease the value of the mean free path, *Figure 5*.

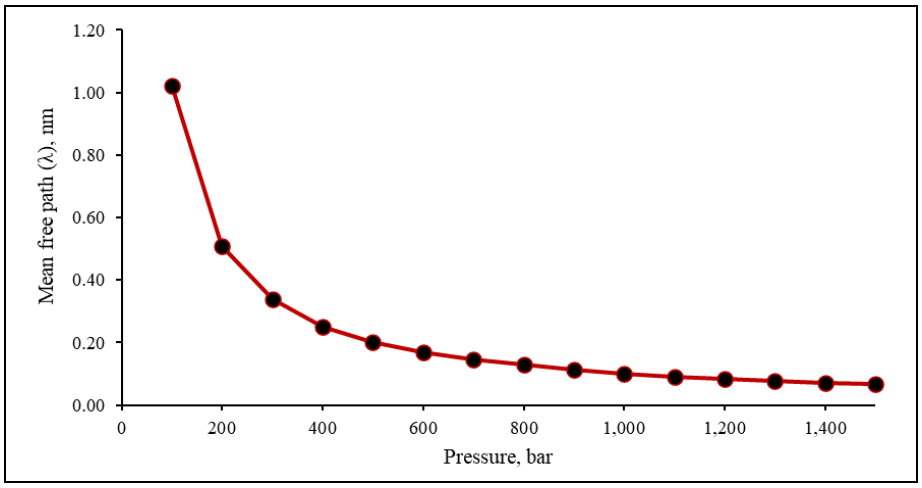

Figure 5

Mean free path vs. pressure diagram, using the investigated reservoir's data

3.2. Knudsen number

When the average mean free path of the gas molecules begins to be comparable or greater than the pore size containing it, the result is a break in the continuum theory. The degree of deviation from this theory is measured with the Knudsen number. The Knudsen number is calculated by the ratio of the mean free path and the pore

diameter ***(Equation 23)***. The value of this number is directly proportional to the mean free path, so as the average distance between the collisions of the molecules becomes smaller the Knudsen number decreases as well.

$$K_n = \frac{\lambda}{d} \tag{23}$$

If the pore diameter is much greater than the mean free path of the contained gas molecules, the value of Knudsen number is between 0 to 10^{-3} [–] and the flow behavior does not differ from the continuum flow [12]. When the mean free path is close to comparable to the pore diameter or exceeds it the flow becomes to alter from Darcy's flow and different types of flow regimes can be distinguished depending on the magnitude of the deviation. *Table 1* represents flow regimes corresponding to Knudsen number ranges [13].

Table 1

Types of different flow regimes as a function of Knudsen number [12]

Knudsen number [-]	Flow regime
$0–10^{-3}$	Continuum/Darcy flow (no-slip flow)
$10^{-3}–10^{-1}$	Slip flow
$10^{-1}–10^{1}$	Transitional flow
$10^{1}–\infty$	Free molecular flow/Knudsen diffusion

The different flow regimes are presented as a function of pressure in *Figure 6*, where different pore diameters are also investigated and the examined formation's properties presented in *Table 2* are shown as a red line.

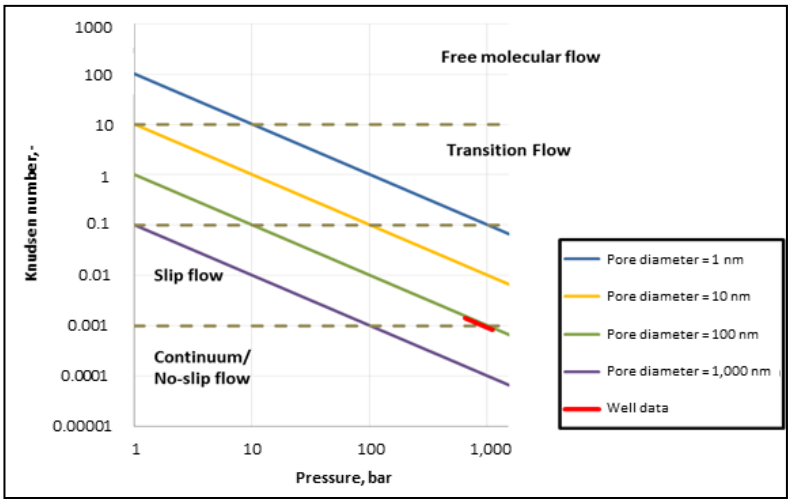

Figure 6

Representation of different flow regimes as a function of pressure and pore diameter

It can be observed that the flow regimes of the investigated formation are between the continuum flow and the slip flow regime. It is quite an interesting result, because as the investigated reservoir's properties are in extreme conditions, very non-continuum flow behavior can be presumed. This controversial observation can be explained by the fact that the value of Knudsen number is proportional to the pressure inversely, meaning that *Equation (24)* is not very accurate at high pressures. That is why it is predicting a mean free path smaller than the collision diameter at very high pressures [14].

3.3. Models

Different flow models investigated in this paper are collected and presented in *Figure 7*. All of them are expressed in an apparent permeability parameter divided by the absolute (or Darcy-constant) permeability. These apparent permeability values are functions of the pressure in all models. This is different than Darcy's model, where a constant value of permeability is determined. These models are expressed in different forms as their applicability is usually acceptable in one or two flow regimes. The derivations of the different models are not detailed in this paper nor the apparent permeability equations of them (the corresponding literature is listed in the references). Two types of flow regimes are investigated in this paper (in addition to the continuum regime). There are six types of models which deal with the slip flow regime and four types which deal with mainly the transitional regime. Also, a model which uses individual equations in case of different regimes is presented. It has to be mentioned that most of the models that account for Knudsen diffusion (typical mechanism in transitional regime besides slip phenomenon) are also suggested in the case of the slip regime, except for the NAP (non-empirical analytical permeability) model, which neglects the slip term and thus cannot describe appropriately the flow in this regime (see *Figure 7*). The models usually suggested to describe slip phenomenon are framed with green and models suggested in case of the transitional regime are framed with red. The following models were used (with references):

- Klinkenberg 1941 [15]
- Jones and Owens 1980 [16]
- Sampath and Keighin 1982 [17]
- Heid et al. 1950 [18]
- Florence et al. 2007 [19]
- Civan 2010 [20]
- Javadpour 2009 [10]
- Azom and Javadpour 2012 [21]
- APF – Darabi et al. 2012 [22]
- Sakhaee-Pour and Bryant 2012 [23]
- NAP – Singh et al. 2014 [24]

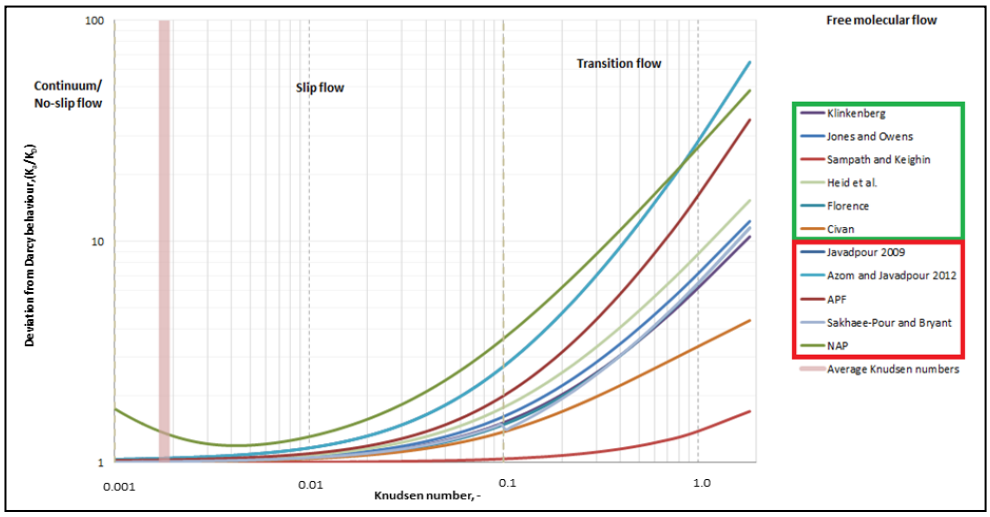

Figure 7. *Comparison of different flow models*

Also, the Knudsen range (different during production) of the investigated reservoir is marked with rose color. We can identify that the apparent permeability values constantly increase with increasing Knudsen number. These models do not underestimate the gas flow rate, as was earlier mentioned in the case of Darcy's flow. The models which account for Knudsen diffusion result in higher apparent permeability values, so higher gas flow rates are expected. These results are inline with the literature [25]. The investigated reservoir data are listed in *Table 2*. The investigated formation was at the depth 5,470–5,478.5 m and 43 core samples were taken along the whole interval, on which the measurements for most basic input data were performed. The Langmuir constants were assumed to be low based on corresponding literature [26].

Table 2

Investigated reservoir's parameters

Name	Symbol	Value	Unit
Absolute permeability	k_∞	0.0035	mD
Average porosity	Φ	2.29	%
Average pore radius	r_{av}	55.22	nm
Reservoir temperature	T	229	°C
Initial reservoir pressure	P_i	1,104.2	bar
Reservoir height	h	8.16	m
Wellbore radius	r_w	5.5	inch
Initial water saturation	S_{wi}	86.1	%
Flowing bottom hole pressure	P_{wf}	650	bar
Drainage radius	r_e	50	m
Langmuir volume	V_L	2	scf/tons
Langmuir pressure	P_L	4,000	psi
Bulk density	ρ_{bi}	2.63	g/cm^3
Average collision diameter	δ_{av}	0.39	nm

4. RESULTS

During production calculation this paper investigated a five-year period. Because of the very small permeability values no forecast was made of high production rates, which were proven by the calculations. The initial production rates and the cumulative gas productions for each model are presented in *Table 3*. Also, deviation from the Darcy permeability values is examined with percentages to the Darcy values. The pressure drop calculations were based on the algorithm presented earlier and open-hole production (radial flow) was assumed.

Table 3

Comparison of the different models' results in case of initial gas production rate and cumulative gas production for a 5-year period

Model	Initial production rate, m^3/day	Deviation from Darcy, %	Cumulative gas production, m^3	Deviation from Darcy, %
Darcy 1856	1,044.4	**0.00**	1,650,517	**0.00**
Klinkenberg 1941	1,048.9	**0.43**	1,657,087	**0.40**
Jones and Owen 1980	1,049.8	**0.51**	1,658,349	**0.47**
Sampath and Keighin 1982	1,044.8	**0.03**	1,651,003	**0.03**
Heid et al. 1950	1,051.2	**0.65**	1,658,349	**0.47**
Florence et al. 2007	1,048.1	**0.35**	1,655,882	**0.33**
Civan 2010	1,048.0	**0.34**	1,655,657	**0.31**
Javadpour 2009	1,063.8	**1.86**	1,677,526	**1.64**
Azom and Javadpour 2012	1,063.8	**1.85**	1,677,500	**1.63**
APF – Darabi et al. 2012	1,062.8	**1.76**	1,676,472	**1.57**
Sakhaee-Pour and Bryant 2012	1,048.8	**0.42**	1,656,902	**0.39**
NAP – Singh et al. 2014	1,994.6	**90.97**	2,714,736	**64.48**

The initial production rate values are so low that they make the formation impossible for economical production through an open-hole section. The necessity of enhanced gas recovery treatment is evident. However, the deviation from the Darcy production is higher in all cases (as was presumed by the models). The NAP, APF, Javadpour 2009 and Azom and Javadpour 2012 models provide higher production rates than the other models. This phenomenon can be elucidated by the fact that the reservoir is at the continuum–no-slip boundary *(Figure 7)* so the necessity of Knudsen flow is not required and the validity of these models during these conditions is questionable. Also, the NAP model yields very high production rates compared to other models, which can be accounted for by the fact that the model does not work properly in the Knudsen range of the reservoir. The other models provide very similar results for initial gas rate and cumulative gas production. As the flow type of the reservoir is very close to the continuum flow regime, it was expected that Darcy's flow calculations will result in almost acceptable production values. This assumption was proven by the calculations.

The reservoir pressure drop is not significant during the examined period because of the very low gas production rates. *Figure 8* shows the reservoir pressure

depletion and the cumulative gas production during the five-year period in the case of the Klinkenberg, 1941 model.

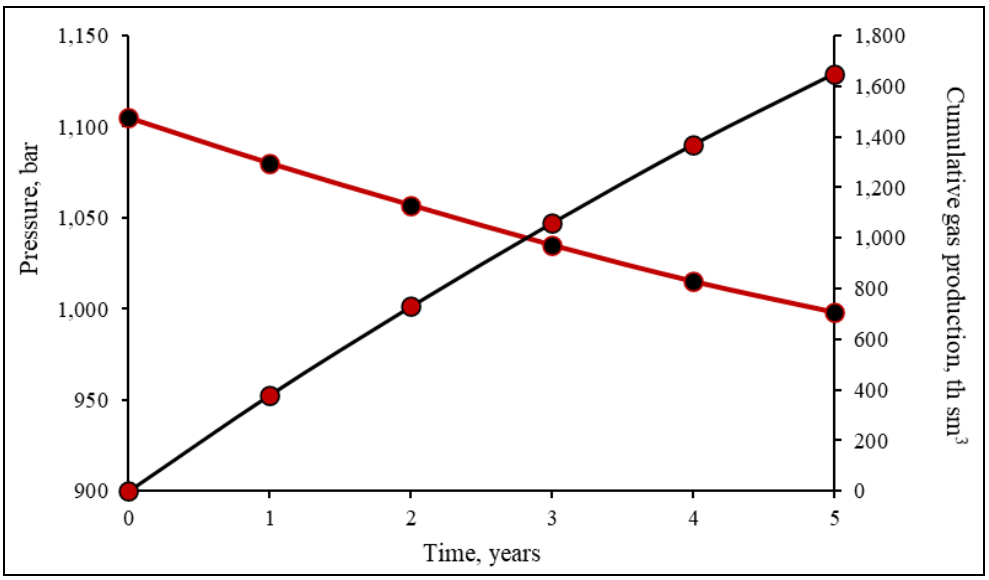

Figure 8
Pressure depletion and cumulative gas production for 5-year period with Klinkenberg, 1941 model

5. MODEL ADAPTABILITY FOR REAL PRODUCTION DATA

Results show that the calculation method suggested by this paper works well in case of the investigated reservoir but comparison of the results was not feasible because there were no available production data from the well. Therefore, another Hungarian natural gas well was built into the model to analyze the behavior of the model. The basic data of the investigated reservoir are shown in *Table 4*. As the reservoir is not a shale gas reservoir but a tight gas reservoir, the value of Langmuir pressure and Langmuir volume were chosen to be 0. There are three different productive zones in this formation and each of them was hydraulically fractured (vertical fracturing treatment). After test geophysical investigation and production tests it was determined that the three different fracture systems connect to each other and behave like one vertical fracture. Therefore, basic data were interpreted in this way. During test production 2,810,800 sm^3 natural gas and negligible amounts of condensate and water were produced. The initial gas production rate was about 36,000 sm^3/day, which coincides with the results forecast by the model suggested in this paper. The basic data and the production data were provided by company MOL Nyrt.

Table 4

Basic parameters of the investigated reservoir

Name	Symbol	Value	Unit
Absolute permeability	k_{∞}	0.008	mD
Average porosity	Φ	8.22	%
Reservoir temperature	T	473.15	K
Initial reservoir pressure	P_i	561	bar
Reservoir height	h	180	m
Area of the reservoir	A	0.02	km^2
Wellbore radius	r_w	0.14	inch
Initial water saturation	S_{wi}	55.4	%
Flowing bottom hole pressure	P_{wf}	266	bar
Fracture half length	x_f	50	m
Length of the flow	L	130	m

The investigated reservoir was in the continuum–slip boundary as well so the simple Darcy's model and the Civan, 2010 model (slip model) was interpolated on the production data, *Figure 9*. As can be seen, there is no excessive deviation between the two models. The interpolated graph fitted acceptably on the measured values, so the model suggested by this paper, works in a practicable range.

Although in case of reservoirs where flow regimes are in different than continuum regime can be calculated by different models

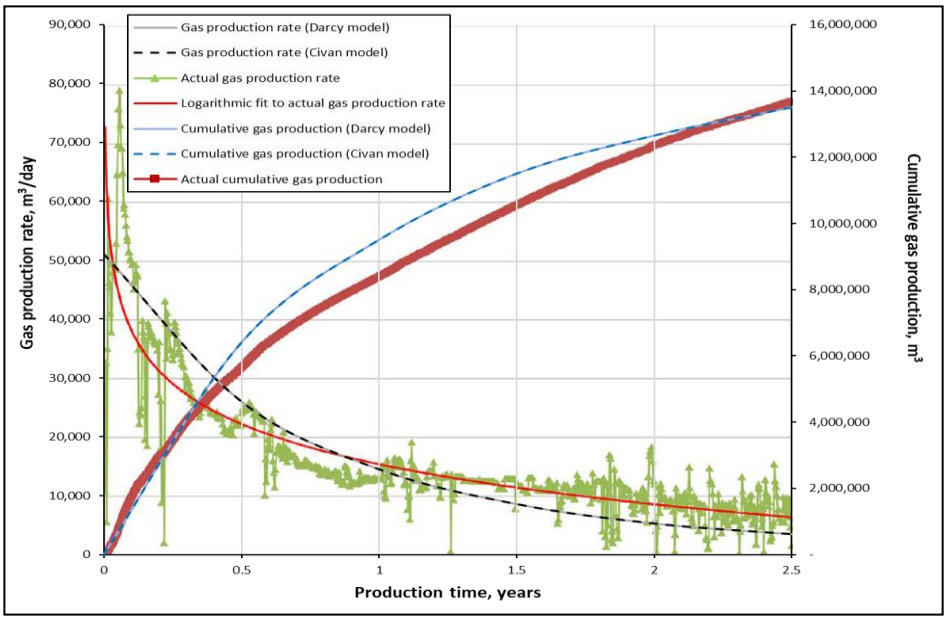

Figure 9

Plotting calculated data to real well data [27]

6. CONCLUSION

This paper described different types of unconventional gas reservoirs and described the different flows which come into prominence due to micro- and nanopore regimes. A Hungarian formation was characterized through the introduced flow equations and a new material balance equation. The material balance, which involves the detailed role of adsorbed gas in the porous matrix, provides reliable calculation of pressure depletion during production and original gas in place.

The performed measurements on the core samples provide the basic input parameters in the calculations. The reservoir is under extreme conditions, so different models had to be evaluated to gain a broader understanding of the reservoir behavior. As the reservoir is in the slip flow regime the most reliable data are assumed to be provided by the slip flow models.

The reservoir production was investigated in a five-year period by the presented calculation algorithm using all models. As no production data were available from the well, gas production data of another Hungarian well were used to investigate the application and adaptability of the model. The results proved the model works in a practicable range.

ACKNOWLEDGMENTS

The research was carried out in the framework of the GINOP-2.3.2-15-2016-00010 *Development of enhanced engineering methods with the aim at utilization of subterranean energy resources* project of the Research Institute of Applied Earth Sciences of the University of Miskolc in the framework of the Széchenyi 2020 Plan, funded by the European Union, co-financed by the European Structural and Investment Funds.

REFERENCES

[1] Haghshenas, B., Clarkson C. R., Chen, S. (2014). *New Models for Reserve Estimation and Non-Darcy Gas Flow in Shale Gas Reservoirs*. Paper presented at the SPE/EAGE European Unconventional Resources Conference and Exhibition, Vienna, Austria, SPE-167789-MS. https://doi.org/10.2118/167789-MS.

[2] Clarkson, C. R., Haghshenas, B. (2013). *Modeling of Supercritical Fluid Adsorption on Organic-Rich Shales and Coal*. Paper presented at the SPE Unconventional Resources Conference-USA, The Woodlands, Texas, USA, SPE-164532-MS, https://doi.org/10.2118/164532-MS.

[3] Wang, F. P., Reed, R. M. (2009). *Pore Network and Fluid Flow in Gas Shales*. Paper presented at the SPE Annual Technical Conference and Exhibition, New Orleans, Louisiana, SPE-124253-MS. https://doi.org/10.2118/124253-MS.

[4] Pápay, J. (2013). *Exploitation of Unconventional Petroleum Accumulations*. Akadémiai Kiadó, Budapest.

[5] Langmuir, I. (1918). The adsorption of gases on plane surfaces of glass, mica and platinum. *Journal of American Chemical Society*, 40 (9), pp. 1361–1403, https://doi.org/10.1021/ja02242a004.

[6] Blount, C. W., Price, L. C. (1982). *Solubility of methane in water under natural conditions: a laboratory study*. Final Report, Idaho State University, Pocatello (USA), Department of Geology, https://doi.org/10.2172/5281520.

[7] Hall, H. N. (1953). Compressibility of Reservoir Rocks. *Journal of Petroleum Technology*, 5 (1), pp. 17–19, SPE-953309-G. https://doi.org/10.2118/953309-G.

[8] Williams-Kovacs, J., Clarkson, C., Nobakht M. (2012). Impact of Material Balance Equation Selection on Rate-Transient Analysis of Shale Gas. *Paper presented at the SPE Annual Technical Conference and Exhibition*, San Antonio, Texas, USA, SPE-158041-MS, https://doi.org/10.2118/158041-MS.

[9] Engler, T. W. (2010). *Multiphase Phenomena—Fluid Flow in Porous Media*. Chapter 5. New Mexico Institute of Mining and Technology, Socorro, New Mexico, pp. 1–55.

[10] Javadpour, F. (2009). Nanopores and Apparent Permeability of Gas Flow in Mudrocks (Shales and Siltstone). *Journal of Canadian Petroleum Technology*, 48 (8), pp. 16–21, https://doi.org/10.2118/09-08-16-DA.

[11] Knight, R. D. (2004). *Physics for Scientists and Engineers: A Strategic Approach*. Pearson/Addison Wesley, San Francisco.

[12] Cussler, E. L. (2009). *Diffusion: Mass Transfer in Fluid Systems*. Cambridge University Press, Cambridge.

[13] Rezaee, R. (2015). *Fundamentals of Gas Shale Reservoirs*. John Wiley & Sons, Inc., Hoboken, NJ, https://doi.org/10.1002/9781119039228.

[14] Javadpour, F., D. Fisher, D., Unsworth, M. (2007). Nanoscale gas flow in shale gas sediments, *Journal of Canadian Petroleum Technology*, 46 (10). https://doi.org/10.2118/07-10-06.

[15] Klinkenberg, L. J. (1941). The Permeability of Porous Media to Liquids and Gases, Paper presented at the Drilling and Production Practice, New York, API-41-200.

[16] Jones, F. O., Owens, W. W. (1980). A Laboratory Study of Low-Permeability Gas Sands. *Journal of Petroleum Technology*, 32 (9), pp. 1631–1640, SPE-7551-PA, https://doi.org/10.2118/7551-PA.

[17] Sampath, K., Keighin, W. C. (1982). Factors Affecting Gas Slippage in Tight Sandstones of Cretaceous Age in the Uinta Basin. *Journal of Petroleum Technology*, 34 (11), pp. 2715–2720, SPE-9872-PA. https://doi.org/10.2118/9872-PA.

[18] Heid, J. G., McMahon, J. J., Nielsen, R. F., Yuster, S. T. (1950). *Study of the permeability of rocks to homogeneous fluids*. Paper presented at the Drilling and Production Practice, New York, API-50-230.

[19] Florence, F. A., Rushing, J., Newsham, K. E., Blasingame T. A. (2007). *Improved Permeability Prediction Relations for Low Permeability Sands*. Paper presented at the Rocky Mountain Oil & Gas Technology Symposium, Denver, Colorado, U.S.A., SPE-107954-MS, https://doi.org/10.2118/107954-MS.

[20] Civan, F. (2010). Effective Correlation of Apparent Gas Permeability in Tight Porous Media. *Transport in Porous Media*, 82, pp. 375–384. https://doi.org/10.1007/s11242-009-9432-z.

[21] Azom, P., Javadpour, F. (2012). *Dual-continuum modeling of shale and tight gas reservoirs*. Paper presented at the SPE annual technical conference and exhibition, San Antonio, Texas, SPE-159584-MS. https://doi.org/10.2118/159584-MS.

[22] Darabi, H., Ettehad, A., Javadpour, F., Sepehrnoori, K. (2012). Gas flow in ultra-tight shale strata. *Journal of Fluid Mechanics*, 710, pp. 641–658. https://doi.org/10.1017/JFM.2012.424.

[23] Sakhaee-Pour, A., Bryant, S. L. (2012). *Gas Permeability of Shale, The University of Texas at Austin*. Paper presented at the SPE Annual Technical Conference and Exhibition, Denver, Colorado, USA, SPE-146944-MS. https://doi.org/10.2118/146944-MS.

[24] Singh, H., Javadpour, F., Ettehadtavakkol, A., Darabi, H. (2014). Nonempirical apparent permeability of shale. *SPE Reservoir Evaluation & Engineering*, 17 (3), pp. 414–424, SPE-170243-PA, https://doi.org/10.2118/170243-PA.

[25] Singh, H., Javadpour, F., Ettehadtavakkol, A., Darabi, H. (2014). Nonempirical apparent permeability of shale. *SPE Reservoir Evaluation & Engineering*, 17 (3), pp. 414–424, SPE-170243-PA, https://doi.org/10.2118/170243-PA.

[26] Badics B., Uhrin A., Vető I., Bartha A., Sajgó Cs. (2011). Medenceközponti földgáz-előfordulás elemzése a Makói-árokban. Hungarian Geological Society, *Földtani Közlöny*, 141 (1), pp. 23–40.

[27] Kiss K. (2014). *Magyarországi repesztések tapasztalatai, üzenetei*. Presentation material, Budapest, 30. 10. 2014, Access date: 10. 10. 2021, Access: http://docplayer.hu/19983811-Magyarorszagi-repesztesek-tapasztalatai-uzenete-kiss-karoly-kutatasi-projektek-vezeto-2014-10-30-budapest.html.

Geosciences and Engineering, Vol. 9, No. 14 (2021), pp. 116–127.
https://doi.org/10.33030/geosciences.2021.14.116

AN OVERVIEW OF OIL WELL DRILLING PROBLEMS IN SHALE FORMATIONS

(Case Study: Asmari Reservoir)

SOBHAN ANVARI

PhD Student, Institute of Petroleum and Natural Gas, Faculty of Earth Science and Engineering, University of Miskolc, Hungary
sobhan_anvari@yahoo.com

Abstract: Shale layers are found in 75% of the drilled sections in Iran, which causes 90% of the problems of instability of wells, and this can cause a number of problems, such as complete or partial collapse of the well or even loss of the well before it reaches its goal. On the other hand, the costs of instability can be reduced when drilling in shale formation using analytical and numerical methods considering the correct parameters. With the right understanding, we can help stabilize it. Preventing the problems caused by shale formations and resolving these problems requires an understanding of the features of the formation, familiarity with the changes caused by the physical and chemical interactions of the fluid, and awarness of the physiochemical properties of the drilling mud.

Keywords: *Oil wells, Drilling, Shale Formations*

1. INTRODUCTION

One of the major problems in drilling and exploration is the existence of deep-seated shale layers during drilling to production oil and gas. Despite extensive studies on the shale layers and their complex properties, the problems of shale layers still raise the cost of drilling oil wells. Most of the research on shale has investigated the physical and chemical properties of its behavior during and after drilling, attempting to stabilize the shale by introducing relationships for changes in drilling mud compounds. The study of shale from the perspective of rock mechanics is a new aspect of the studies that is being developed in recent years. One of the important issues in studying the stability of horizontal wells is the determination of in situ stresses. According to research, rock strength is a more important factor in rock stability than other parameters such as elastic properties of rock, drainage conditions, and layering surfaces [4, 19]. Shales containing clay minerals can react with aqueous base drilling mud and the inflation created by this reaction causes instability. In addition, shale rocks are weakly cemented and hardened at genesis and they are washed and eroded by the flow of mud. Another factor in the high tendency of shales to be unstable is their very high pressure.

Because the shales have very low permeability in the picodarcy to microdarcy range, and often because of the high initial deposition rate, the shales have much higher pressure than other sediments. Due to the low permeability of the shale, the mud cake does not form effectively in the well wall, so the formation does not have a good shield against well hydraulic pressure. On the other hand, induced hydraulic pressures due to low permeability are not able to diffuse rapidly within the formation to reduce effective stresses. Taken together, these factors increase the instability of the well. Drilling in the Iranian reservoirs where the shale layers are found is no exception and there are many problems for drilling companies. Asmari reservoir, one of the largest oil reservoirs in Iran, has shale layers and in this paper we will discuss its shale formations, look at shale types and their instability as investigated in theory and then take a critical look at the research that has been done on this field.

Studies by numerical methods can be attributed to the work of Low and Anderson in 1958 where, for the first time, using the thermodynamic relationships between water movement and ion exchange, they were able to propose a relationship called the osmotic pressure relationship. According to their research, to stabilize the well wall, a fluid with the lowest activity should be used, thereby reducing the osmotic pressure, which in turn would lead to stability and lowering the inflation of the shale wall [12]. Mohammadzade Sani investigated the stability of the well wall in the shale formation by FLAC3D software [16]. Mengjiao et al. investigated the model of wall instability in shale formations [14], which included parameters such as pro-elastic and chemical effects [3].

2. MINERALOGY OF CLAYS

Clay is a generic term that used to describe sediments, soils and very fine rocks. It is asoil material that aggregate one or more clay minerals with possible tinctures of quartz (SiO_2), metal oxides (Al_2O_3, MgO, etc.) and organic matter.Geologic clay deposits are mostly composed of phyllosilicate minerals containing variable amounts of water trapped in the mineral structure. Clays are plastic due to particle size and geometry as well as water content, and become hard, brittle and non-plastic upon drying.

This clay feature is due to the presence of some clay minerals in their structure. Clay minerals are fine-grained aluminosilicate minerals with microscopic structure. In the mineralogical classification, clay minerals fall into the group of sheet silicate minerals, because their main structure is layered and made of aluminum and silicate sheets. Each layer is like a thin sheet that it is called the single layer. Examples of sheet silicate minerals are mica and vermiculites, which are divided into thinner layers along their cleavage. Depending on the type of repeating plates in the mineral structure, clay minerals can also be divided by the number of silicate to aluminum plates, such as 1 : 1, 1 : 2, 2 : 2, etc. Clay is also called a batch of particles less than 2 microns in diameter that contains most of the clay minerals [23].

Most excavated clays have the same composition, structure and are derived from the weathering of igneous minerals. They later became sedimentary rocks due to

their transport and compaction. Each clay network consists of two tetrahedral silicon plates and one central aluminum octahedral plate. The corners of the tetrahedral plate are located toward the center of the network and form one layer with one of the octahedral hydroxyls. These two panels are horizontal, continuous and separated in the Z direction. The O^{-2} layers of each tetrahedral are adjacent to each other and between them there is a weak link and a Well-formed cleavage panel. Between these networks is water formation, so that both hydrogen atoms are opposite an oxygen layer [23]. The difference between the different clay minerals is in the deposition of aluminum in the central octahedral layer and the silicon in the tetrahedral layers, as well as the location of the other cations. This combination causes electrical instability, which is compensated by the absorption of cation into the intercrystalline region [21]. Diagenesis of clay minerals occurs in the following order:

- feldspar (mother minerals, weathered)
- smectite
- mixed-layer clays (periodically smectite and illite)
- illite and muscovite.

The conversion of clay minerals from each step to the next is accelerated by catalysts such as burial depth and geothermal heat. In this cycle, the activity for water absorption and cation exchange is gradually reduced [19]. Hydration and dispersion are two major mechanisms when reacting water with clay and shale formations. This reduces the compressive strength of these rocks [24].

3. CALCULATION METHOD OF VERTICAL, MINIMUM HORIZONTAL AND MAXIMUM HORIZONTAL STRESSES OF THE SHALE LAYER OF THE ASMARI FORMATION

Using log well data, it can be found that the shale layer occurs from the depths of 3,915 to 3,930 meters and because of the high shale gauge ratio (SGR) value at a depth of 3,915 m and the shale being pure, this depth has been chosen as the basis for the horizontal section studied to obtain vertical, minimum horizontal, and maximum horizontal stresses. The vertical stress is calculated by [25]

$$a_v = y \times h \,, \tag{1}$$

Where y is the average density of rocks from the surface of the earth to a depth of 3,915 meters in g/cm^3, and h is the given height in meters (depth 3,915 m). According to the average lithological density of the well, the vertical stress *vs* at the depth of 3,915 m was 98.17 MPa. To obtain the minimum and maximum horizontal stresses ($S_{H\ min}$ and $S_{H\ max}$), Anderson's fault theory is used to determine the stress regime. The values of the minimum and maximum horizontal stresses can be calculated using *Equations (1)* and *(2)* for different fault conditions [25].

Table 1

Relationships used to obtain mechanical and resistive properties of shale

Parameters in the equations	Equations
V_p is the longitudinal wave speed in meters per second and ΔT_p is the time of passing the wave length. [6]	$V_p = \frac{1}{\Delta T_P}$
σ_c is uniaxial compressive strength in MPa and V_p is the longitudinal wave velocity in kilometers per second.	$\sigma_c = 0.77 V_p^{2.93}$
$\emptyset$ is the angle of internal friction in degrees, and v_p is the longitudinal wave velocity in meters per second. [25]	$\Phi = sin^{-1}(\frac{V_p - 100}{V_p + 100})$
C is adhesion. S_0 is uniaxial compressive strength. μi is the angle tangent of internal friction. [25]	$2C = S_0[(\mu_i^2 + 1)^{\frac{1}{2}}\_\mu_i$
v_c is the transverse wave velocity v_p is the longitudinal wave velocity in meters per second. [15]	$\frac{V_p}{V_s} = 1.89$
ΔTS is the transverse wavefront in second per meters and the transverse wave speed is in meters per second. [6]	$\Delta T_s = \frac{1}{V_s}$
Ed is a dynamic elastic modulus in MPa, ρ is the density in kilograms per cubic meter, v_p is the longitudinal wave velocity in meters per second and v_s is the transverse wave velocity in meters per second. [17]	$E_d = \rho V_s^2 \frac{(3V_P^2 - 4V_s^2)}{(V_P^2 - V_s^2)}$
ν is the Poisson's coefficient, v_p is the longitudinal wave velocity in meters per second and v_s is the transverse wave velocity in meters per second. [17]	$v = \frac{V_P^2 - 2V_s^2}{2(V_P^2 - V_s^2)}$
ES is a static elastic modulus in GPa and v_p is the longitudinal wave velocity in meters per second. [10]	$E_s = 0.076 V_P^{3.23}$
G is the shear modulus, E is a static elastic modulus and V is Poisson's coefficient. [25]	$G = \frac{E}{2(1 - v)}$
K is the modulus of the bulk, E is a static elastic modulus and V is Poisson's coefficient. [25]	$K = \frac{E}{3(1 - 2v)}$

Normal faulting $$\frac{\sigma_1}{\sigma_3} = \frac{S_v - P_p}{S_{H_{min}} - P_p} \leq [(\mu^2 + 1)^{\frac{1}{2}} + \mu]^2 \quad (2)$$

Reverse faulting $$\frac{\sigma_1}{\sigma_3} = \frac{S_{H_{max}} - P_p}{S_v - P_p} \leq [(\mu^2 + 1)^{\frac{1}{2}} + \mu]^2 \quad (3)$$

Where σ_1 is the principal maximum stress, σ_3 is the principal minimum stress, SV is vertical stress, $S_{H\,max}$ is the maximum horizontal stress, $S_{H\,min}$ is the minimum horizontal stress, P_P is the pore pressure of the formation and μ is the angle of internal friction. By placing a value of 34.4 MPa for the pore pressure at high relationships, the value of $S_{H\,max}$ is 301.2 MPa and the value of $S_{H\,min}$ is 49.5 MPa (according to unpublished documents from the South Oil Company).

Assuming $S_{H\,max}$ as the vertical line and $S_{H\,min}$ as the horizontal line, the stress polygon can be plotted for the desired depth. This polygon defines the possible values of minimum and maximum principal stresses at any depth based on Anderson's fault theory as well as Moore-Coulomb's fault theory with a friction coefficient and pore pressure [1]. This polygon of the stress is plotted in *Figure 1*.

The optimal weight of the drilling mud can be determined by calculating the amount of collapse pressure and fracture pressure according to the stress conditions in a vertical well. If the calculated values of the collapse pressure (P_{Wf}) are greater than the actual mud pressure value in the well, the well will fail. Likewise, if the calculated values of failure pressure (P_{Wf}) are less than the actual value of mud pressure, the well will fail and it will be disrupted [2].

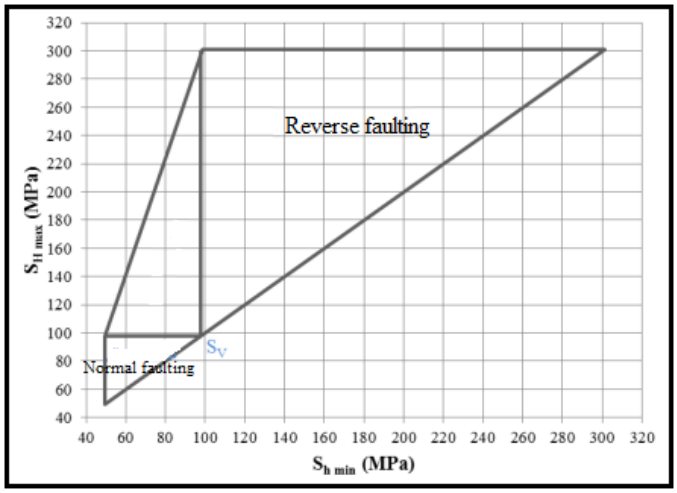

Figure 1

Stress Polygon for a depth of 3,915 meters and a pore pressure of 34.4 MPa

4. ADVANTAGES AND DISADVANTAGES OF OIL SHALE

Oil shales are distributed around the world and most of them are in the United States. By 2007, Brazil, Estonia and China were extracting oil shale. Geological surveys were carried out in Iran in the southern Alborz region in 1955 and in Ghalikoh and Zardkoh Lorestan in the year 1979, according to the Exploration Management Announcement. Experiments with oil shale in the region have shown that the grade of

the oil exceeds the world average. However, due to the impoverished areas and high costs of production, extraction and production of these resources is not currently a priority. In terms of estimating the volume of these reserves, according to an initial estimate made by the American company TOSCO in 1955, a significant amount of available reserves has been announced. Projects are currently being developed to estimate the volume of these reserves in the National Petroleum Exploration Management [5].

5. KEY PARAMETERS OF GAS SHALE EVALUATION

Among the parameters used to evaluate the gas shale, the following can be mentioned: Total Organic Carbon (TOC) (wt%): Its value can be estimated using different well logs or through laboratory analysis.

Maturity: Maturity is one of the important parameters for evaluating oil shales, which can be investigated through geochemical and mapping data. As can be seen in *Figure 2*, in immature rock (Ro < –0.5) the gamma diagram has a high irregularity, whereas in adult rock (Ro = 1) this irregularity is very low. Also, the separation rate (ΔlogR) of the resistivity and sonic diagram is high in adult rock and therefore will show more TOC. However, these two diagrams in the immature rock are completely irregular and show little separation. Geochemical parameters such as vitrinite reflectance coefficient, maturity index biomarkers and maturity-related carbon isotopes can be mentioned [20].

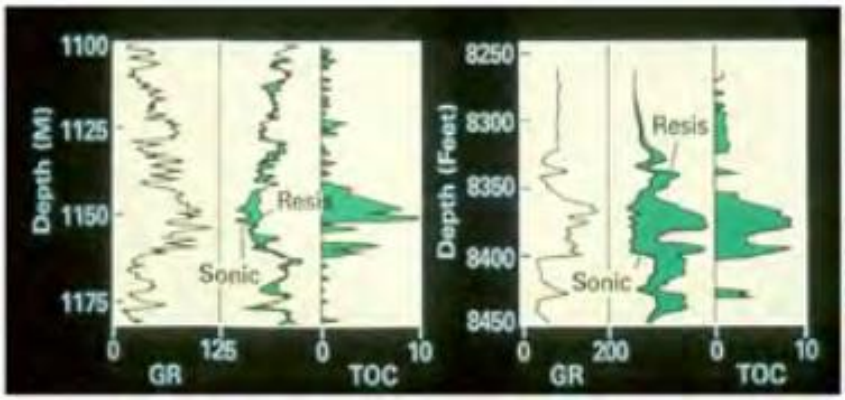

Figure 2

Diagrams used in maturity study (left in immature rock & right in mature rock)

Geochemical parameters (hydrocarbon type and quality): The type of kerogen can be determined using hydrogen index versus oxygen index (HI/OI) graphs or the atomic ratio of oxygen to hydrogen. T_{max} and other parameters can also be used for other evaluations such as maturity.

Total porosity: It can be used to evaluate porosity using a rock sample crushing method and also based on neutron, sonic and density diagram data.

6. WAYS TO DEAL WITH INSTABILITY WHEN DRILLING IN SHALE LAYERS

One of the major problems in drilling and production is the existence of deep-sea shale layers during drilling for oil and gas extraction. Despite many studies on shales and their complex properties, problems caused by the presence of shale layers still raise the cost of drilling oil wells. Most of the research on shale has investigated the physical and chemical properties of its behavior during and after drilling and has attempted to make the shale drilling mud composition more stable by introducing relationships [4, 18]. Chemical instability is often found in shale formations and is strongly influenced by drilling fluid composition. Shale is the most complex rock and is not well understood to this day. Shale properties include low porosity and permeability due to the large amount of clay minerals. Chemical reaction with aqueous base drilling fluids may cause serious problems in the stability of the well wall. Finally, the most effective way to solve or manage problems caused by shale instability may be weight, type, chemistry and particles of drilling mud, as well as the strategy of drilling a wall pipe [22]. Investigating shale from a rock mechanics perspective is a new aspect of the studies that has been under development in recent years. Determination of horizontal stresses is one of the important issues in the study of stability of horizontal wells. Changes in pore pressure have a significant effect on well stability during shale drilling, ecause shale has low permeability, as mentioned, and the flow of ions and water in it is very slow. It is argued that during drilling, there is a major pressure change near the well wall and there will be a large inductive pore pressure gradient in that small area.

7. INVESTIGATION OF DRILLING PROBLEMS IN CRACKED SHALE LAYERS OF DASHTAK FORMATION

Problems in the drilling industry include dealing with shale formations and controlling the instability and loss of wells in these layers. In recent years we are witnessing continuous research in the study and production of new mud and polymer materials in the mud industry. All of these moves are aimed at finding a viable, low-cost solution to hydrocarbon resources. One of the most important problems in drilling wells in the Fars region used to reach the huge gas reserves in the Ofogh-e-Dahrom is crossing the shale Dashtak Formation. There are several drilling problems associated with one of the thickest and most important formations of Iran, which in the gas reservoirs of Ofogh-e-Dahrom acts as an excellent rock cover. The numerous mud waste in this formation have causes many problems in drilling wells in this region. Thus, drilling professionals are always been looking for solutions to overcome these problems.

The presence of waste and falling of the well wall not only increases the cost of drilling due to the high cost of materials used in mud, but also causes other major problems such as the instability of the well and the clogging of drilling pipes. Also, the residue left in the well due to the shale loss should not be ignored. Residual operations also require a great deal of time and expense in drilling operations. Residual operations in the shale formation are more difficult than in calcareous formations due to

the waste and loss of the shales. Therefore, detailed studies should be carried out on drilling in this formation or in shale layers in general [13].

Shale layers of the Borgan Formation

Identification and detection of clay minerals begins with sampling. Depending on the type and number of experiments, the core and shale sediments of the formation are sampled. It is advisable to specify the exact location of the sample for each of the experiments in the area map. The Borgan Formation of the Cretaceous is one of the most important rocks of the Persian Gulf hydrocarbon reservoirs. The Borgan Formation is an oil field consisting of fine-grained to medium-grained sandstones, rock clay, calcareous shales and carbonate-limited sequences [7, 9]. According to the type of experiments, the required number and amount of shale cores from the Borgan Formation at depths of 2,208 to 2,254 m wells were sampled by the employer. Experiments and identification methods were determined and implemented using the laboratory experiences of colleagues at the Petroleum Industry Research Institute as well as the results of studies in related published articles [11]. These samples will be used for experiments to study and identify clay minerals among shale layers including X-ray diffraction (XRD) analysis, scanning electron microscopy (SEM), X-ray fluorescence (XRF) and more. In this experiment, based on the results of different experiments on samples of core wells, it can be stated that the major minerals of shale formations samples are quartz and clay minerals. Kaolinite, with a frequency of 66%, and illite, with a frequency of less than 12%, are the most abundant clay minerals in the samples and quartz is the most abundant mineral, up to 32%. The size of the quartz particles is mainly in the range of silt to fine sand.

8. INVESTIGATION OF DRILLING PROBLEM OF SHALE AND MARNI FORMATIONS

Habibnia and Dinarvand [8] studied the Maron oilfield, one of the most important fields in the Zagros oil basin (40 km east of Ahvaz). From the geological point of view, the field is located in the northern of Dezful and between the Koopal, Aghajari, Ramin, Shadegan and Ramshir fields, as shown in *Figure 3*. According to [8], 320 wells had been drilled in the field up to that point (2012 or 2013). The extensive presence of shale sediments along with high amounts of marn in the stratigraphic column has caused many problems during the drilling of wells in this field. Therefore, conducting this study in this field is essential and can provide valuable results for tackling the problems of tube entrainment. In their study, 18 shale samples and more than 30 marn samples from 8 wells with different depth intervals were tested. Since most shale minerals are composed of silicates, hydrofluoric acid (HF) was used as one of the main materials of the designed fluid. First, the powdered sample was sifted uniformly and placed in a pill making machine. The tablets were pressurized and prepared by applying a force of 60 kN. The pills were carefully weighed and then placed in different solvents. After 20 minutes, these pills were weighed again. The results are presented in *Table 2*. The observed weight difference indicates the degree of disintegration [8].

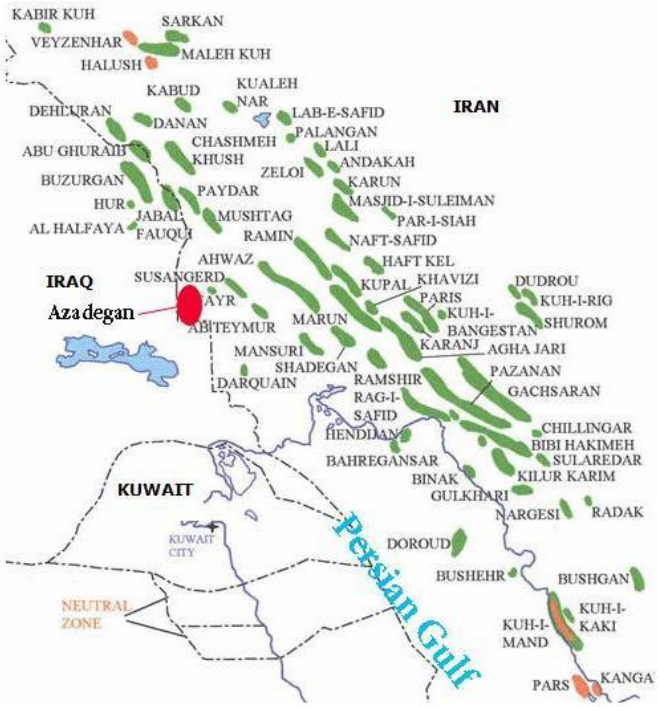

Figure 3
The position of the Maron oilfield and its adjacent fields

Table 2
Results of using different solvents with one type of pills

Original material	Solvent	Time to minute	Result
HF2%	Urban water	20	Inflation
HF5%	Urban water	20	There was not much difference, but the appearance of the pill became more fragile and corrupted
HF5%	Water saturated with NaCl to prevent shale in-flation	20	1 – Reduce the corrosive power of acid. 2 – Weight difference was negative due to NaCl deposition 3 – No shale Inflation
HF5%	Alcohol	In less than a few minutes, the pill was completely destroyed	High disintegration and low inflation

Original material	Solvent	Time to minute	Result
HF2%	Alcohol	In less than a few minutes, the pill was completely destroyed	High disintegration power and low inflation (best result)

Achieving meaningful results without affecting the shape and size of drill cutting requires uniform grading and the conditions used in various experiments. That is why all the samples used in the experiment were prepared by first grinding mill and then in the form of pills of equal size, done by a special template designed by the researchers. Using the results obtained from the experiments performed, the best combination of the quenching fluid and its properties were found to be:

- HF acid as the main dispersant of shale;
- HCl acid to dissolve impurities and create a contact area for the main acid;
- Alcohol as an accelerator of action [8].

9. CONCLUSION

Well instability in drilling operations can be due to formation leaching, erosion of the well. Of all the formations that exhibit extreme instability, shales have been identified as the most problematic in that 90% of the problems of instability of wells are related to drilling in shale layers. According to the well log data studied, Anderson's fault relationships, using the Mogi-Coulomb fracture criterion reveal that the stress regime is normal in the studied well range. Optimization of mud weight is essential to reduce well fall and problems associated with related to it and to reduce drilling mud invasion into the formation. To stabilize the well wall, the mud pressure must be selected that is between the collapse pressure and the fracture pressure.

Due to low porosity and permeability, low efficiency and the high cost of oil and gas shale, countries with less conventional resources pay less attention to this source. However, in recent decades, in the United States, due to the rise in fossil fuel prices, oil shale has been exploited. Harvesting from shale sources is dependent on fuel prices and technology availability. The presence of nitrogenous and oxygenated compounds gives rise to specific properties such as gravity and specific odor in shale oil.

REFERENCES

[1] Ahmadi, M., Soleymani, M., Salehi Siyavoshni, N. (2010). Stability of oil wells in Ahvaz Shale layers. *Monthly magazine Oil Research*, No 63, pp. 12–18. (In Persian)

[2] Al-Ajmi A. M., Zimmerman R. W. (2006). Stability analysis of vertical boreholes using the Mogi-Coulomb failure criterion. *Int. J. Rock Mech. & Min. Sci. & Geomech*., 43, 1, pp. 1–15.

[3] Chen, G., Chenevert, M. E., Sharma, M. M., Mengjiao, Yu. (2003). A Study of wellbore stability in shales including poroelastic, chemical and shale layers. *Monthly magazine Oil Research*, No 63, pp. 12–18. (In Persian)

[4] Chen, X., Tan, C. P., Detournay, C. (2002). The impact of mud infiltration on wellbore stability in fractured rock masses. *SPE/ISRM Rock Mechanics Conference*, Society of Petroleum Engineers, 20th October 2002, Irving, Texas.

[5] Department of Energy Management, International Institute for Energy Studies. Country Hydrocarbon Balance Questionnaire (2008). Publication: Tehran, International Institute for Energy Studies 2009. *Hydrocarbons Division*, pp. 15–40. (In Persian)

[6] Fjaer, E., Holt, R. M., Horsrud, P., Raaen, A. M., Risnes, R. (2008). Geological aspects of petroleum related rock mechanics. *Developments in Petroleum Science*, No. 53, pp. 103–133.

[7] Ghazban. F. (2009). *Petroleum Geology of the Persian Gulf*. University of Tehran Press.

[8] Habibnia, Bahram, Dinarvand, Navid (2013). Investigation of the Drilling Dilemma of shale and Marn Formations and Fluid Design in Maron OilField. *Advanced Applied Geology Journal*, Issue 10, pp. 48–53. (In Persian)

[9] Honarmand, J. Moalemi, S. A., Lotfpour, M. (2009). Investigation of Lithofacies, Sedimentary Environment and Sequence Stratigraphy in Bourgan Formation in Northwest of Persian Gulf. *Stratigraphy and Sedimentology Research, Journal of Isfahan University of Basic Sciences*, 37 (2), pp. 135–150. (In Persian)

[10] Horsrud, Per (2001). Estimating mechanical properties of shale from empirical correlations. *SPE Drilling & Completion*, 16 (2), pp. 68–73.

[11] Kurdi, M., Bashari A. (2013). Identification of clay minerals of Scorpion Formation (Bourgan Sand) and their impact on the Persian Gulf reservoir rock. *Scientific Journal of Oil & Gas Exploration and Production*, 1382 (5), pp. 16–17. (In Persian)

[12] Low, P. F., Anderson, Duwayne M. (1958). Osmotic pressure equations for determining thermodynamic properties of soil water. *Soil Science*, 86 (5), pp. 251–253.

[13] Mengjiao, Yu., Chenevert, E. Martin (2003). Chemical-mechanical wellbore instability Model for shales: accounting for solute diffusion. *Journal of Petroleum Science and Engineering*, No. 38, pp. 131–143.

[14] Miller, S. L. M., Stewart, R. R. (1990). Effects of lithology, porosity and shaliness on P and S-wave velocities from sonic logs. *Canadian Journal of Exploration Geophysics*, 26 (1–2), pp. 94–103.

[15] Mohammadzade Sani, M. (2013). *Wellbore stability design in shale formations*. Petroleum engineering master's thesis, Faculty of Engineering, Kerman Shahid Bahonar University. (In Persian)

[16] Najibi, Ali Reza, Ghafoori, M., Lashkaripour, G. R., Asef, M. R. (2015). Empirical relations between strength and static and dynamic elastic properties of Asmari and Sarvak limestones, two main oil reservoirs in Iran. *Journal of Petroleum Science and Engineering*, 126, pp, 78–82.

[17] Ottesen, S., Kwakwa, K. A. (1991). A multidisciplinary approach to in-situ stress determination and its application to wellbore stability analysis. *SPE/IADC Drilling Conference*, Society of Petroleum Engineers, Amsterdam, Netherlands.

[18] Passey, Q. R., Creaney, S., Kulla, J. B., Moretti, F. J., Stroud (1990). A practical model for organic richness from porosity and resistivity logs. *AAPG Bulletin*, 74 (12), pp. 1777–1794.

[19] Patel, Arvind, Stamatakis, Emanuel, Friedheim, James E., Davis, Eric (1994). *M-I Drilling Engineering Manual*. 5th Ed. chapter B and 11, MI-SWACO pub., Texas, USA.

[20] Rahman, M. K., Naseby, D., Rahman, S. S. (2000). Borehole collapse analysis incorporating time-dependent pore pressure due to mud penetration in shales. *Journal of Petroleum Science and Engineering*, 28 (1–2), pp. 13–31.

[21] Rieke, Herman, H., Ghilingarian, George V. (1998). *Compaction of Argillaceous Sediments*. Chapter Y, Elsevier Scientific Pub. Co., New York.

[22] Van Oort, Eric. (2003). On the Physical and Chemical Stability of Shales. *Journal of Petroleum Science and Engineering*, Vol. 7A, pp. YT.YTO.

[23] Zoback, Mark D. (2007). Reservoir Geomechanics. New York, Cambridge University Press.

Geosciences and Engineering, Vol. 9, No. 14 (2021), pp. 128–139.
https://doi.org/10.33030/geosciences.2021.14.128

PROXY MODEL FOR HYDROCARBON RECOVERY IN A SEVEN-SPOT WATERFLOODED WELL PATTERN

DÁNIEL BÁNKI[1] – ZOLTÁN TURZÓ[2, *]

[1, 2]*Petroleum and Natural Gas Institute, Faculty of Earth Science and Engineering,*
University of Miskolc
[2]*turzoz@uni-miskolc.hu*

Abstract: This article is about establishing an artificial modeling environment using real data, then creating special formulae in order to estimate the recovery factor of the depletion of the reservoir model. The key concept is that these aids in the form of formulae can be very useful, economic and fast methods to help reservoir simulation. Waterflooding was examined in previous years and a sensitivity analysis was conducted several times. First the parameters were screened for impact and importance, then the structure of the resulting proxy model was chosen, along with the accuracy, both based on the focus of investigation itself, which is the recovery factor. The artificial reservoir environment is a seven-spot water flooded well pattern in an initially undersaturated oil reservoir. The results in this particular study are three formulae which are capable of predicting the recovery factor with a satisfactory error margin after five, ten, and fifteen years of production as a function of the initial produced fluid rate target.

Keywords: *reservoir simulation, proxy model, recovery factor estimation*

1. INTRODUCTION

The aim of analytical formulae, proxy models, and any mathematical short-term estimation tool is to help make complex calculations simple and to aid in fast decision making. The accuracy of these is always less than a normal modeling system's performance in this area, and often more application borders need to be set up in order to keep the formula working, but all these fall into the normal nature and behavior of the application of these methods. The benefit is more rapid decision making, due to the fact that for example in reservoir simulation no big simulation runs are needed to find out essential results of smaller modifications, thus saving both time and money.

This nature of descriptive science has always been part of reservoir engineering, geophysics, drilling engineering and so on [1]. One can call these rules of thumb, empirical formulae, or base functions, but the idea is the same: to provide an easier, more affordable tool for performing relatively small calculations, rough estimations etc. In order to have a better understanding of and justification over decisions made during the simulation and regression workflow, a short summary of previous studies is needed.

The first step in examining the behavior of complex hydrodynamic systems is to find a suitable environment for investigation [5]. This step may seem easy, but in the practical world of reservoir simulation this is the first challenges to overcome. The reason is quite simple: in this area of science, if somebody is familiar with the development, constraint and un-readiness of a field data reservoir model, it is not hard to conclude that if we would like to observe and describe something from the beginning, these environments are far from ideal. The magnitude of uncertainty and the size and reliability of these models are perfectly good for industrial use, but are less suitable base for an academic research project [1] [6].

The next step further is the introduction of artificial models, but this process brings up more problems to solve, even before any investigation is started. First and foremost, when using reservoir simulators, several iterational processes and flow equations are being solved in the background, and inside the solution chain there are also some empirical formulae. All in all, it is not sufficient to have artificial and real data sewn together; one has to have realistic artificial datasets. The pressure, composition, soluted content of gas within the oil phase and phase density according to this must be realistically paired up with the saturation functions, and then this set of data has to imported into an also realistic environment in terms of pressure, temperature, depth, contacts, etc. Even when using multiple real data sources, cautious attention has to be used to generate a hydrodynamic system which really could have been generated naturally.

As an example, if the PVT data are imported from real measurements of a heavy oil mixture with the lack of some intermediate hydrocarbons, then in theory the density and solution gas oil ratio can be imported from another real dataset, but in this case the density should be quite a bit higher than normal oil density, and the solution gas oil ratio should not be too big, hence the fact that this composition cannot really hold solution gas in the liquid phase without proper intermediate content. Usually, that is the reason why PVT datasets are almost always imported from the same source. Saturation functions (relative permeability, capillary pressure), can, in theory, be originated from different sources, but the same rules apply in their implementation.

After setting up a stable and realistic modeling environment, the well and production data is the next step. For this, a seven-spot pattern was used with peripheral waterflooding (six injectors) and one production well. If the dynamic variables are set, the sensitivity analysis is the following procedure. In this case the variable was the starting liquid rate target. The accurate rate changes throughout the production period due to natural behavior of production rate decline, but for convenience, later on, the desired starting rates will be referred as production rate. Once a desired rate is set, the production can only keep up that rate for a certain amount of time, and then as depletion follows, the oil production rate will decline.

With the results for the recovery factor after 5, 10, 15 years of production, the datasets for regression were basically gained, but before fitting a formula onto the

dataset, the validity borders and even the extents of the data ranges have to be investigated and post processed. Once the "valuable" data remain, the next step is regression in order to find out the best correlation between the starter rates and the recovery factor. In particular, three third-degree polynomial formulae were found and 2D and 3D response surfaces were also generated.

2. MODEL SETUP AND PROPERTIES

In this chapter, the main characteristics of the reservoir modeling environment will be discussed. In order to establish dynamic flow modeling, it is necessary to start with the static environment, the grid, and the static reservoir properties themselves. Then the fluid, rock and saturation parameters are added, such as compressibilities, reference depths and pressures, relative permeability and capillary pressure datasets, densities etc. As a final configuration, well placement, completion data, wellbore sizes, and skin factors are added, and in the last section production rates and limits and injection controls are added for customized depletion. The datafile ends with the timestep controls, and in the last section there is also possibility to tune the solution controls, for example the maximum number of non-Newtonian iterations, etc.

2.1 Grid, geometry and reservoir parameters

The main aim was to generate an artificial reservoir model depleted with waterflooding, and for this, a seven-spot well pattern was chosen. The inclusive grid consists of 13 × 9 × 10 cell blocks, each block is 360 × 360 feet, with a thickness of 15 feet. This is the main frame, from which, using cell deactivation, the hexagonal shape of the well-pattern was carved out, leaving 77 cells out of the original 117 in each layer. Cell layers are defined for modeling, but for regions, lithological layers should be established. That means in this case, that out of the 10 cell layers, 5 "lithological" units were formed, each having different porosity and permeability values. The environment mimicked is a sandstone reservoir, so the porosity-permeabilities values fit into this trend and scale. The depth of the cell layer tops and the regarding poro-perm data can be found in *Table 1*.

Table 1

Regions, porosities and permeabilities of the reservoir

Layer	Region	Top of structure [ft]	Porosity [%]	Permeability [mD]
1	1	7,800	15	170
2		7,815		
3		7,830		
4	2	7,845	20	600
5		7,860		
6	3	7,875	15	170
7	4	7,890	18	200
8		7,905		
9	5	7,920	20	600
10		7,935		

The top of the reservoir is at 7,800 ft in depth, with the 10 ×15 feet cell thickness yielding a total reservoir thickness of 150 feet. The oil-water contact is set to 8,200 feet, acting as a semi-closed reservoir with a passive aquifer, hence the transformation of the pore volume higher than the oil-water-contact (OWC). The initial average reservoir pressure is 3,316 psi. The pressure and the solution gas-oil ratio were set to yield an undersaturated oil reservoir at the start of the simulation. [3] A 3D picture of the grid with the active cells, major extents and the wells is shown in *Figure 1*.

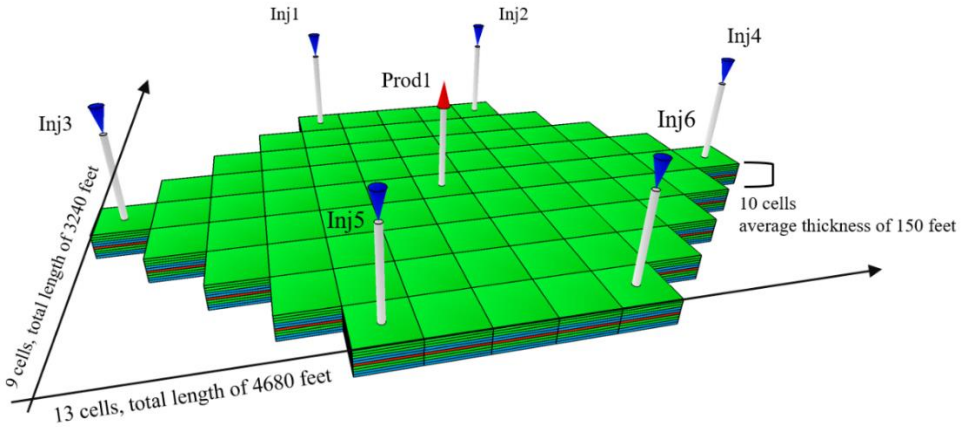

Figure 1

Geometry, extent and injection and production well positioning of the reservoir

2.2 Fluid properties and saturation functions

The initial calculation of the modeling process is called equilibration, often regarded as time zero calculation. Based on the built-up grid, the rest of the cells should also be filled with fluid parameters. From the reference pressures, depths, hydrostatics with the densities, capillary pressure and relative permeability curves equilibrium is calculated in order to yield the initial fluid in place data before even the first timestep of dynamic modeling is reached [4].

For the success of this equilibration, the next process is to implement all the fluid properties needed. Density of the phases for oil, water and gas were 52.9989, 66.7593 and 0.0651035 in lb/ft^3, respectively. For both water and reservoir rock, a reference pressure and compressibility data pair were also used. For PVT data, real fluid measurement was used, where datasets included bubble point pressure, formation volume factor and viscosity in terms of gas-oil ratio for oil, and formation volume factor with viscosity for the gas phase. The reason not including these here is the length and size of the datasets: only for the oil phase, one set of PVT data is more than three pages. As an example, a graph for the viscosity vs pressure vs solution gas oil ratio for the oil phase is displayed in *Figure 2*.

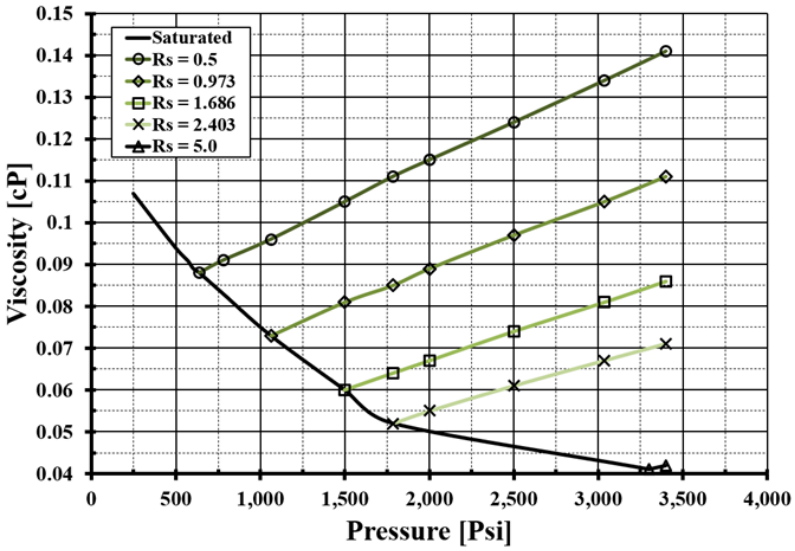

Figure 2. *Effect of different solution gas-oil ratios on viscosity*

In order to have any quantitative result on fluid flow within the cells, the content of the cells is calculated with the usage of saturation functions. Under this expression, a set of water-oil and gas-oil relative permeability curves and a matching water-oil capillary pressure curve are defined. [2] The input is in tabular format, and the simulator will yield the non-existing data ranges later on by using spline interpolation. These datasets have to be treated as one unity; even in artificial model establishment, the saturation function should come from one specific fluid system. The values for relative permeabilities in the water-oil system are used as an example in *Figure 3*.

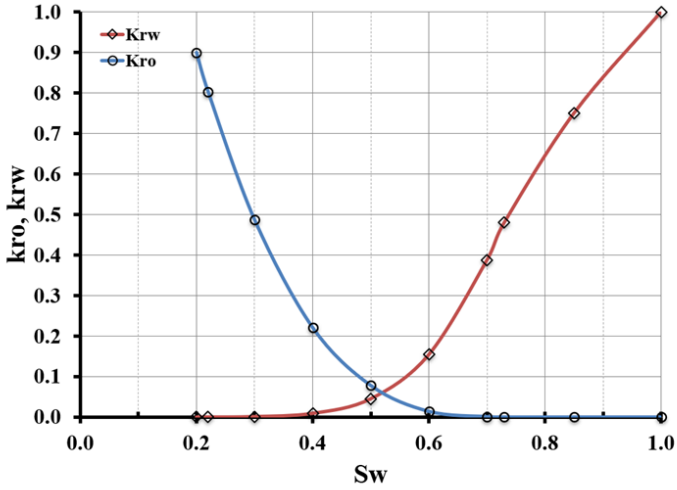

Figure 3. *Water-oil relative permeability data*

2.3 Well specifications and production criteria

For a seven-spot pattern type, the layout of the wells in the waterflooded reservoir model has six injector wells at the peripheral corners of the hexagonal shape and a single producer in the middle of the grid. The diameter of the tubing for each one is 0.625 feet, and all near wellbore vicinity zones have a unified skin factor of 7.5. According to completion all wells are open in every cell layer. These values and options may be too idealized, but the aim of the study is to examine recovery factor based on initial rate only. Of course in a real reservoir management scenario there is a big step of optimizing depletion, but in this case that change would also alter the outcome and focus of the study.

The reservoir is depleted using waterflooding for pressure maintenance and displacement towards the production well. In order to keep the liquid rate controlled, a specific liquid rate of 2,000 STB/day primary liquid production rate is set up. To aid displacement, reservoir voidage replacement was used with a multiplier of 0.95 for the injector wells, which were under group control based on the actual liquid outtake of the producer well. To prevent the production of gas and the formation of a secondary gas cap, a flowing bottomhole pressure limit was also set for the producer. Checking the solution GOR of the initial reservoir conditions and matching it with the corresponding bubble point pressure from the PVT datasets, a pressure limit of 1,400 psi was set to ensure that this value is always higher than the actual bubble point, and as since the average reservoir pressure is even higher than that, the formation of a secondary gas cap was prevented.

2.4 Time variables, base case characteristics

The size of the timesteps was 30 days, and based on the number of the timesteps (185), total simulation time was around 15 years. The values described in this chapter are considered as the base case values for the sensitivity analysis. Based on this, 35 other production rate-based scenarios yielded the data for regression in the sensitivety analysis. The graphs in *Figure 4* show the main characteristics and behavior of the base case scenario. For this display, flowing bottomhole (BHP) and average reservoir pressures (FPR), oil production rate (FOPR), gas-oil ratio (GOR), watercut (FWCT), and recovery factor (FOE) were selected.

During the depletion period, the reservoir pressure is decreasing mildly due to the controlled voidage replacement. GOR, as a constant, is a good indication of no free gas in the system. Regarding flowing bottomhole pressure, the line moves together with reservoir pressure up the point when the desired oil and liquid rate cannot be managed. The liquid rate is insufficient due to pressure decrease, and the oil rate cannot be held because – as the watercut curve indicates – there is a water breakthrough in roughly the tenth year of production. The recovery factor increases monotonously as long as the oil production rate is constant, but after reaching the extents of this depletion, the steepness is reduced. If the production period were longer, the recovery factor curve would converge to a possible maximum value.

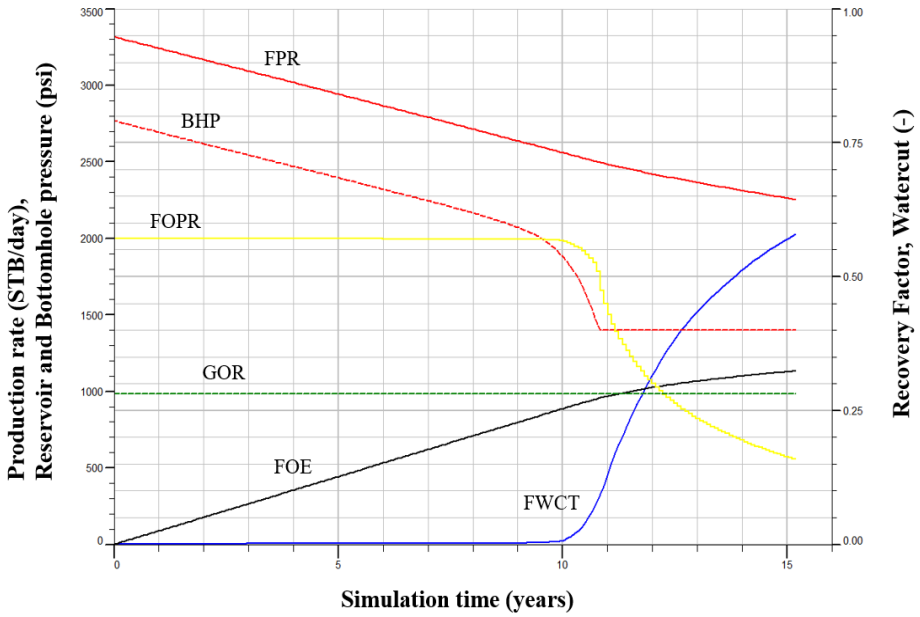

Figure 4. *Main characteristics of the base case scenario*

3. SENSITIVITY ANALYSIS AND REGRESSION

After establishing the main model, running and understanding the base-case scenario, the next step of investigation was the sensitivity analysis, which in this study focuses on checking the recovery factor at 5, 10 and 15 years of production if the initial liquid target changes. For this, a total set of 36 scenarios was established. The results of the analysis, the production start rates in stb/day and the corresponding recovery factor values can be found in *Table 2*.

From these, minor adjustments should be made to increase later accuracy of the formula and decrease unwanted error in the regression. At selected points, the predefined initial values were set, though at high preferred initial values, the reservoir cannot even bear that rate even at the start. That means that after this critical rate, basically only the numbers were changed in the scenarios, but the outcome was the same. A critical rate of 7,300 STB/day was found to be the first rate that cannot be sustained by the reservoir from the start date. For the sake of objectivity, in *Table 2*, all the results are included, but the values shown in italics were removed due to these reasons. In other words, if for regression the rate is changing but the outcome is the same, that will fail any attempt to find correlation at that part of the data, and will generate significant error in the fit, as the regression will try to use best fit, and shift the fitted curve towards these false datasets, which is undesirable.

Table 2

Recovery factors based on initial rate after 5, 10 and 15 years of depletion

Rate	RF 5	RF 10	RF 15
100	0.0064	0.0127	0.0191
200	0.0127	0.0254	0.0381
300	0.0191	0.0381	0.0572
400	0.0254	0.0508	0.0762
500	0.0318	0.0635	0.0953
600	0.0381	0.0762	0.1143
700	0.0445	0.0889	0.1334
800	0.0508	0.1016	0.1524
900	0.0572	0.1143	0.1715
1000	0.0635	0.1270	0.1905
1200	0.0762	0.1524	0.2286
1400	0.0889	0.1778	0.2661
1600	0.1016	0.2032	0.2959
1800	0.1143	0.2286	0.3126
2000	0.1270	0.2539	0.3226
2200	0.1397	0.2771	0.3294
2400	0.1524	0.2908	0.3346
2600	0.1651	0.2998	0.3386
2800	0.1778	0.3063	0.3418
3000	0.1905	0.3113	0.3444
3200	0.2032	0.3152	0.3465
3400	0.2159	0.3183	0.3483
3600	0.2286	0.3209	0.3498
3800	0.2413	0.3231	0.3511
4000	0.2537	0.3249	*0.3522*
4500	0.2720	0.3284	*0.3544*
5000	0.2800	0.3308	*0.3558*
5500	*0.2844*	*0.3323*	*0.3568*
6000	*0.2869*	*0.3331*	*0.3573*
7000	*0.2888*	*0.3338*	*0.3577*
8000	*0.2888*	*0.3338*	*0.3577*
10000	*0.2888*	*0.3338*	*0.3577*
12000	*0.2888*	*0.3338*	*0.3577*
16000	*0.2888*	*0.3338*	*0.3577*
20000	*0.2888*	*0.3338*	*0.3577*

The next adjustment is due to the shape, in other word the mathematical structure of the recovery factor curve itself. As discussed previously, after the breakthrough, or after several years of high depletion rate, the curve itself will tend towards the possible maximum value, and become flat afterwards. This, as generally having the same effect as being above the critical rate, will also affect the fit. In order to eliminate this, the datasets were only included to the point where there is at least 0.1–0.5% change in the recovery factor between the two neighboring scenarios. These are also in italics in the table. For 5 and 10 years, the last scenario is 5,000 stb/day, and for 15 years, due to being at the maximum for a long period, is 3,800 stb/day. The recovery factor curves are shown in *Figure 5*.

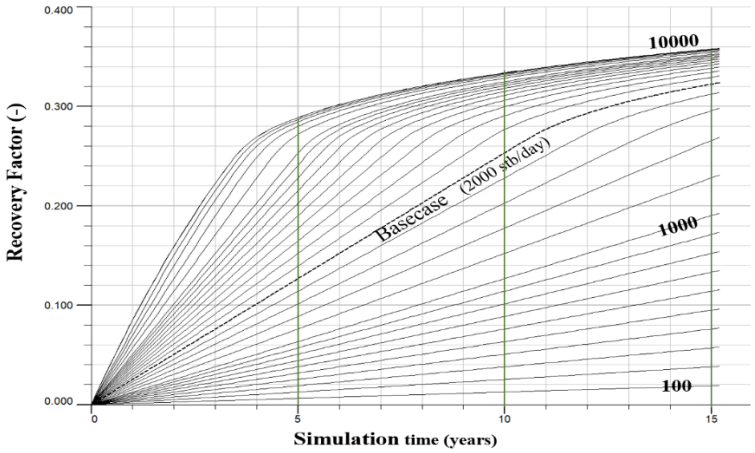

Figure 5. *Recovery factor curves of the sensitivity analysis*

Regression was applied after the datasets were chosen. Based on the behavior of the Recovery factor curve, the idea to split the time period into three discrete formulas was described in [8]. To sum it up, as the recovery factor curve has very distinct parts, the mathematical functions to fit those parts are specific, too. Therefore, having one formula for the entire timespan will not lead to the desired accuracy. In addition, companies have production plans for discrete time periods, so the idea can still be applied when the desired timespan is known. As a result, three distinct datasets were fitted with functions. In previous work examining water breakthrough, the logarithmic fit proved to be successful, but in a form of a log scale straight line equation [8]. In this study the resulting best fit after the ln-ln plot was a third-degree polynomial. The maximum allowed difference in estimated and simulated recovery factor was set to 1.5%. The plotted datasets with the fitted curves are displayed in *Figure 6.*

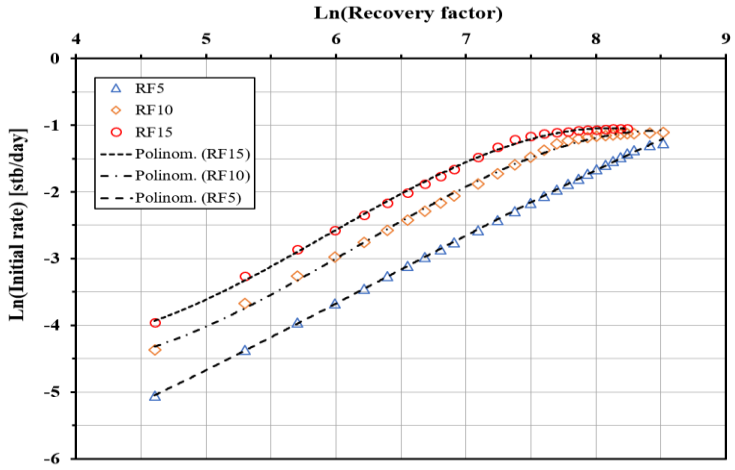

Figure 6. *Dataset and fitted functions for the recovery factors*

The parametric form of the fitted function is described in *Equation 1*, and the coefficients for the three regressions are listed in *Table 3*.

$$ln[RF] = a_1[ln(lrate)]^3 + a_2[ln(lrate)]^2 + a_3[ln(lrate)] + c \quad (1)$$

Table 3

Coefficients, R^2 values and average differences of the fitted functions

Timespan	a1	a2	a3	c	R^2	avg. difference in Rf
Rf 5 year	–0.0098	0.1855	–0.1535	–7.3219	0.9997	–0.26%
Rf 10 year	–0.0667	1.2285	–6.4207	5.7121	0.9980	+0.14%
Rf 15 year	–0.0793	1.4124	–7.2716	7.3504	0.9986	+0.32%

Near the end of the three periods, at the highest rates for each, the recovery of the reservoir model approaches the possible maximum of the system. If we take only the linear part on the ln-ln fit, the accuracy is better, but of course the validity range is smaller. Because the correlation between the initial liquid rate and the recovery was changing shape at the end of the 5-, 10- and 15-year depletion periods, a polynomial fit seemed to be better, with controlled degree. The end result is a third-degree polynomial with the right curvature at the end of the datasets. In terms of accuracy, there is a strictly linear part, which will have some errors when approached with a polynomial. The concept of accuracy was to define the time period and give a solution with the lowest average error [7]. If the production time is even longer, or the breakthrough is postponed, then a further split of the fit is suggested, to have both a linear part and a polynomial part of the fitted curve. Another possible approach for the short-term forecast to have high accuracy is to only take the linear part into consideration when applying the fit. The error of the formulae is displayed in *Figure 7*.

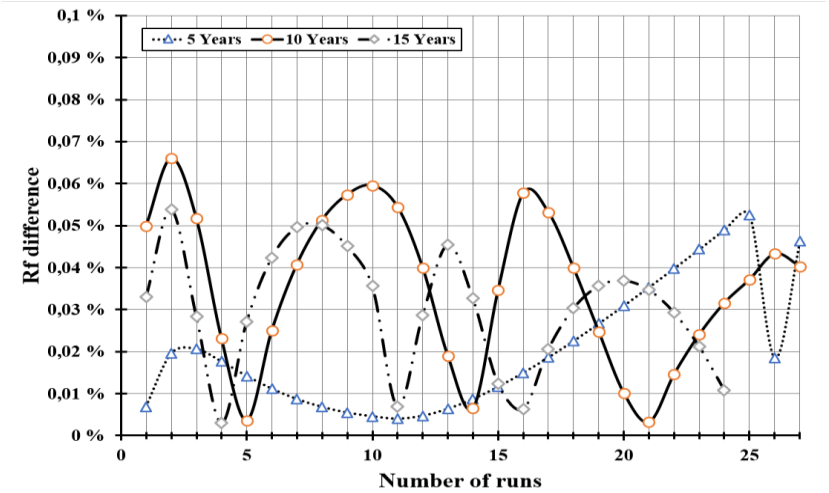

Figure 7. *Accuracy of the fitted functions*

4. RESULTS AND CONCLUSIONS

The aim of the study was to generate a proxy model – in other words, analytical formulae – in order to estimate the recovery of an artificial reservoir model. In this article the examined reservoir was an undersaturated oil reservoir depleted by water-flooding, using a seven-spot well pattern with peripheral water injection and central oil production. The produced fluid was set to be only oil and water with the introduction of a minimum flowing bottomhole pressure limit in order to keep the entire flowing system in the reservoir and at the sandface single phase. For this purpose, first the modeling grid and reservoir properties were implemented in simulation software, then the fluid and well properties were added, to create a base-case scenario. After creating a stable base case, sensitivity analysis was conducted to gain datasets of recovery factors of 5, 10 and 15 years of production, respectively, as a function of the initial liquid production rate stated in the datafile. The results in order of increasing recovery factor can be found in *Figure 8*.

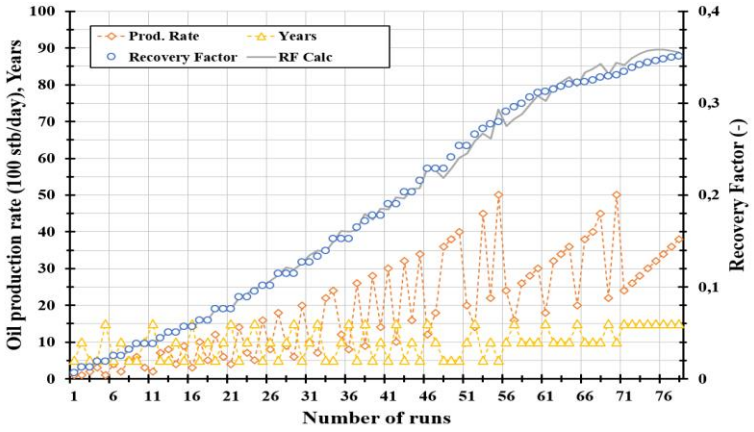

Figure 8. *Results of the calculation with increasing recovery factor*

After the removal of duplicate and false datasets, a regression was performed on the remaining datasets in each case, resulting in third-degree polynomial formulae that are capable of estimating the recovery factor with a maximum error margin of 0.07% (in terms of RF difference). The results are displayed in *Equations (2)–(4).*

$$ln[RF\,5] = -0.0098[ln(lrate)]^3 + 0.1855[ln(lrate)]^2 - 0.1535[ln(lrate)] - 7.3219 \quad (2)$$

$$ln[RF\,10] = -0.0667[ln(lrate)]^3 + 1.2285[ln(lrate)]^2 - 6.4207[ln(lrate)] - 5.7121 \quad (3)$$

$$ln[RF\,15] = -0.0793[ln(lrate)]^3 + 1.4124[ln(lrate)]^2 - 7.2716[ln(lrate)] - 7.3504 \quad (4)$$

For further application, these types of formulae can also be used to generate charts of the solution, and it is also possible to establish a three-dimensional response surface, such as that seen in *Figure 9*. Note that in this particular case, hence the three

distinct equations, the points between the functions in the figure are results of simple linear interpolation for display purposes only.

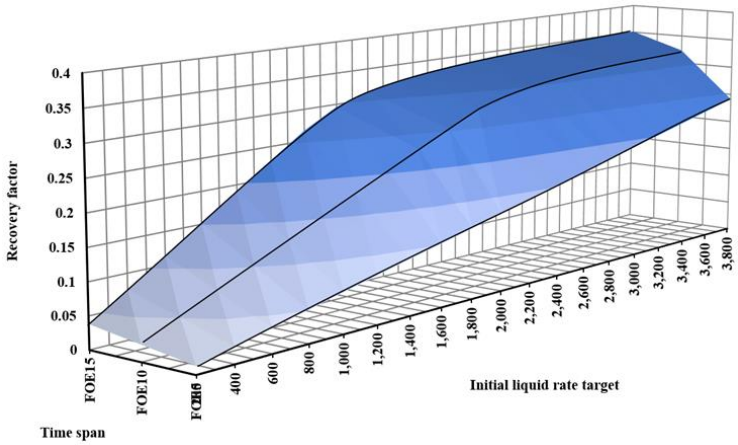

Figure 9. *3D surface generated from the formulae*

REFERENCES

[1] Gokhale, S.S. (1998). *Analytical Modeling, Encyclopedia of Distributed Systems*. Kluwer Academic Publishers, Amsterdam.

[2] Papay, J. (2003). *Development of Petroleum Reservoirs.* Budapest, Akadémiai Kiadó.

[3] Schlumberger Information Solutions (2008). *ECLIPSE Blackoil Reservoir Simulation*. Houston, Schlumberger.

[4] Schlumberger (2012). *ECLIPSE Reference Manual.* Houston, Schlumberger.

[5] Robinson, S. (2014). *Simulation: The Practice of Model Development and Use*. 2nd ed., London, Palgrave Mcmillan.

[6] Bánki D., Jobbik A: (2016). Dynamic modeling of hydrocarbon reservoirs using finite difference methods and derivation of analytic formulae for easier forecasting, *Proc. ISCAME Conference*, Debrecen, October 13–15, 2016.

[7] Bánki, D., Turzó, Z. (2020). Aiding Reservoir Simulation and Maintenance Using analytical Formulae, *Műszaki Földtudományi Közlemények*, Miskolc, Volume 89, pp. 207–215.

[8] Bánki, D., Turzó, Z. (2020). Application of analytical formulae in recovery factor estimation of hydrocarbon reservoirs. *Proc. XX. Ph.D. Conference proceedings*, Budapest PEME Egyesület, November 12, 2020.

Responsible: Prof. dr. Péter Szűcs Vice-Rector
Published by the Miskolc University Press under leadership of Attila Szendi
Responsible for duplication: Erzsébet Pásztor
Technical editor: Csilla Gramantik
Proofreader: Zoltán Juhász
Number of copies printed:
Put to the press: May 2022
Number of permission: MERT-2022-100-ME
HU ISSN 2063-6997